5. AUTOMOTIVE METALS – STEEL

A. NSF Funding for the Development of 3rd Generation Advanced High-Strength Steels (AHSSs) (ASP 280[i])

Project Manager: Roger A. Heimbuch
Auto/Steel Partnership (A/SP)
2000 Town Center Drive, Suite 320
Southfield, Michigan 48075-1123
(248) 945-4770; fax: (248) 356-8511; e-mail: rheimbuch@a-sp.org

Chairman: Ronald Krupitzer
American Iron and Steel Institute (AISI)
2000 Town Center Drive, Suite 320
Southfield, Michigan 48075-1123
(248) 945-4761; fax: (248) 352-1740; e-mail: krupitzerr@autosteel.org

Technology Area Development Manager: Joseph A. Carpenter
(202) 586-1022; fax: (202) 586-1600; e-mail: Joseph.Carpenter@ee.doe.gov

Field Project Officer: Aaron D. Yocum
(304) 285-4852; fax: (304) 285-4403; e-mail: aaron.yocum@netl.doe.gov

Expert Technical Monitor: Philip S. Sklad
(865) 574-5069; fax: (865) 576-4963; e-mail: skladps@ornl.gov

Contractor: United States Automotive Materials Partnership (USAMP)[i]
Contract No.: DE-FC05-02OR22910 through the National Energy Technology Laboratory

Objectives

- Conduct the fundamental research required to develop 3rd Generation Advanced High-Strength Steels (AHSSs) that are higher in strength and more formable than currently available commercial grades of AHSSs with the potential of being more cost effective than stainless steels and twinning-induced plasticity (TWIP) steels.

Approach

- Conduct fundamental steel research at universities that can lead to the development of a cost-effective family of 3rd Generation AHSSs that can be applied for mass reduction in the auto body.
- Utilized National Science Foundation (NSF) processes to manage the research.
- Provide a portion of the funding (25%) through this project for fundamental research required to develop 3rd Generation AHSSs.
- Additional funding will be provided directly by the Department of Energy (DOE, 25%) and the NSF (50%).

Accomplishments

- NSF Advanced High-Strength Steel Workshop held October 22-23, 2006, Arlington, Virginia.
- NSF Advanced High-Strength Steel Proposal Panel Review held April 10-11, 2007, Arlington, Virginia. Eight proposals, from 30 submitted, were selected for funding using the NSF process and a budget allocation prepared by NSF. The research projects will be carried out over three years.
- NSF will notify the appropriate Principal Investigators (PIs) and universities of their grants and track and document the research projects following NSF standard practices.

Future Direction

- An industry-based steering committee is being formed to interface with the researchers.
- An annual progress review of 3rd Generation AHSS research is being planned which will include the NSF research, work from the Department of Energy (DOE) National Laboratories and other research programs. The intent is to share progress, identify gaps in the research program and identify areas where additional support would be valuable.

Introduction

One of the tasks of the ASP 240 Future Generation Passenger Compartment project (see 5.I) was to run the structural-optimization codes with unrestricted strength limitations to define the upper strength bound for auto-body steel for optimized mass reduction. Several areas of the body were found that would benefit from higher strength.

An additional 5 to 8% mass reduction is possible in those areas of the vehicle. Based on the specific areas of the body, estimates were made of the forming characteristic needed to make those types of parts. A window-of opportunity was defined ranging from 600 MPa/40% elongation to 1600 MPa/20% elongation for a cost-effective 3rd Generation AHSS family. It was recognized fundamental steel research would be required to develop steels in that property range. A collaborative effort by NSF, DOE, AISI and A/SP has been put together to fund eight university research proposals, using the NSF processes, to fund the supporting fundamental research to develop steels with the desired properties.

Objective

The objective of this project is to provide a portion of the funding (25%) for the fundamental research required to develop a cost effective family of 3rd Generation AHSSs that can ultimately be applied for mass reduction in the auto body. Additional funding will be provided directly by DOE (25%) and NSF (50%). The research will be done utilizing the processes of the NSF. If the research is successful, it will provide the basis for the commercial development of cost-effective 3rd Generation AHSSs by the A/SP steel members.

Project Status

A NSF Advanced High-Strength Steel Workshop was held October 22-23, 2006 in Arlington Virginia. As a result of that workshop, the NSF requested proposals for basic research to support the development of a family of 3rd Generation AHSS. A NSF AHSS Proposal Panel Review was held April 10-11, 2007, in Arlington, Virginia. Eight proposals, from 30 submitted, were selected for funding using the NSF process and a budget allocation was prepared by NSF. The research projects will be carried out over three years starting the academic year 2007-2008. The following table shows the PI, institutions and titles.

University	Professor	Topic
Carnegie Mellon University	Warren Garrison	AHSS through microstructure and mechanical properties
Case Western Reserve University	Gary Michal	AHSS through C partitioning
Catholic University of America	Abu Al-Rub Rashid	AHSS through particle size and interface effects
Colorado School of Mines (CSM), Ohio State University (OSU)	David Matlock (CSM) and Robert Wagoner (OSU)	Collaborative GOALI Project Formability and Springback of AHSS
Drexel University	Surya Kalidindi	FEM using crystal-plasticity simulation modeling tools
OSU	Ju Li	Multi-scale modeling of deformation for design of AHSS
University of Missouri-Rolla	David C. Van Aken	AHSS through nano-acicular duplex microstructures
Wayne State University	Susil K. Putatunda	High-strength, high-toughness bainitic steel

Conclusions

NSF is in the process of initiating the research contracts with the eight selected universities. Reporting of the research will follow the normal processes of NSF and brief summaries will appear in future editions of this annual report.

Future Work

An industry-based steering committee is being formed to interface with the researchers**.** An annual progress review of 3rd Generation AHSS research is being planned which will include the NSF research, work from the DOE National Laboratories and other research programs. The intent is to share progress, identify gaps in the research and identify areas where additional support would be valuable.

Acknowledgements

The support and guidance of Dr. Mary Lynn Realff of the NSF, Dr. Joseph Carpenter of the DOE and Ronald Krupitzer of the AISI in developing and implementing this research initiate is greatly appreciated. Dr. Joycelyn Harrison is the successor to Dr. Realff as NSF monitor of the grants.

References

The NSF Report, "Advanced High Strength Steel Workshop Oct.22-23, 2006, Arlington, Virginia" by Professor Robert Wagoner, Department of Material Science and Engineering, The Ohio State University, Columbus, OH.

---

[i] Denotes project 280 of the Auto/Steel Partnership (A/SP), the automotive-focus arm of the American Iron and Steel Institute (AISI). See www.a-sp.org. The A/SP co-funds projects with DOE through a Cooperative Agreement between DOE and the United States Automotive Materials Partnership (USAMP), one of the formal consortia of the United States Council for Automotive Research (USCAR) set up by Chrysler, Ford and General Motors to conduct joint, pre-competitive research and development. See www.uscar.org.

B. High-Strength Steel Joining Technologies (ASP 070[i])

Project Manager: Michael S. Bzdok
Auto/Steel Partnership (A/SP)
2000 Town Center, Suite 320
Southfield, MI 48075-1123
(248) 945-4778; fax: (248) 356-8511; e-mail: mbzdok@a-sp.org

Co-chair: John C. Bohr
General Motors Corporation (GM) – Controls, Robotics, and Welding
30300 Mound Road – Mail Code 480-109-164
Warren, MI 48090-9015
(810) 602-8276; fax: (586) 947-1039; e-mail: johnc.bohr@gm.com

Co-chair: Eric Pakalnins
Chrysler LLC
800 Chrysler Drive – CTC-CIMS 482-00-11
Auburn Hills, MI 48326-2757
(248) 576-7454; fax: (248) 576-7490; e-mail:ep18@chrysler.com

Technology Area Development Manager: Joseph A. Carpenter
(202) 586-1022; fax: (202) 586-1600; e-mail: joseph.carpenter@ee.doe.gov

Field Project Officer: Aaron D. Yocum
(304) 285-4852; fax (304) 285-4403; e-mail: aaron.yocum@netl.doe.gov

Expert Technical Monitor: Philip S. Sklad
(865) 574-5069; fax: (865) 576-4963; e-mail: skaldps@ornl.gov

Contractor: U.S. Automotive Materials Partnership (USAMP)[i]
Contract No.: DE-FC05-02OR22910 through the National Energy Technology Laboratory

Objective

- The objective of the High-Strength Steel Joining Technologies project team is to provide welding and joining expertise to the A/SP lightweighting projects to facilitate the increased use of advanced high-strength steels (AHSS). Additional project objectives include augmenting the technical knowledge pertaining to welding of AHSS through applied research and development of industry standards for quality acceptance and weldability testing of AHSS.

Approach

- Anticipate needs of the A/SP lightweighting projects and conduct applied research to address identified technology gaps.
- Determine welding parameters to produce quality welds, then statically and dynamically test welds produced at these parameters to quantify individual weld structural performance (see Figure 1). Tensile shear strength, impact energy and fatigue life are typically evaluated.
- Utilize commercially-available equipment or equipment typically found in existing manufacturing facilities for AHSS feasibility assessments. Utilize other, new technologies as necessary for lightweighting implementation.

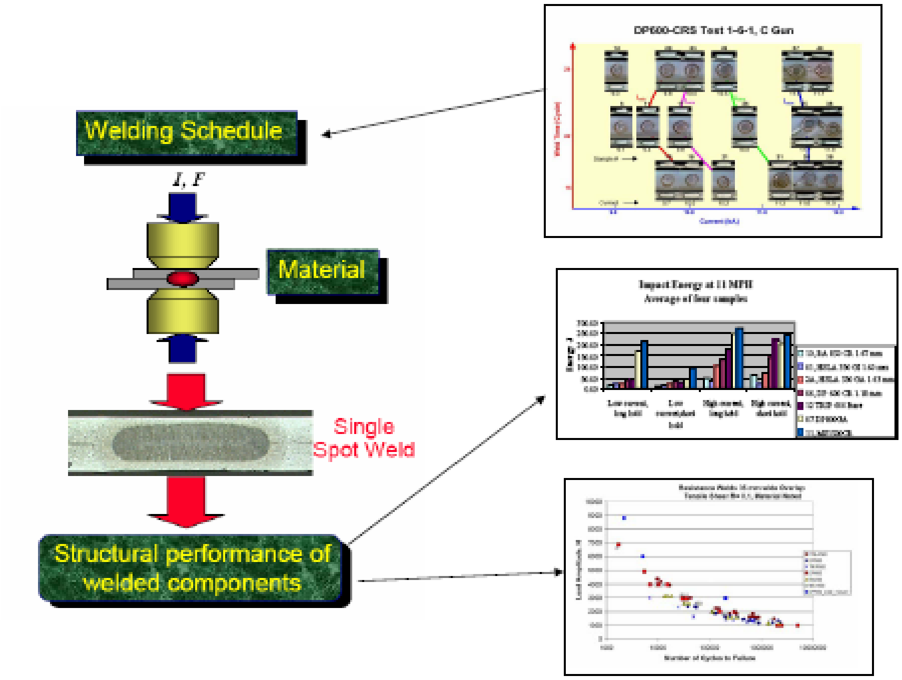

Figure 1. Resistance spot welding.

- Focus on materials classified as Group 3 and 4 (see Figure 2), as well as specific materials recommended by the A/SP Lightweight Structures Group.

Group: Tensile Strength (MPa):	**1. Low Strength < 350**	**2. Intermediate Strength 350-500**	**3. High Strength > 500 - 800**	**4. Ultra High Strength > 800**
Typical Materials:	**Mild 140YS/270TS BH 180YS/300TS BH 210YS/320TS BH 240YS/340TS**	**BH 260YS/370TS HSLA 280YS/350TS HSLA 350YS/450TS DP 300YS/500TS**	**DP 350YS/600TS TRIP 350YS/600TS DP 500YS/800TS TRIP 500YS/800TS CP 700YS/800TS**	**DP 700YS/1000TS MS 950YS/1200TS MS 1150YS/1400TS MS 1250YS/1520TS HS 950YS/1300TS**
Note: Steels with a minimum tensile strength above 500 MPa (Groups 3 and 4) are generally considered Advanced High Strength Steels (AHSSs). Source: International Iron and Steel Institute (IISI), *Advanced High Strength Steel (AHSS) Application Guidelines, 6 June 2006*				

Figure 2. IISI steel classifications for welding.

- Investigate the use of process finite-element modeling to predict weld-quality characteristics and optimize weld-process parameters (see Figure 3). Utilize simulation for future projects to develop weld-process optimization and weldability assessments. Validate simulation results with experimental data.

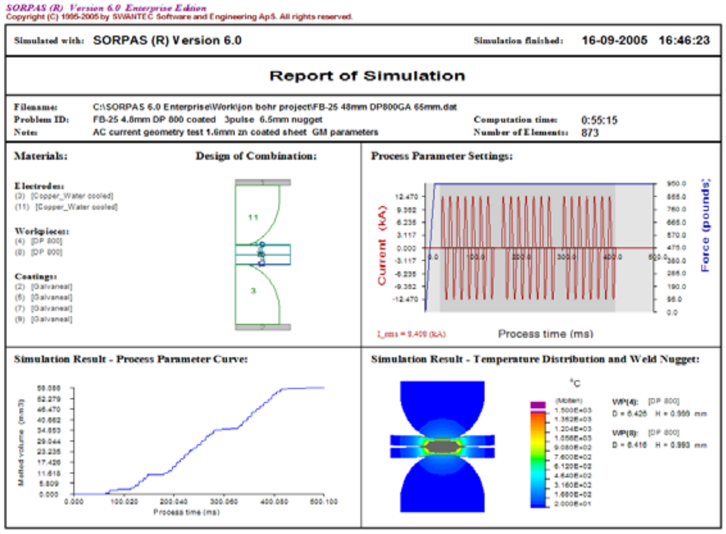

Figure 3. Process Simulation Report for resistance spot welding of DP780 Utilizing B-Nose Electrode and 3-Pulse Weld Schedule.

Accomplishments

- Produced and distributed public-project-result compact discs (CDs) and member-company toolkit CDs entitled "An Investigation of Resistance Welding Performance of Advanced High-Strength Steels," a Resistance Spot Weld (RSW) Design of Experiment (DoE) project (see Figure 4).
- Produced and distributed public-project-result CDs and member-company-toolkit CDs entitled "Advanced High-Strength Steel (AHSS) Weld Performance Study for Autobody Structural Components," a final project report of the Structural Weld Sub-Group (SWSG) study. Project included test matrix for evaluation of processes including metal inert gas (MIG), laser-assisted MIG, and plasma-assisted MIG (see Figure 4).
- Produced and distributed public-project-result CDs and member-company-toolkit CDs entitled "Impact Testing of Advanced High-Strength Steel (AHSS) Resistance Spot Welds at Various Temperatures," a study to quantify the effect of temperature on impact strength (see Figure 4).
- Produced and distributed public-project-result CDs and member-company-toolkit CDs entitled "Modeling Projection Welding of Fasteners to AHSS Sheet using Finite-Element Method," a study to model the projection welding of a hex-flanged weld nut using SORPAS with a cylindrical-block model.
- Produced and distributed public-project-result CDs and member-company-toolkit CDs entitled "Weld Lobe Development and Assessment of Weldability of Common Automotive Fasteners (Studs and Nuts) Using the Drawn Arc Welding Process" (see Figure 4). The purpose of this study was to determine the feasibility of welding studs to dual-phase (DP) and hot-stamped boron (HSB) steel, compare performances between cold-rolled steel and the above-mentioned steels, and develop a weld matrix for specific stud/material combinations (see Figure 5).

Figure 4. A/SP joining team project CDs.

AUTO STEEL PARTNERSHIP - DRAWN-ARC WELDING STUDY 2006

Emhart Teknologies

FASTENER DESCRIPTION:	M6 Stud/Nut
FASTENER PLATING:	Zinc-Nickel
EMHART FASTENER PART#:	39050
BASE MATERIAL TYPE:	DP980
BASE MATERIAL PLATING:	Galvaneal
BASE MATERIAL THICKNESS:	1.0 mm

WELD CURRENT (I) in Amps	20	25	30	35	40	45	50	55	60
1500									
1450									
1400									
1350									
1300									
1250			5	5	5	5			
1200			5	5	5	5			
1150			5	4	5	5			
1100			2	5	5	5	5		
1050			5	5	5	4	5		
1000			1	5	5	5	5		
950			2	5	5	4	5		
900			3	1	5	3	5		
850			2	1	1	4	5		
800			1	1	1	2	1		
750			1	1	1	1	5		
700			1	1	1	1	4		
650									
600									
550									
500									

WELD TIME (t) in milliseconds

EQUIPMENT
DCE 1500 WELD CONTROL
ETF12 FEEDER
LM WELD HEAD

WELD PROGRAMMING PARAMETERS	
LIFT	1.20mm
PENETRATION	-1.8 mm
START DELAY	250ms
Varc PILOT LIMIT	15.0V to 33.0V
Varc WELD LIMIT	15.0V to 33.0V
WELD TIME	+/- 6ms
WELD CURRENT	+/- 30Amps
STUD NEGATIVE POLARITY	

Figure 5. Drawn arc-weld matrix.

- Supported development of an automotive-industry AHSS resistance-weld-quality standard American Welding Society (AWS) D8.1M:2007 and provided technical support for development of an AHSS fracture-classification matrix for the standardization effort. The American National Standard Institute (ANSI) has completed the balloting process and was published in January 2007 (see Figure 6).

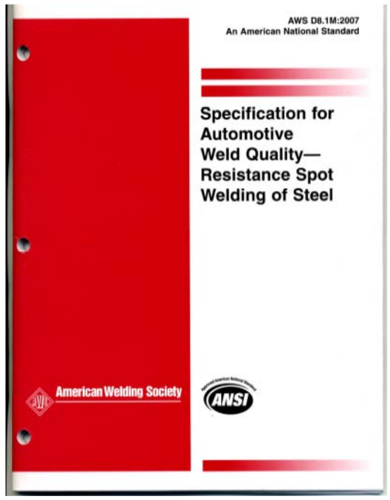

Figure 6. AWS/ANSI D8.1M:2007.

Future Direction

Future team activities include supporting welding development for the A/SP AHSS Application Guidelines Project Team and developing welding-parameter and joint-performance data for specific applications on AHSS automotive body prototypes. Future project work also includes:

- Complete development of a DoE methodology for material characterization and for assessing manufacturing feasibility of spot-welding AHSS.
- Develop software application to support common deployment and analysis of the AHSS Design of Experiment test method.
- Publish A/SP-recommended AHSS starting RSW schedules.
- Develop arc-weld procedures for various weld filler metals and AHSS joints, including determining the hot-cracking susceptibility and filler-metal compatibility of sheet AHSS materials.
- Create arc-weld design rules for the various lightweight chassis project teams' use.
- Complete a comprehensive study on Joint Efficiency that will allow joining-process comparisons for weld repair or substitution.

Introduction

The purpose of this project is to evaluate the weldability of the new AHSS currently being considered by the automotive companies as a solution to lightweighting without compromising cost or structural strength. The project intent is to evaluate various grades, thicknesses, and joining processes.

Initially, resistance welding was evaluated. Subsequent projects extended to metal inert gas (MIG), laser-assisted MIG, and plasma-assisted-MIG joining processes. Additional evaluations have included projection-nut welding and drawn-arc stud and nut welding to AHSS.

SWSG MIG/Laser Project

The arc-welding processes have historically been, and are today, commonly used in the manufacture of automotive structures. Recent increased usage of AHSS in automotive designs posed a desire to evaluate the application of arc-welding processes relative to the joining of AHSS.

This project establishes suitable welding parameters for AHSS material iterations (DP 600, DP 780, DP 800, DP 980 and high-strength low-alloy (HSLA) 350). Material section thicknesses ranged from 1.0 mm to 3.4 mm. Five arc-welding processes (Gas-Metal Arc Welding (GMAW)-Pulse/AC, GMAW-Pulse/DC, Laser-GMAW, Laser, and Laser-Plasma) were examined in this operation.

Special consideration was given to the acceptance criteria for this project's welds. The standards of the three original equipment manufacturers (OEMs) were reviewed and a derivative acceptance standard was established for this study. Hardness/metallographic, impact, and yield/tensile properties related to the resulting weldments are presented as the results of this investigation.

A summary review of the results indicates:

- AHSS materials were successfully joined with the processes studied.
- Weld processes utilizing filler material demonstrated better results than processes with no filler material.
- Laser-welded lap joints generally failed in the weld metal, while GMAW fillet joints generally failed in the heat-affected zone (HAZ).
- Filler material/electrode strength had no direct effect on the weldment strength.
- Material strength and/or thickness gauge had no influence on laser-welded joint strength.
- Zinc-coated materials demonstrated high levels of porosity without a controlled/ engineered gap.

The project has been completed. The Project Team has produced and distributed public-project-result CDs and member-company-toolkit CDs entitled "Advanced High-Strength Steel (AHSS) Weld Performance Study for Autobody Structural Components."

Low-Temperature Impact Project

To date, performance data have only been reported under ambient-temperature conditions, and effects of extreme temperatures on impact of RSW of AHSS steels have not been considered. The objective of this study was focused on the impact performance through impact energy and peak load of various stack-up combinations of AHSS and mild steels at a large range of possible application temperatures. The conducted experiments provide a better understanding of the effects of extreme cold/hot weather conditions of RSW joints. The dynamic responses to low- and high-speed impact loading are investigated, which interact with the effects of stack-ups and temperature. The results show that impact energy and peak load are significantly different in magnitude, trend and scattering/variation. This study also shows that impact energy is more sensitive to material combinations than peak load.

The project has been completed. The Project Team has produced and distributed public-project-result CDs and member-company-toolkit CDs entitled "Impact Testing of Advanced High-Strength Steel (AHSS) Resistance Spot Welds at Various Temperatures."

Assessing Weldability of Projection-Welding Fasteners Using FEA

While the Joining Technology effort has been directed towards RSW, little focus has been directed toward projection-welding of traditional fasteners to AHSS sheet. Weld schedules and expected weld properties of projection-welded joints between fasteners and AHSS sheet are expected to differ from those in traditional material combinations. The highly-alloyed chemistry of AHSS and tailored material properties can result in undesirable properties after these materials are welded. Furthermore, the dissimilar-metal combination that is typical of projection welding of fasteners, adds complexity to the issue as a result of different base-metal properties and weld-metal dilution. In this sense, optimization of the weld process may be difficult as it requires an understanding of the effects of process parameters on the properties of the weld and surrounding base metal.

The projection-welding process of an M12/1.75/30 hex-flange 3-projection weld nut to 1.2-mm thick DP 780 hot-dip galvanized (HDG) AHSS sheet has been modeled using SORPAS.

The following conclusions have been found:

- A cylindrical-block model is best suited to this application. The axisymmetric geometry assumes one projection that encircles the entire nut resulting in a low current density. The rectangular-block model results in excessive deformation in the nut body and requires reinforcement.

- The modeled results show strong correlation with experimental cross-sections.
- Increasing the weld current results in an increase in weld size.
- Increasing the weld force results in a decrease in weld size.
- Increasing the weld time to four cycles results in an increase in weld width, but has little effect on weld height.
- Increasing the weld time beyond four cycles has no effect on weld size.
- A peak in power during the first four cycles due to contact resistance causes rapid melting and collapse of the projection.
- Decreasing current density after collapse limits further nugget growth.
- Increasing the weld time results in an increase in HAZ size, but can also result in lower cooling rates.
- Modeling and experimental results indicate the projection-weld nut in this study to be weldable to DP 780 HDG sheet material under various conditions.

The project has been completed. The Project Team has produced and distributed public-project-result CDs and member-company-toolkit CDs entitled “Modeling Projection Welding of Fasteners to AHSS Sheet using Finite-Element Method.”

Lightweight Rear Chassis Structures

The Lightweight Rear Chassis Structures team (see 5.J) of the A/SP needed assistance in welding a lightweight design from DP 600, 800, and 980 materials. After obtaining the various materials, the Joining Team proceeded to evaluate the weldability of these materials and to test weld the combinations prescribed for a rear-end structure. The Joining Team established the weld parameters and assisted the prototype source in making the structure. Weld parameters were delivered to the Lightweight Rear Chassis Structure team along with mechanical and chemical properties of the test materials.

Drawn-Arc Stud and Nut Welding to AHSS

Drawn-arc welding (DAW) is a well-established process for attaching studs to a variety of material type, thickness and coating combinations in automotive construction. The application of DAW is consistent with new automotive designs and manufacturing strategies that continually focus on ways to reduce costs. DAW provides a combination of short cycle time for stud attachment (high productivity) and adaptability to automation. Technological improvements in DAW equipment have resulted in increased application of the process.

The focus of this study was to determine whether drawn-arc stud welding can be performed on a consistent basis to new materials like DP steel and HSB steels. The approach of this study was to determine the feasibility of welding studs to DP and HSB steels, compare performances between cold-rolled steel and the above-mentioned steels, and develop a weld matrix for specific stud/material combinations.

Results indicate that the fasteners chosen for this study can be welded to the DP steel and HSB steel. Nut welding to HSB steel provided very interesting test results. Also, interesting to note was that certain geometries of a stud or nut are required to weld to HSB steel. These geometries also allow the automation of DAW process to be used for a variety of bracket configurations.

The project has been completed. The Project Team has produced and distributed public-project-result CDs and member-company-toolkit CDs entitled “Weld Lobe Development and Assessment of Weldability of Common Automotive Fasteners (Studs and Nuts) Using the Drawn Arc Welding Process.”

Conclusions

Additional welding issues will be addressed during 2008 by the Joining Technologies Team funded by USAMP lightweighting initiatives and as member-company in-kind contributions.

Presentations and Publications

1. Donald F. Maatz, Jr., RoMan Engineering Services, "Advanced High-Strength Steel (AHSS) Weld Performance Study for Autobody Structural Components." Presented at the March 7, 2007 Great Designs in Steel Seminar in Livonia, Michigan. Paper presented at the MS&T'07 Conference at Cobo Center, Detroit, Michigan
2. Dr. Siva Ramasamy, Emhart Teknologies, "Drawn Arc Welding of Fasteners to Advanced High Strength Steels." Presented at the March 7, 2007 Great Designs in Steel Seminar in Livonia, Michigan
3. Dr. Siva Ramasamy, Emhart Teknologies, "Weld Lobe Development and Assessment of Weldability of Common Automotive Studs and Nuts with the Drawn Arc Welding Process." Paper presented at the MS&T'07 Conference at Cobo Center, Detroit, Michigan.

---

[i] Denotes project 070 of the Auto/Steel Partnership (A/SP), the automotive-focus arm of the American Iron and Steel Institute (AISI). See www.a-sp.org. The A/SP co-funds projects with DOE through a Cooperative Agreement between DOE and the United States Automotive Materials Partnership (USAMP), one of the formal consortia of the United States Council for Automotive Research (USCAR) set up by Chrysler, Ford and General Motors to conduct joint, pre-competitive research and development. See www.uscar.org.

C. Hydroform Materials and Lubricants (ASP 060[i])

Project Manager: Bart Clark
Auto/Steel Partnership (A/SP)
2000 Town Center, Suite 320
Southfield, Michigan 48075-1123
(248) 945-4776; fax: (248) 356-8511; e-mail: bclark@a-sp.org

Chairperson: Ronald Soldaat
Dofasco, Inc.
1330 Burlington Street East
P.O. Box 2460
Hamilton, Ontario, Canada L8N 3J5
(905) 548-7200; fax: (905) 548-4250; e-mail: Ronald_Soldaat@dofasco.ca

Technology Area Development Manager: Joseph A. Carpenter
(202) 586-1022; fax: (202) 586-1600; e-mail: joseph.carpenter@ee.doe.gov

Field Project Officer: Aaron D. Yocum
(304) 285-4852; fax: (304) 285-4403; e-mail: aaron.yocum@netl.gov

Expert Technical Monitor: Philip S. Sklad
(865) 574-5069; fax: (865) 576-4963; e-mail: skladps@ornl.gov

Contractor: United States Automotive Materials Partnership (USAMP)[i]
Contract No.: DE-FC05-02OR22910 through the National Energy Technology Laboratory

Objective

- Develop mechanical-test procedures and forming-limit diagrams for tubes.
- Improve the accuracy and confidence in finite-element modeling (FEM) of tubular hydroforming.
- Investigate the fabricating and performance characteristics of tailor-welded tubes (TWTs).
- Develop an understanding of steel and lubricant requirements for hydroforming using a combination of experiments and FEM.
- Support the work of other A/SP project teams when they investigate hydroformed structural components.
- Validate the performance benefits of hydroforming in automotive structures.

Approach

- The approach taken in this project is first to gain a basic understanding of the hydroforming process and potential issues, then apply the understanding to support other A/SP project teams in vehicle applications.
- The investigation encompasses various steel grades and gauges of steel tubing, including TWTs and advanced high-strength steel (AHSS), in free-expansion and corner-fill processes using several types of lubricants.
- The work has been divided into several phases.
  - Phase 1 – Investigate free-expansion and corner-fill characteristics.
  - Phase 2 – Investigate effects of pre-bending, lubricants and end-feeding on hydroforming limits.
  - Phase 3 – Investigate some of the pre-bending parameters for the hydroforming process.
  - Phase 4 – Investigate some of the bending parameters for AHSS tubing.

- Phase 5 – Determine the experimental forming limits of steel tubes.
- Phase 6 – Develop methods for empirical prediction of tube forming-limit diagrams and analysis of hydroforming data.
- Phase 7 – Investigate tubes made from tailor-welded blanks of varying grades and thicknesses.
- Phase 8 – Demonstrate the benefits of tube hydroforming through projects focused on real-world applications.

Note: Delays in obtaining sheet stock and tubes caused Phases 3 and 4 to follow Phases 5 and 6.

Accomplishments

During the report period (October 1, 2006 – September 30, 2007) the following were accomplished:

- Completed additional inside and outside corner-fill experiments with 90°-bent, interstitial-free (IF) and dual-phase (DP) 600 tubes with welded end caps to study the effect of elimination of tube end feed. Completed draft report.
- Completed experimental study on the hydroforming of TWTs fabricated from tailor-welded blanks of varying thicknesses of high-strength low-alloy (HSLA) 350 and DP 600 sheet steels. Tests included free-expansion and straight-tube corner-fill.
- In March 2005, the team was challenged to demonstrate the manufacturability of an AHSS hydroformed-TWT, lightweight, automotive front-rail. The team has taken on this challenge and accomplished the following to date:
  - Procured steels and tooling to fabricate tubes made from tailor-welded blanks with six different thicknesses/grades of high-strength steel.
  - Procured tooling to fabricate the front frame rail from the above tubes.
  - Soutec Soudronics in Switzerland fabricated the TWTs for the hydroforming process. Forming the TWTs, although eventually successful, proved to be very technologically challenging.
  - Procured special tooling dies for the hydroforming process
  - Began the process of bending the TWTs to fit the dies, which bending had been unsuccessful to date due to wrinkling and splitting.
- Developed a concept for a burst-testing-criteria fixture and identified a contractor to build it.
- Developed a proposal for a project concerning, “Investigation of Fabricating Dual Phase and TRIP Steel Tube from an ERW Production Line.” Project has been awarded to a contractor and the required sheet steels have been acquired.
- Developed a proposal for a project, “Stress and Strain Measurements under Non-Linear Loading through Tube Fracture for Improved Modeling and Prediction,” which involves controlled stress-path expansion of tubes. Quotes have been received in response to a request for quote (RFQ) and are in the process of being reviewed.

Future Direction

During fiscal year 2008, the Hydroforming Materials and Lubricant team plans to accomplish the following:

- Proceed with AHSS TWT bending trials for the front-rail project and gain an understanding of the effect of the process variables.
- Upon successful AHSS TWT trials, fabricate and determine the manufacturing parameters of a hydroformed front frame rail in support of the work performed by Lightweight Front Structures, ASP 110 (see annual report for fiscal year (FY) 2006). These rails will be further tested by the Strain Rate Characterization project Team, ASP 190 (see 5.G)
- Complete report for the hydroforming of HSLA 350 and DP 600 TWTs and make documentation available to A/SP member companies.
- Complete report on the hydroforming of DP 600 and IF Bent Tubes with Welded End Caps and make documentation available to A/SP member companies.

- Conduct the project, "Investigation of Fabricating Dual Phase and TRIP Steel Tube from an ERW Production Line."
- Conduct the project, "Stress and Strain Measurements under Non-Linear Loading through Tube Fracture for Improved Modeling and Prediction."

Introduction

Hydroformed steel tubes have been used in the automotive industry to form components that meet structural objectives, particularly strength and rigidity, at optimal mass. One of the most significant advantages of tubes is that they are monolithic closed sections and, as such, exhibit significantly greater stiffness in torsion than conventional open sections such as "C" and "hat" shapes. Eliminating the need for weld flanges, which are required to join two open members into a closed member, offers a potential for reducing vehicle mass. The use of hydroformed tubes is limited largely by lack of knowledge of the capabilities and parameters of hydroforming processes and the effects of those processes on the tubes.

This project was undertaken to investigate and quantify the capabilities and parameters of various hydroforming processes so that automotive designers and engineers can utilize a wider range of tube configurations and predict with reasonable accuracy the performance of hydroformed components. Hydroforming tubes made from high-strength and AHSS, and particularly tubes made from tailor-welded blanks, are of particular interest because of the potential reduction of mass associated with materials of higher strength and optimal thickness.

Discussion

The Hydroforming Process

Hydroforming is a process in which a tube is placed into a die shaped to develop the desired configuration of the tube. Water is introduced into the tube under very high pressures causing the tube to expand into the die. The tube ends can be held stationary or moved inward during the process to end-feed material into the die cavity. ---

The process has two distinct stages, shown in Figure 1. The first stage is free expansion (Figure 1a). It continues until the tube contacts the die wall (Figure 1b). In the second stage, corner filling, the tube is in contact with the surface of the die, which constrains subsequent deformation (Figure 1c). During this stage, the tube expands into the corners of the cavity, accomplishing corner fill. A tube that has been hydroformed is shown with the die in Figure 2. Note that the test was continued until the tube failed.

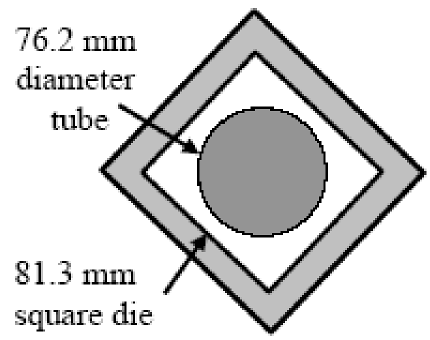

Figure 1a a) Free Expansion

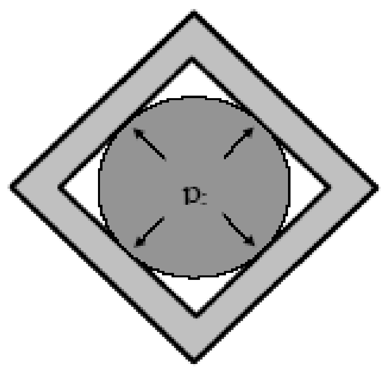

Figure 1b b) Contact with die wall

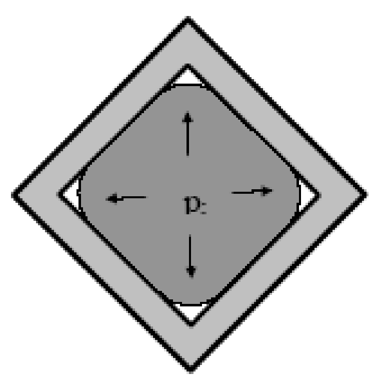

Figure 1c c) Corner filling

Figure 2. A hydroformed tube and die.

During corner fill, the tube slides against the die; therefore, friction between the tube and die affects the process, and the lubricant used in the process becomes a significant parameter.

Forming-Limit Diagrams (FLD)

During tube fabrication and during both stages of hydroforming, the tube undergoes plastic strain. The amount of plastic strain that can occur before the material fractures is predicted in stamping processes that utilize flat sheet steel by using a forming-limit diagram (FLD). The FLD is determined by the properties of the material. The hydroforming process is preceded by tube forming and sometimes pre-bending of the tube, both of which induce strains in the material and alter its properties. Before a FLD can be developed for the hydroforming process, the strain history – that is, the strain induced in the material prior to hydroforming – must be known.

An FLD is required for any successful computer simulation of hydroforming. Therefore, in addition to experiments with tube expansion to determine the effects of axial compression and tension in combination with internal pressurization, the effects of pre-bending and pre-forming on subsequent formability was addressed. Collected data were used to develop FLDs for tubular hydroforming of straight tubes. These data will be used to develop guidelines for optimizing bending operations.

Presently, the formability limits for pre-bent steel in tubular hydroforming are poorly understood. Accuracy needs to be addressed and improved to allow optimum application of tubular hydroforming in the lightweighting of vehicles.

Hydroforming Tailor-Welded Tubes

The Project Team began work on hydroforming TWTs. The work is being conducted on 76.2-mm (3”) outside diameter (OD) tubes made from two material grades and two thicknesses. The test consists of five TWT configurations:

1) Baseline: 1.5-mm DP 600 single material tube
2) 1.5-mm DP 600 butt welded to 1.5-mm DP 600
3) 1.2-mm DP 600 butt welded to 1.5-mm DP 600
4) 1.5-mm HSLA 350 butt welded to 1.5-mm DP 600
5) 1.5-mm HSLA 350 butt welded to 1.2-mm DP 600

The blanks were butt welded before the tubes were formed. In all cases the tubes are 508-mm (20-inches) long.

The finished tubes were sent to the testing laboratory where they were analyzed. The laboratory found that tube concentricity was not adequate in some cases to allow conventional hydroforming, because it was not possible to maintain an adequate seal between the tube ends and the end caps, where water is introduced. At the suggestion of the laboratory and with the approval of the Hydroforming Team, the laboratory welded the end caps. Free expansion tests have been completed and the results are being analyzed.

Vehicle Front Structural Rail

In March, 2006, the Hydroforming Team began an initiative to fabricate a front structural rail, based on a design developed by the Lightweight Front Structures (LWFS) Team, ASP 110. LWFS had developed designs for a front rail for two vehicles. The first was the target vehicle. The second had 20% less mass than the target vehicle, which is a reasonable assumption based on anticipated secondary effects resulting in lower mass in systems such as suspension, powertrain and roof structure.

Two design concepts were developed for each vehicle and both concepts were optimized by using tailor-welded blanks. The first design concept in each case requires conventional stamping processes to form a "hat-shaped" member with a "top plate" spot-welded at the "hat" section flanges. The second concept utilizes a tailor-welded tube consisting of six different grades/gauges of steel. The TWT design did not address attachment to contiguous vehicle components.

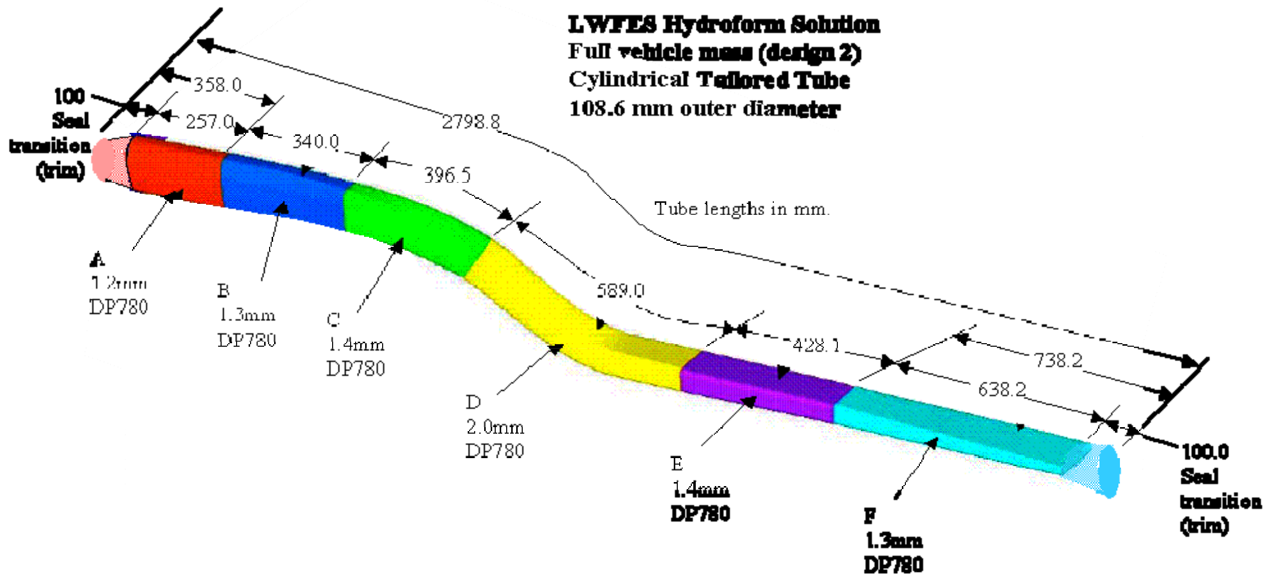

Figure 3. Hydroformed rail for full vehicle mass.

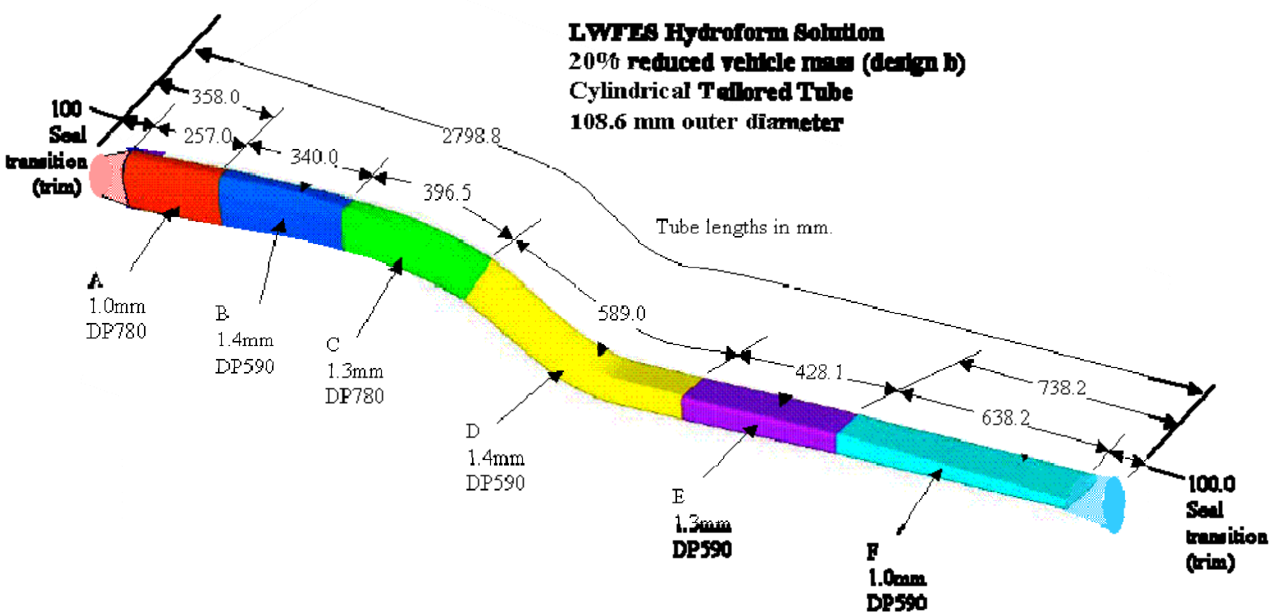

Figure 4. Hydroformed rail for 20% reduced vehicle mass.

The blank lineup for the rail in the target vehicle is shown in Figure 3 and the lineup for the rail in the vehicle with 20% reduced mass rail, in Figure 4. It is noteworthy that the rail for the full mass vehicle utilizes DP 780 steel in 1.2-mm to 2.0-mm thickness, while the rail for the 20% reduced mass vehicle utilizes both DP 780 and DP 590.

The Project Team agreed that the purpose of the front-rail initiative is a manufacturing-feasibility study. For this reason, no effort will be made to correct the hydroforming tools to bring the end product within dimensional-tolerance limits. Rather, the hydroforming supplier will be asked to utilize his experience to produce tubes as close as possible to dimensional tolerances, then perform comprehensive dimensional studies on the tubes to learn the effects of the fabrication process, such as springback and die release.

The Team selected a hydroforming supplier and a tube manufacturer, both of whom have state-of-the-art equipment and expertise, are willing to stretch their current technology and are willing to make significant in-kind contributions to the project.

The hydroforming tools have been procured, the tube-forming tools have been procured, and fabrication of the tubes has been completed. Work on the bending of the tubes is in progress.

Burst Criteria

The Hydroforming Team also recognized the need to develop burst criteria for hydroformed tubes. To date, a test fixture has been prescribed and a vendor has been selected to design and build the fixture. The second phase of this initiative will be the actual tests.

Future Work

During FY 2008, the Hydroforming Materials and Lubricants Team will pursue the following work:

- Gain an understanding of issues affecting bending of AHSS tailor-welded tubes.
- Manufacture front rails from TWTs to both designs (target vehicle and 20% reduced mass vehicle, Figures 3 and 4).
- Perform analyses on hydroformed rails.
- Complete the project on the hydroforming of DP 600 and IF Bent Tubes with Welded End Caps and make test documentation available to A/SP member companies.
- Conduct the project, "Investigation of Fabricating Dual Phase and TRIP Steel Tube from an ERW Production Line."
- Conduct the project, "Stress and Strain Measurements under Non-Linear Loading through Tube Fracture for Improved Modeling and Prediction."

Conclusions

Analysis of tests run during this reporting period indicates that:

- Tube bending can significantly limit subsequent tube formability and needs to be accounted for in part design.
- Tube-bending speed has only a minor effect on bending strains and subsequent hydroforming. Bending radius, however, has a large impact.
- Lubricant selection is important as it affects bending and hydroforming strains.
- Tube end feeding is very beneficial for achieving complex geometries.
- FLDs based on sheet-forming technology are useful for predicting necking strains in free-expansion hydroforming, but bursting in closed-die hydroforming requires further understanding.

Presentations and Publications

1. "Hydroforming Group," Auto/Steel Partnership Program Review, Department of Energy, September 21, 2005.
2. "Hydroforming Committee," A/SP SPARC financial planning review, July 18, 2006.
3. "Hydroforming Materials and Lubricants," Auto/Steel Partnership Department of Energy Peer Review meeting was conducted on Friday, December 1, 2006
4. "Influence of Lubricant in Bending & Hydroforming Evaluations" presentation by Jean Reid at ASTM D02 Petroleum Products and Lubricants Committee workshop/symposium on Tribological Challenges of Metal Deformation Fluids, Florida, June 17, 2007.

5. "Tube Hydroforming Phase V: Experimental Forming Limits of Steel Tubes" IRDI report, March 2007 (awaiting publication by A/SP Technology Transfer Team)
6. "Influence of Bending Parameters on the Hydroforming of IF and DP 600 Tubes" IRDI report, March 2007 (awaiting publication by A/SP Technology Transfer Team)
7. "Hydroforming Materials and Lubricants (ASP060) - Project Description Sheet, Statement of Project Objectives and Presentation," A/SP Project Review and Budget meeting, July 17, 2007.

---

[i] Denotes project 060 of the Auto/Steel Partnership (A/SP), the automotive-focus arm of the American Iron and Steel Institute (AISI). See www.a-sp.org. The A/SP co-funds projects with DOE through a Cooperative Agreement between DOE and the United States Automotive Materials Partnership (USAMP), one of the formal consortia of the United States Council for Automotive Research (USCAR), set up by Chrysler, Ford and General Motors to conduct joint, pre-competitive research and development. See www.uscar.org.

D. Sheet-Steel Fatigue Characteristics (ASP 160[i])

Project Manager: Bart Clark
Auto/Steel Partnership (A/SP)
2000 Town Center, Suite 320
Southfield, Michigan 48075-1123
(248) 945-4776; fax: (248) 356-8511; e-mail: bclark@a-sp.org

Chair: Raj Mohan Iyengar, Ph.D.
Severstal North America Inc
3001 Miller Road
P.O. Box 1631
Dearborn, MI 48121-1631
(313) 317-1303; fax (313) 337-9372; e-mail rmohan@severstalna.com

Technology Area Development Manager: Joseph A. Carpenter
(202) 586-1022; fax: (202) 586-1600; e-mail: joseph.carpenter@ee.doe.gov

Field Project Officer: Aaron D. Yocum
(304) 285-4852; Fax (304) 285-4403; e-mail: aaron.yocum@netl.doe.gov

Expert Technical Monitor: Philip S. Sklad
(865) 574-5069; fax: (865) 576-4963; e-mail: skladps@ornl.gov

Contractor: United States Automotive Materials Partnership (USAMP)[i]
Contract No.: DE-FC05-02OR22910 through the National Energy Technology Laboratory

Objectives

- Compile the test data generated in the previous phases of the project into a user-friendly database that can be used in all phases of design and structural analysis of sheet-steel vehicle bodies.
- Investigate the fatigue life of joints formed by spot welding, adhesive bonding and weld bonding (a combination of spot welding and adhesive bonding).
- Explore the fatigue response of advanced high-strength steels (AHSS) after being subjected to metal inert gas (MIG) and laser-welded joining and compare this behavior with that of standard automotive steels.
- Assist the Joining Technology team (see 5.B) in identifying the optimum welding parameters for laser- and MIG-welded joints, and develop a fatigue test program.

Approach

- Investigate the fatigue characteristics of resistance spot welding, a fusion process in which the metal pieces to be joined are melted and re-solidified via a brief high-voltage electrical pulse, forming an alloy with a distinctly different microstructure than that of the parent metals. At the intersection of the weld nugget, or button, and the faying surfaces, a crack-like discontinuity is formed which is often the site of initial crack growth. In addition, the weld nugget itself may contain discontinuities (such as porosity), which can also become sites at which fatigue cracks form. The amount and type of discontinuities and, thus, the fatigue properties can be affected to a considerable extent by the welding process. The microstructures of the joined metals are also changed in the area adjacent to the weld, which area is known as the heat-affected zone (HAZ).
- Investigate the fatigue characteristics of adhesive bonding, which substitutes an entirely different material in place of the weld to act as the load-bearing connection. The adhesive must adhere to the metals being joined and resist interfacial fatigue failure at the adhesive/metal interface and within itself (cohesive failure).

- Investigate the fatigue characteristics of weld bonding, which is a combination of adhesive bonding and spot welding.
- Investigate the previously unknown, or at best little known, factors that are expected either to improve impact durability or facilitate their modeling and simulation.
- Reduce the spot-weld, adhesive-bonded, and weld-bonded test data to a form that is useful to design engineers who perform vehicle structural analysis.
- Develop a test program to investigate the fatigue performance of gas metal arc welding (GMAW), a fusion welding process which results in continuous joints. However, under GMAW (or MIG), a third "filler" metal is introduced under an arc and shielding gas and, akin to spot-welding, alloys and microstructures are formed which are different from the metals being joined.
- Identify the parameters, including metal grades, metal thicknesses, coatings and joint configurations that impact the fatigue performance of GMAW welded joints.

Accomplishments

- Completed testing of spot welds in mild steel and ultra-high-strength boron steel and placed online the knowledge base developed from the results.
- Completed a detailed study of effect of geometric parameters on fatigue lives of spot-welded specimens.
- Developed a specification for fabricating MIG- and laser-weld specimens, submitted a request for quotation, selected a contactor and awarded a construction contract.
- Completed fatigue testing of MIG-welded specimens created by the Joining Technologies Team, ASP 070.
- Completed fabrication of test specimens for Phase 1A MIG-weld fatigue testing.
- Completed weld fatigue testing for single-lap-shear, MIG-welded test specimens.
- Initiated weld testing of double-lap-shear and perch-mount specimens.

Future Direction

- The project team will complete the Phase 1A of its own program of fatigue testing MIG welds.
- Specimen specifications for Phase 1B testing will be completed and Phase 1B will be initiated.
- Detailed analyses and interpretations of the test results will be conducted to develop appropriate parameters that capture the effect of weld and specimen geometry on fatigue performance.

Introduction

Future and near-future vehicle designs are faced with several stringent requirements that impose conflicting demands on the vehicle designers. Safety, particularly crash-energy management, must be improved while vehicle mass and cost are contained.

AHSSs, judiciously selected and applied, are currently the best candidates to achieve low-cost (compared with aluminum (Al), magnesium (Mg) and plastics), reliable materials for meeting these mandates. As structural components are optimized and thinner gauge, higher-strength materials are assessed, the fatigue lives of the areas where loads are transferred become increasingly important considerations. To assess the performance of a component in the design phase, the fatigue characteristics of not only the base material but the joints where loads are transferred, must be known. This project has essentially completed testing various grades of steel and steel coupons that have been spot welded, adhesively bonded and weld bonded. Testing of GMAW and laser-welded joints is under way.

Discussion

The effort to evaluate the fatigue characteristics of spot welds began in the 2002 fiscal year with presentations by key researchers on the current state of the work at Chrysler Corporation, Ford Motor Company, and General Motors Corporation. Based on these presentations, the Sheet-Steel Fatigue Project Team has produced results beneficial to all three companies. Early in the planning, the A/SP Joining Technologies Team was consulted, and that team prepared the samples that were tested. This interaction ensured that the samples were joined using consistent procedures that were properly controlled and in adherence to the best current practices in sheet-metal joining in the automotive industry.

The following fatigue test parameters were agreed upon and carried out:

- Two modes of testing: tensile shear (Figure 1) and coach-peel (Figure 2).
- A single thickness (1.6 mm) was selected to ensure that results were comparable between steel grades. A thinner gage (0.8 mm) was selected for a small satellite study (one AHSS and one high-strength low-alloy (HSLA)) on the effect of gage thickness on fatigue.
- Because no such data were available for AHSSs, several grades in this class were tested.
- Testing was done at two stress ratios, R, 0.1 and 0.3. The stress ratio R is defined as the ratio of the minimum stress to the maximum stress in the test cycle. Maximum and minimum values are algebraic, with tension designated as positive and compression negative.
- Eleven steel grades were tested.
- While the majority of testing was performed on spot-welded joints, the fatigue performance of adhesive-bonded and weld-bonded joints was explored in several tests series.

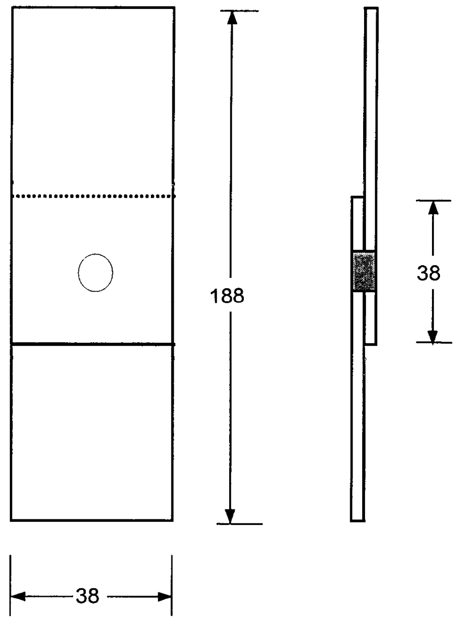

Figure 1. Spot-welded lap-shear test specimen.

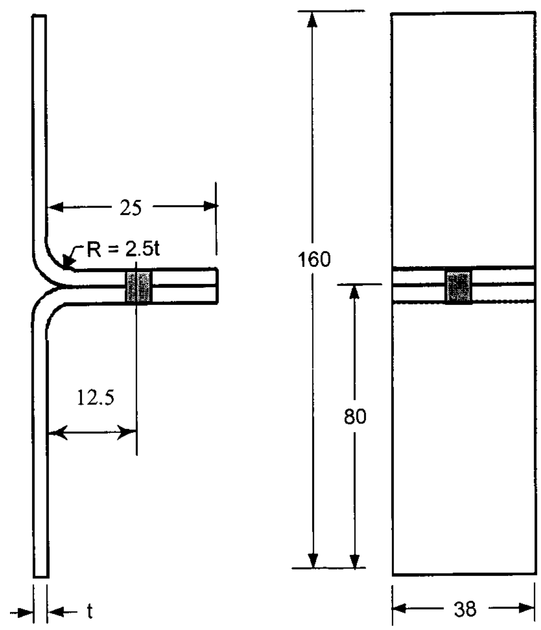

Figure 2. Coach-peel test specimen.

Two testing sources, of the nine invited to submit testing proposals, were selected to perform the fatigue experiments: The University of Missouri at Columbia, Missouri, and Westmoreland Mechanical Testing and Research, Inc. in Youngstown, Pennsylvania.

As the testing progressed and results were analyzed, the following tests were added for comparison purposes:

1. Testing at specified R ratios means that the maximum and minimum loads are constant throughout a given test. However, as the maximum load is increased to generate fatigue curve data, the minimum loads also increase. This process is valuable for establishing baseline data. However, in the real world, load amplitudes can be expected to be variable. For this reason, automotive-spectrum load tests, set to two different predetermined scalings, were run.
2. To investigate the effect of button size, fatigue studies were performed on specimens with a welding schedule that produced a smaller weld button.
3. At the request of the Joining Technologies Team, three test series were run using wide samples (125 mm vs. the standard 38 mm). The wider samples minimize rotation of the weld under load and allow negative R ratios to be explored.

GMAW Joints

GMAW welding is the second most common welding process used on vehicle structures, with the rate of applications increasing yearly. GMAW or MIG welds are used not only on body members and sub-frames in passenger cars, but also in frames for larger passenger vehicles, light trucks and sport-utility vehicles (SUVs). Therefore, the test samples will be made from two thickness groups: a thinner gage of 1.6 mm for body applications and a thicker gage of 3.4 mm for frame applications. These target thicknesses, primarily based on material availability, represent typical, as-welded material thicknesses found in body and frame applications, respectively.

Frame members do not generally require as much formability as do body members, and they offer excellent opportunities for mass reduction through downgaging. Therefore, tests on frame joints will ultimately employ higher-strength materials than those specific to body members, but often result in similar numbers of welds and amount of weld area.

The Team agreed to four specimen designs for testing. Each explores a different loading mode and reveals different information about the material/joint performance: butt weld (Figure 3), single-lap-shear (Figure 4), double-lap-shear (Figure 5), and perch mount (Figure 6).

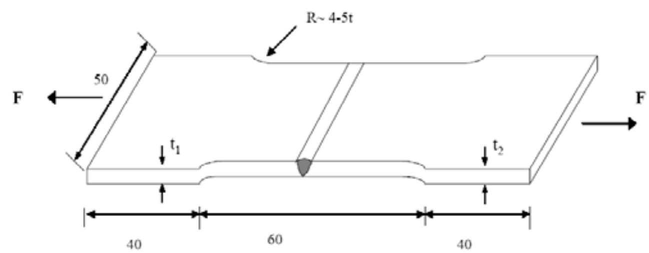

Figure 3. MIG butt-welded specimen.

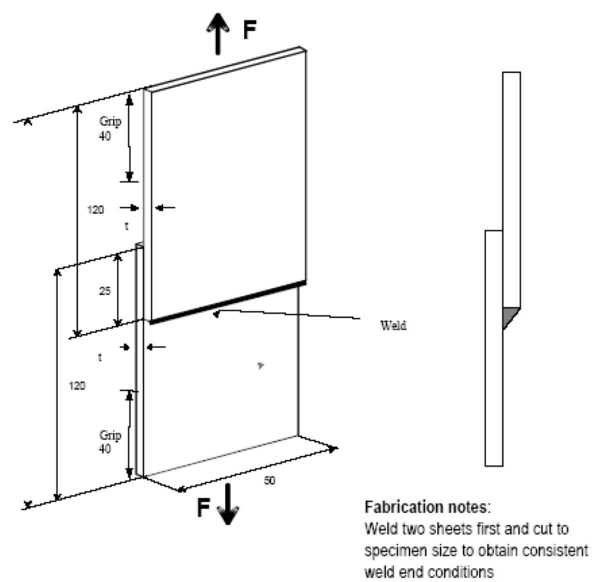

Figure 4. MIG-welded, single-lap-shear specimen.

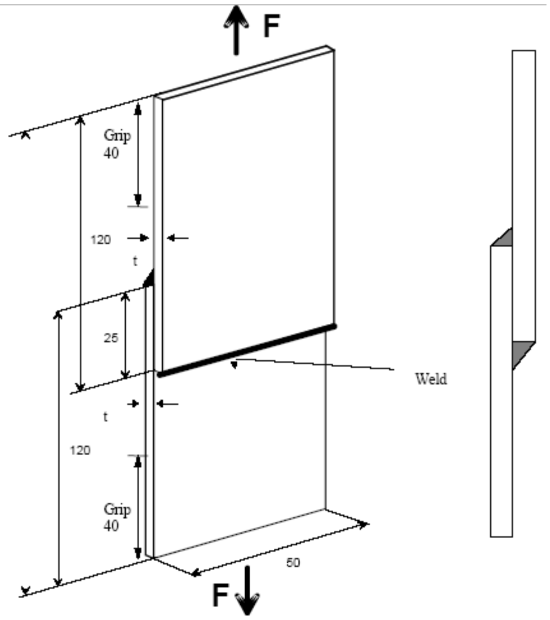

Figure 5. MIG-welded double-lap-shear specimen.

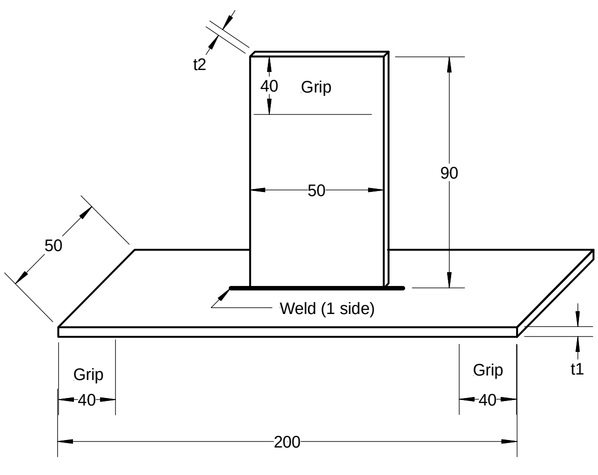

Figure 6. MIG welded perch mount specimen.

Results – Spot welds

Plotted in Figure 7 are all the tensile-shear and coach-peel fatigue results for all nominal 1.6-mm gage materials with 7-mm-diameter spot welds, conventional steels and AHSS included. Data labels ending in R0.1 indicate R=0.1 loading and data labels ending R0.3 indicate R=0.3 loading. Runouts are plotted but not otherwise indicated in this figure.

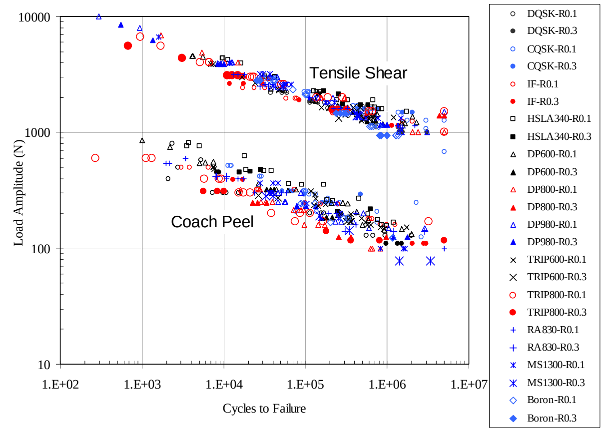

Figure 7. Fatigue results for all 1.6 mm thick, 7 mm diameter nugget spot-welded materials.

Two thicknesses of HSLA340 (1.0 mm and 1.78 mm) and two thicknesses (1.53 mm and 0.83 mm) of dual phase (DP 600) are compared in Figure 8. The nominal button size for all specimens was 7.0 mm and the welding parameters were held as similar as possible between the gages/grades without compromising strength. It was expected that the thinner gages would show shorter life because of the intrinsically higher stresses in the joint; this result was indeed found in both materials.

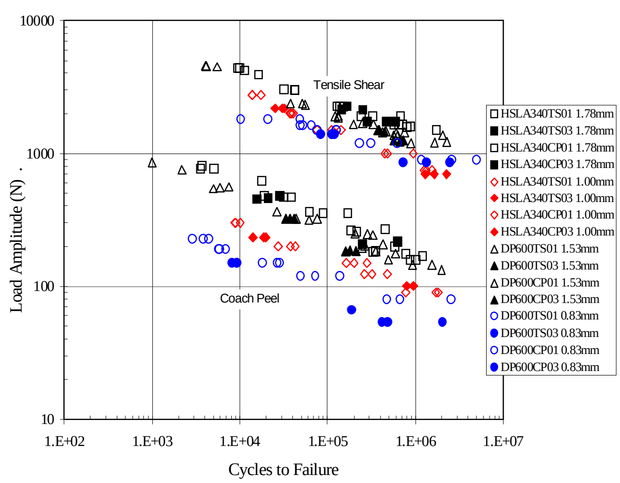

Figure 8. Effect of thickness on fatigue performance.

Results – Fusion Welds

Fatigue testing of specimens containing the fusion weld line within the width of the specimen was conducted to assist the Joining Technology team in identifying the optimum welding parameters for laser- and MIG-welded joints. The dimensions of the specimens are shown in Figure 9a and 9b. The weld location was centered between the edges of the sample and the robot travel was 25 mm total. This produced a weld with a start and a stop within the gage section of each specimen. GMAW welding of the DP 780 AHSS was performed with 70 ksi and 90 ksi filler wires while GMAW welding of the DP 600 AHSS was performed with only 70 ksi filler wire. No filler was used with the laser welds.

The DP 600 results of the fatigue, shown in Figure 10a, indicate no significant difference in performance between the AC, DC or laser-assisted GMAW welding processes. Similarly, the performance of the DP 780 GMAW welds (Figure 10d) was not influenced by either the process type or the strength of the filler material used. Similar observations may be made concerning the laser processing presented in Figure 10b and 10c. The mean stress appears to be an insignificant factor in the fatigue performance of fusion-welded joints. This behavior can be seen in all of the graphs in Figure 10.

Conclusions

Analysis of test results indicates that, for the specimen geometries and steel grades selected for this study, the fatigue performance of a spot weld is independent of the base-metal strength. This finding supports the initial understanding that the melting and resolidifying processes associated with spot welding form new alloys and, thus, making the properties and coating of the material(s) being joined, and the welding parameters, insignificant contributors to fatigue performance.

Similarly, the results clearly indicate that, within either the GMAW- or laser-weld groups, the type of weld does not seem to influence the fatigue performance (e.g., for GMAW it does not matter if the weld is AC, DC, or laser-assisted).

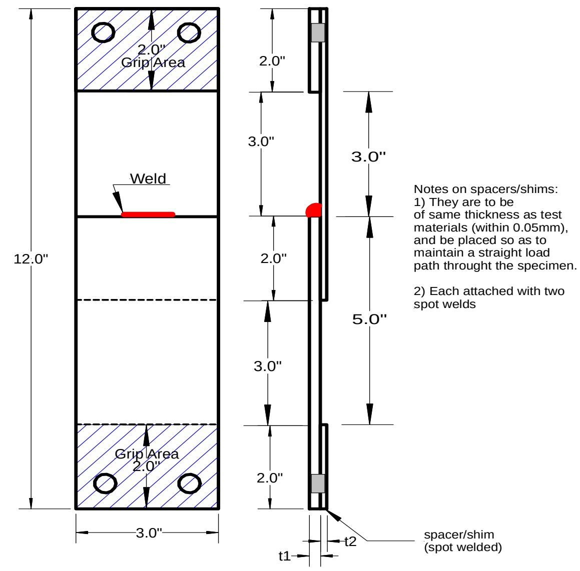

Figure 9a. Schematic of specimens for GMAW. Dimensions in mm.

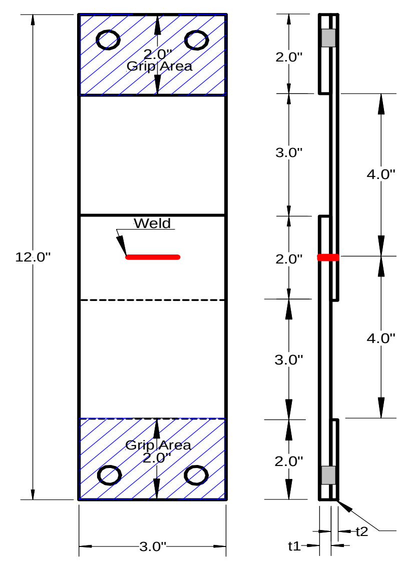

Figure 9b. Schematic of specimens for laser-weld fatigue tests. Dimensions in mm.

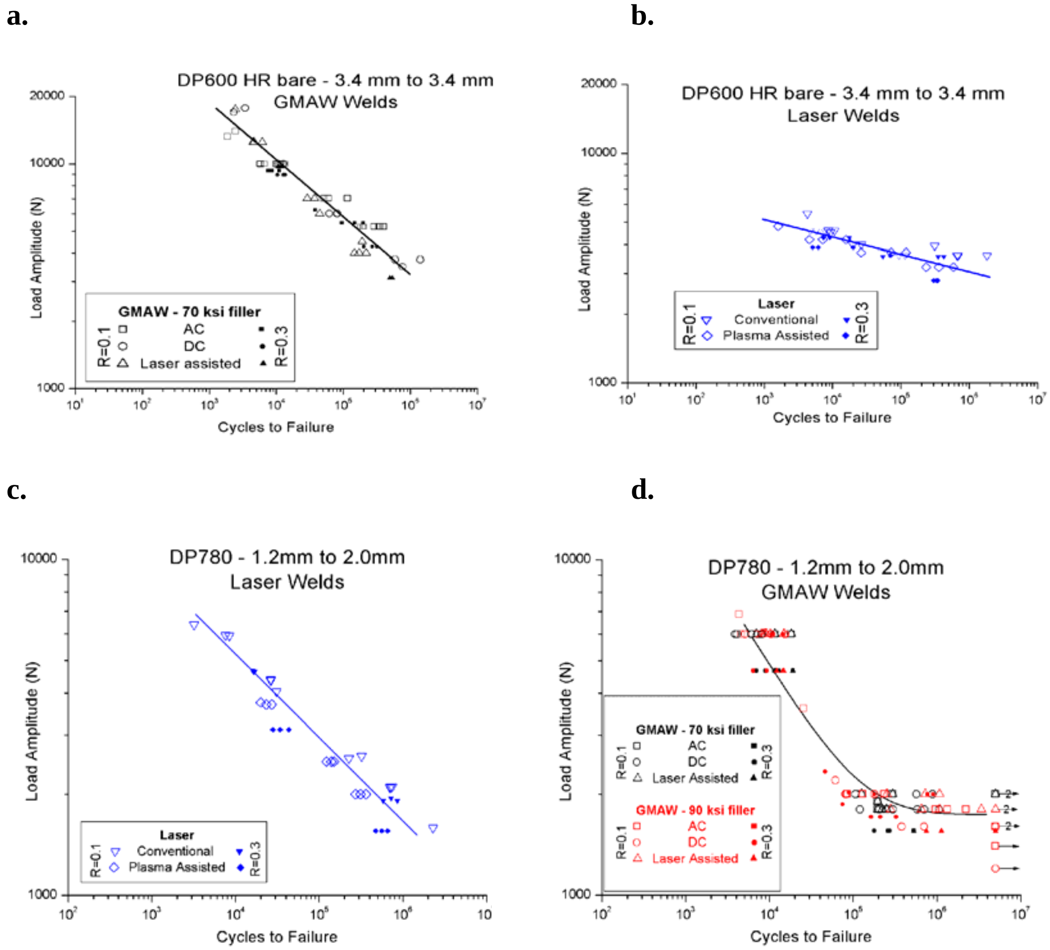

Figure 10. Fatigue-performance evaluation of GMAW and laser welds in two AHSSs: DP 600 hot-rolled, bare, and DP 780 coated. Specimens for DP600 are 3.4 mm to 3.4 mm while the specimens for DP 780 are 1.2 mm to 2.0 mm.

<u>Presentations and Publications</u>

1. "Sheet Steel Fatigue Group", Auto/Steel Partnership Program Review, Department of Energy, September 21, 2005.
2. "A/SP Sheet Steel Fatigue Committee", Joint Policy Board, Feb. 1, 2006.
3. J.J.F. Bonnen, Hari Agrawal, Mark A. Amaya, Raj Mohan Iyengar, HongTae Kang, A. K. Khosrovaneh, Todd M. Link, Hua Chu Shih, Matt Walp, Benda Yan, "Fatigue of Advanced High Strength Steel Spot Welds," 2006, Society of Automotive Engineers, SAE-2006-01-0978, pp. 19. *Republished in 2006 SAE Transactions.*
4. Kang, HongTae, "Evaluation of Spot Weld Fatigue Damage Parameters" 2006, Society of Automotive Engineers, SAE-2006-01-0978, pp. 19. *Republished in 2006 SAE Transactions.*
5. "Spot Welds, MIG Welds and their effect on the fatigue of AHSS steels," Mar. 10, 2006 (A/SP Frame group).
6. "Sheet Steel Fatigue Committee," A-S/P SPARC financial planning review, July 18, 2006.
7. "Spot Welds, MIG Welds and their effect on the fatigue of AHSS steels," Mar. 10, 2006 (Joining group).
8. "Fatigue of MIG Welds" AISI Wheel Task force meeting, Nov 18, 2005.
9. ASP Team Review, Dec. 15, 2005.
10. "Fatigue of AHSS SpotWelds," 2nd Annual Ford AHSS Conference, Oct. 18, 2005.

11. J.J.F. Bonnen and R. Mohan-Iyengar, "Fatigue of Spot Welds in Low-Carbon, High-Strength Low-Alloy, and Advanced High-Strength Steels and Fatigue of Fusion Welds in Advanced High-Strength Steels," 2006 Proceedings of the International Automotive Body Congress (IABC 2006), pp 12, 2006.
12. H.-T. Kang, J. J. F. Bonnen, and R. Mohan Iyengar, "Sources of Variability in the Fatigue Strength of Spot Welded Specimens," Proceedings of Materials Science & Technology Conference, Detroit, September 2007.
13. J. J. F. Bonnen and R. Mohan Iyengar, "Fatigue Performance of Conventional and Advanced High-Strength Steel Spot Welds," presented at the special symposium marking the 20th Anniversary of Auto-Steel Partnership, held as part of the Materials Science & Technology Conference, Detroit, September 2007.

---

[i] Denotes project 160 of the Auto/Steel Partnership (A/SP), the automotive-focus arm of the American Iron and Steel Institute (AISI). See www.a-sp.org. The A/SP co-funds projects with DOE through a Cooperative Agreement between DOE and the United States Automotive Materials Partnership (USAMP), one of the formal consortia of the United States Council for Automotive Research (USCAR), set up by Chrysler, Ford and General Motors (GM) to conduct joint, pre-competitive research and development. See www.uscar.org.

E. Tribology (ASP 230[i])

Project Manager: Pat V. Villano
Auto/Steel Partnership (A/SP)
2000 Town Center Drive, Suite 320
Southfield, Michigan 48075-1123
(248) 945-4780; fax: (248) 356-8511; e-mail: pvillano@a-sp.org

Project Chairman: David J. Meuleman
General Motors Corporation (GM)
Manufacturing Engineering
2000 Centerpointe Parkway
Mail Code 483-520-266
Pontiac, Michigan 48341
(248) 753-5334; fax: (248) 753-4810; e-mail:david.meuleman@gm.com

Technology Area Development Manager: Joseph A. Carpenter
(202) 586-1022; fax: (202) 586-1600; e-mail: joseph.carpenter@ee.doe.gov

Field Project Officer: Aaron D. Yocum
(304) 285-4852; fax (304) 285-4403; e-mail: aaron.yocum@netl.doe.gov

Expert Technical Monitor: Philip S. Sklad
(865) 574-5069; fax: (865) 576-4963; e-mail: skladps@ornl.gov

Contractor: United States Automotive Materials Partnership (USAMP)[i]
Contract No.: DE-FC05-02OR22910 through the National Energy Technology Laboratory

Objectives

- Identify the tribological factors that contribute to successful stamping of advanced high-strength steels (AHSSs). This includes the achievement of consistent, moderate coefficient of friction; minimized tool wear; and minimized galling/die pick-up.
- Identify the changes in the tribological system required by the use of galvanneal verses hot-dip-galvanized (HDG) coatings on AHSSs.
- Update the current A/SP lubricant testing procedure to accommodate the new AHSSs and the lubricants that can be used with them.

Approach

- Examine wear rates of different die materials, die-surface treatments and lubricants with AHSSs.
- Comparison of wear rates with different lubricants and die materials.
- Evaluation of methods of improving die life.
- Optimized lubricants/die combinations for AHSSs.
- Conduct a die-wear test and analysis consisting of seven individual One-Factor-at-a-Time (OFAT) tests totaling 550,000 pieces.
- Die-wear testing to include dual-phase (DP) 980, high-strength low-ally (HSLA), and DP 600 steels.

Accomplishments

- Completed Phase 1 report “Enhanced Stamping Performance of High Strength Steels with Tribology.”
- Completed Phase 2 report “Effect of Stroke Length and Penetration on Die Wear.”
- Completed Phase 3 report “Enhanced Stamping Performance of High Strength Steels with Tribology.”

- Completed Phase 4 Test work “Improve the Life of High Strength Steel Stamping Dies.”
- Completed a Trim Die study to evaluate wear rates with American Iron and Steel Institute (AISI) A2 and AISI S7 when using AHSS and ultra-high-strength steel.

Future Direction

- Develop wear-rate model to predict die life.
- Gather wear test data to substantiate model.
- Correlate model with production data as AHSSs come into production.
- Conduct experiment using five commercially-available, trim-steel/coating combinations to be examined for wear resistance.

Introduction

OFAT Project

Based on Phase 4 test results, a new OFAT project was initiated where a selected number of variables were further tested. These included extended testing (to 100,000 strokes) of the best performing die-material/die-coating combination, testing of DP 780 and DP 980 steels and examination of weight loss in the draw beads as a measure of wear. Extreme wear of trim steels was also observed when trimming the DP 980 steel. An analysis of the data was conducted and we are waiting completion of the final report.

Final Phase 4 Improving the Life of High-Strength Steel Stamping Dies

All testing and analysis work has been completed; however, there is still ongoing work to be done to get the final report finished. The following are the conclusions from the study.

- Restraining force or stress is most influenced by sheet thickness and bead radius.
- Thinning strains confirm the stress factors.
- A significant interaction was found between base steel and thickness: the strain difference between the HSLA and DP 600 increases as sheet thickness increases.
- Wear-volume measurements show both abrasive and adhesive wear. The type of wear was generally related to the type of bead coating.
- In general, adhesion was heaviest with the galvanized sheet while abrasion was heaviest with the galvaneel sheet.
- The effect of wear on restraining force and thinning strain was not directly related to one type of wear, but more on the nature of the worn surface with pick-up generally increasing restraining force.
- Unexpectedly, abrasive wear did not, in many cases, lead to reduced restraining force rather than a restraining-force increase with increased abrasive wear.
- These results appear to be sensitive to bead material with the uncoated AISI D2 steel showing the strongest tendency for increased restraining force with increased abrasive wear.
- The effectiveness of the wax-based, dry-film lubricant (DFL) was less than expected, possibly due to melting.
- Run-in during the initial 4,000 strokes was plotted and shows a significant variation in restraining force during the run-in phase.
- The restraining force with the CrN-coated beads achieved stability much sooner than with the uncoated D2 beads.

The team is struggling over the best way to translate the results and still make the data available to the A/SP membership. Some of the results, however, were presented at the Great Designs in Steel Seminar that was held in March 2007.

Technical Papers for Publication

Six technical papers are being written from past work and are expected to be made available to various trade publications.

---

[i] Denotes project 230 of the Auto/Steel Partnership (A/SP), the automotive-focus arm of the American Iron and Steel Institute (AISI). See www.a-sp.org. The A/SP co-funds projects with DOE through a Cooperative Agreement between DOE and the United States Automotive Materials Partnership (USAMP), one of the formal consortia of the United States Council for Automotive Research (USCAR), set up by Chrysler, Ford and General Motors (GM) to conduct joint, pre-competitive research and development. See www.uscar.org.

F. High-Strength Steel Stamping Project (A/SP 050[i])

Project Manager: Michael S. Bzdok
Auto/Steel Partnership (A/SP)
2000 Town Center, Suite 320
Southfield, Michigan 48075-1123
(248) 945-4778; fax: (248) 356-8511; e-mail: mbzdokl@a-sp.org

Co-chair: James Fekete
General Motors Corporation
Body Manufacturing Engineering
2000 Centerpointe Parkway
Pontiac, Michigan 48341
(248) 753-5324; fax: (248) 753-4810; e-mail: jim.fekete@gm.com

Co-chair: Changqing Du
Chrysler LLC
800 Chrysler Drive
Auburn Hills, Michigan 48326
(248) 576-5197; fax: (248) 576-0230; e-mail: CD4@chrysler.com

Technology Area Development Manager: Joseph A. Carpenter
(202) 586-1022; fax: (202) 586-1600; e-mail: Joseph.Carpenter@ee.doe.gov

Field Project Officer: Aaron D. Yocum
(304) 285-4852; fax (304) 285-4403; e-mail: aaron.yocum@netl.doe.gov

Expert Technical Monitor: Philip S. Sklad
(865) 574-5069; fax: (865) 576-4963; e-mail: skladps@ornl.gov

Contractor: U.S. Automotive Materials Partnership (USAMP)[i]
Contract No.: DE-FC05-95OR22363 through the National Energy Technology Laboratory

Objectives

- Determine how to accurately predict and control the amount of springback and other deviations from the desired stamping geometry for parts made from advanced high strength steel (AHSS) prior to construction of production tooling.
- Develop part-design and manufacturing-process guidelines that can be recommended to automotive design and manufacturing engineers for the purpose of reducing springback and other part distortions.
- Investigate and analyze fractured materials for the purpose of understanding the fracture mechanism in terms of material properties and processing effects.

Approach

The approach of the High-Strength Steel (HSS) Stamping project is to:

- Predict AHSS stamping springback through finite-element analysis (FEA).
- Control AHSS stamping springback by developing knowledge of part-design geometries that affect flange springback and die processes that control springback.

- Develop predictive tools related to fracture in AHSS based upon an investigation and analysis of fractured material property microstructural characterization.

Accomplishments

The significant accomplishments of A/SP AHSS Stamping Group are as follows:

- Modified tooling for stretch-forming processes of AHSS auto-body structural components to neutralize the residual stresses that cause springback and sidewall curl. Predictable results have been shown for high-strength low-alloy (HSLA) 350 and dual-phase (DP) 600 MPa. The tooling was additionally modified for DP 780 MPa and DP 980 MPa. Panel measurements and data analysis have been reported upon. Identified additional processes to control springback, sidewall curl and panel twist.
- Modified panel geometry to show an alternative approach to control springback. Effective use of stiffening beads and other part-shape modifications and use of process variables are being recommended to product designers for control of twist, undercrown and springback based upon case studies of AHSS part developments.
- Utilized Multi-Process Master Shoe Die and Sub-Die inserts that are capable of a variety of part shapes and processes. The master shoe has a high-pressure hydraulic cushion that can be programmed for various process control features. Sub-die inserts for an Underbody Longitudinal Rail, a Cowl Cross Bar and a Body Center Pillar were modified and run in tryout. Completed detailed data analyses and developed part and process conclusions and recommendations based upon the analyses.
- Completed seven case studies of AHSS part developments by working through the original equipment manufacturers (OEMs). Applications guidelines studies were completed on a roof-rail reinforcement, three “B” pillar reinforcements, two “A” pillar reinforcements, and a rear rail.
- Initiated an investigation of shear fracture of AHSS with the Edison Welding Institute (EWI), in cooperation with the Ohio State University, to perform analyses directed at understanding the basic characteristics of fractures at a microstructural level.
- Initiated an investigation, at Wayne State University, of shear fracture in DP and transformation-induced plasticity (TRIP) steels that included: the key material parameters needed to predict fracture; fracture criteria based on these material parameters; and guidelines to develop predictive tools and develop standardized test for predicting failures in sheared edge stretching and breakage on a radius.
- Modified “15-Flange Die” for use in evaluating stretch-flanging capability of DP and other AHSS materials.

Future Direction

Partner companies have observed fractures in parts subjected to stretch flanging or stretching over a die radius. This phenomenon is not currently predictable. For this reason, the project team has solicited, received and evaluated proposals for work in the area of fracture analysis to support future formability analysis in dies. The project work has been awarded to the EWI and has started during the 2007 fiscal year. Focused project work is targeted at delivering:

- Key material parameters needed to predict fracture for the various conditions investigated.
- Fracture criteria based upon those key material parameters.
- Guidelines for development of predictive tools related to fracture.

The 15-Flange Die is to be utilized for further evaluation of stretch-flanging capability of AHSS including:

- Improved evaluation of microstructural effects.
- Include effect of shear-affected zone caused during trimming.
- Optimize process for best edge-stretch ability and maximum tool life.

Die trials with the new Multi-Process Die and programmable hydraulic cushion are continuing. This die is designed as a master die set and pressure system that will accept sub-die inserts to produce a variety of structural parts, such as underbody rails, cross bars and side-structure pillars. Additional, varied stamping processes for draw- or form-die actions can be developed with this tool.

Additional applications guidelines case studies are proposed to be completed at the rate of three per quarter by obtaining one study from each OEM per quarter and contracting additional case-study assistance.

Introduction

AHSS combining high strength and superior formability compared to the traditional HSLA steels are increasingly being used in automotive applications to deliver superior vehicle safety performance, while at the same time provide opportunities for mass reduction. AHSSs have high initial work-hardening rates as well as high tensile strengths. These characteristics, which make the material attractive to design engineers, also create challenges in the stamping and manufacturing processes, especially in terms of dimensional control. Stamped parts exhibit more springback after forming, compared to their lower-strength steel counterparts.

To address these issues, the A/SP initiated enabler projects, focusing on stamping and springback experiments using tools of production components, as well as understanding how best to simulate the forming processes using computer FEA models. To date, various classes of automotive parts have been studied, fabricated from AHSS with tensile strengths varying from 600 to 980 MPa.

Various process-control methods have also been investigated as means to control springback. So far, the method employed for controlling springback involves trial-and-error in the experiments, which is time consuming and costly. The need for accurate computer models for predicting springback is therefore apparent.

FEA has been widely used in the automotive industry for vehicle designs and manufacturing feasibility. Over a period of twenty years, a high level of confidence has been achieved using FEA to predict cracking and wrinkling in metal-forming processes. However, it remains a challenge to accurately predict springback, particularly for those parts with twists and sidewall curls. Numerous studies have been carried out to correlate computer prediction to experimental results. It has been shown that the material models, element formulations, friction and contact algorithms are important parameters affecting simulation accuracy. Other studies have also demonstrated the sensitivity of springback predictions to numerical parameters such as mesh size, number of through-thickness integration points, tooling traveling speed, contact-interface parameters, etc. During the last decade, FEA software developers and users have been investing much effort into the solution of springback-prediction problems. A steady improvement has been seen in the prediction capability and methodology.

In this study, experiments and computer simulations were conducted on an automotive rear rail. Various DP steels were used with tensile strength levels of 600, 780 and 980 MPa. Simulations were carried out using various numerical parameters (mass scaling, adaptive levels and mesh coarsening) in order to study their effects on the prediction accuracy. In the die-tryout experiments, various forming process variables were also investigated including pad forces, blank-hold forces and die configurations (drawing versus crash forming). Experimental results as well as the corresponding FEA simulation results were evaluated.

Discussion

The Project Group has focused on experimenting with a multi-process research die with sub-die inserts (Figure 1) to produce various automotive structural components by a variety of processes. This die has the necessary higher holding pressures and controlled processes required for working the higher-strength materials.

A programmable, hydraulic-pressure cushion is the main component of this system that provides the means of stretch forming the metal and controlling springback.

Sub-die inserts in the multi-process master shoe die enable stamping of underbody, cross-car and body-side structural components with a variety of stamping processes.

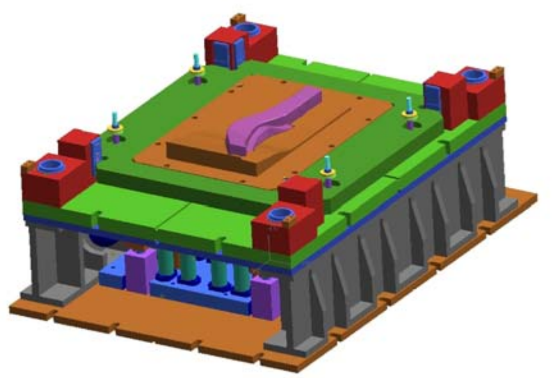

Figure 1. Lower half of multi-process die.

Sub-die inserts in the multi-process master shoe die enable stamping of underbody, cross-car and body-side structural components with a variety of stamping processes.

Rear Longitudinal Rail Sub-Dies

Tryout utilized three different stamping processes: draw action, with part on post or part on binder, and form die with upper pad. Materials included 1.6-mm and 2.2-mm DP 600 MPa steel and 1.6-mm DP 780 MPa and DP 980 MPa steel. Tryout resulted in identification of a forming process that lowered press forces and used material more efficiently (Figure 2). However, part dimensions were still outside acceptable ranges, so efforts with the higher-strength grades to improve the springback control with "shape set" features such as lock steps, added to the forming process.

Figure 2. Rail stampings by three processes.

Cowl Cross Member Sub-Die

A Cowl Cross Member sub-die is also part of the program. This stamping tryout also shows that the higher-strength steels are more easily formed than drawn for some panel configurations (Figure 3).

Figure 3. Cowl cross-bar processes.

The project examined die (forming) processes and material grades for their effect on part quality/dimensional accuracy and press-force/energy requirements.

Overall, the goal was to develop product/process-design guidelines for AHSS. The Cross Cowl Stamping trials covered the following materials: HSLA 350; DP 600; DP 780; and DP 980. The following three stamping configurations were examined: Cushion Draw with 340-mm-wide blank; Crash Form with 340-mm-wide blank; and Crash Form with 280-mm-wide blank.

The goal of the experiment was to form three parts for each material/stamping combination. Following stamping, each test part was scanned, laser trimmed, and re-scanned. Thus, only one set of parts were used for this study. Binder Force (cushion draw) and Pad Force (all forming processes) were established experimentally prior to conducting the trials and all trials were conducted under a single-press set-up.

Overall, satisfactory parts were stamped from all four materials and the three forming processes. Two areas were prone to wrinkles, the top surfaces near each end of the part. It is noted that production parts exhibit this same condition. Splits did occur with DP 980 but they were confined to an area off-part and could have been induced by holes laser cut for locating the blank.

The parts were examined through strain analyses, dimensional analyses (untrimmed and trimmed), and forming-tonnage requirements. Production drawn (toggle) and trimmed parts were included where appropriate comparisons could be constructed. Highlights of the analyses include:

- Surface strains were measured in four areas. Major- and minor-strain levels for DP 780 and DP 980 appear to be more uniform than HSLA 350 and DP 600.
- In the plan view, this part exhibits curvature on one side and is straight on the other side. The side with curvature had more side-wall curl but less opening angle (springback) than the straight side. For the respective side, there was more opening angle in the center, but curl increased towards the ends.
- The majority of springback is material related. Trimming had the second largest effect on overall springback followed by forming process and blank width.
    - The amount of springback increased parabolically with the material strength. For example, DP 980 had three times the springback of DP 600.
    - Trimming caused springback to increase by approximately 30%.
    - Drawing produced about 20% more springback than crash form.
    - Springback increased about 10% with the reduced blank size using the crash-form process.
- A typical increase in forming tonnage due to material grade was less than half the increase in tensile strength.

It is emphasized this part has open ends. Parts with closed ends create an entirely different forming condition and thus many of the aforementioned observations may not hold.

Body-Side Center-Pillar Sub-Die

A sub-die for a body-center pillar has also been completed and modified through tryout to optimize results (Figure 4)**.**

Figure 4. Body-side center pillar.

This part is crucial to the body-side structure for meeting side-impact requirements. It is also typically difficult to stamp in medium-strength grades due to springback, twist and undercrown. The higher-strength grades increased the manufacturing difficulties.

During tryout, several features were added to the part to enable stamping in DP 780 material. Changes were made to the product shape to take up excess metal and features were added to stiffen the part. Split- and fracture-free stampings were then made from both DP 780 and DP 980 material. Parts have been scanned and dimensional analysis has been contracted.

Phase two of the project will complete the dimensional evaluation of both untrimmed and trimmed parts. Using this information and FEA analysis, computer-guided compensation will be used to re-cut the die to achieve dimensional accuracy of the part.

Summary

By recording the results of innovative forming processes, case studies for specific structural parts have been presented, along with product-design and stamping-process guidelines for industry reference, when making product applications of the AHSS materials.

In addition, stamping-press tonnages are being recorded, along with impact loads, press-signature analysis and die-cushion-pressure requirements for the stamping industry's information. This will aid in better understanding the machine and equipment requirements for manufacturing components from this material.

Conclusions

Preliminary conclusions of the information indicate:

- Increases in material strength result in increases in forming-force requirements for typical automotive parts having open ends.
- Binder-force requirements can result in significant increases in forming force at ram positions relatively far from the bottom of the stroke. This effect far outweighs the material-property effects on press-force requirements.
- Active binders also result in significant increases in press-energy requirements. This has the potential to reduce throughput if the time required to recover the energy stored in the press flywheel exceeds the design stroke rate of the part.

Further stamping tryouts of DP 600, DP 780, and DP 980 will be conducted on typical automotive underbody, cross–car and side-structural members with new tooling and multiple processes. These materials, in lighter gauges than currently employed, will assist the weight-reduction and structural-performance goals of the Future Generation Passenger Compartment (see 5.I) and other lightweighting project groups in the A/SP.

Stamping experiments and LS-DYNA simulations were conducted on an AHSS automotive rear rail. The experimentally-obtained springback results were compared with those from the numerical simulation. The following conclusions are obtained:

- Both the experimental and the simulation results showed that the draw-form process produced more springback than the crash-form process; and the amount of springback increased with the material strength.
- The FEA predicted springback match to the experiments was seen to be dependent upon material strength. Reasonably good prediction accuracy was obtained for the DP 600 parts.
- The correlation between the predicted and the experimental results for DP 780 and DP 980 parts is not as good as that for DP 600 (Figure 5). Further study is needed to improve the predictability for higher-strength materials.

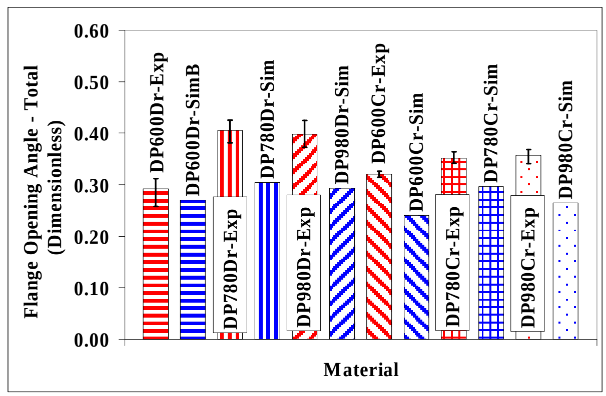

Figure 5. Correlation simulation vs. experimental.

- Increasing mass scaling and reduced adaptive levels will deteriorate the prediction accuracy. Mesh-coarsening prior springback analysis does not greatly affect the prediction results.

Presentations and Publications

1. C. Du, Chrysler LLC; X. M. Chen, United States Steel Corporation; T. Lim, Dofasco Inc., T. Chang, Severstal North America, P. Xiao and S.-D. Liu, Generalety, LLC, "Correlation of FEA Prediction and Experiments on Dual-Phase Steel Automotive Rails." Paper submitted to the Numiform 2007 Conference, Aveiro, Portugal. Paper presented at the MS&T'07 Conference at COBO Center, Detroit, Michigan.
2. James R. Fekete, General Motors Corporation and Stephen K. Kernosky, Ford Motor Company, "Characterization of Press Tonnage

Requirements during Stamping of Dual Phase Steel." Paper published at the 2007 SAE Congress in Detroit, Michigan.

---

[i] Denotes project 050 of the Auto/Steel Partnership (A/SP), the automotive-focus arm of the American Iron and Steel Institute. See www.a-sp.org. The A/SP co-funds projects with DOE through a Cooperative Agreement between DOE and the United States Automotive Materials Partnership (USAMP), one of the formal consortia of the United States Council for Automotive Research (USCAR, www.uscar.org), set up by Chrysler, Ford and General Motors to conduct joint pre-competitive research and development.

G. Strain-Rate Characterization (ASP 190[i])

Project Manager: Pat V. Villano
Auto/Steel Partnership (A/SP)
2000 Town Center Drive, Suite 320
Southfield, Michigan 48075-1123
(248) 945-4780; fax: (248) 356-8511; e-mail: pvillano@a-sp.org

Chairman: Kathy Wang
General Motors Corporation (GM)
2000 Centerpoint Parkway
Pontiac, Michigan 48341
(586)-986-1173; fax: 586-986-8722; e-mail: kathy.wang@gm.com

Lead Scientist: Srdjan Simunovic
Oak Ridge National Laboratory (ORNL)
Oak Ridge, TN 37831-6359
(865) 241-3863; fax: (865) 574-7463; e-mail: simunovics@ornl.gov

Technology Area Development Manager: Joseph A. Carpenter
(202) 586-1022; fax: (202) 586-1600; e-mail: Joseph.Carpenter@ee.doe.gov

Field Project Officer: Aaron D. Yocum
(304) 285-4852; fax: (304) 285-4403; e-mail: aaron.yocum@netl.doe.gov

Expert Technical Monitor: Philip S. Sklad
(865) 574-5069; fax: (865) 576-4963; e-mail: skladps@ornl.gov

---

Contractor: United States Automotive Materials Partnership (USAMP)[i]
Contract No.: DE-FC05-02OR22910 through the National Energy Technology Laboratory

---

Objectives

- Develop new experimental set-ups for characterization of crashworthiness and strain-rate sensitivity of advanced high strength steels (AHSSs) and AHSS structural designs.
- Replicate impact conditions that occur in automotive impact by simpler and more manageable experiments in order to generate meaningful data for computer modeling.

Accomplishments

- Developed experimental set-up procedures for new crashworthiness characterization test based on parallel-plates buckling, a procedure developed at the University of Dayton Research Institute (UDRI).
- Developed and conducted constant-velocity crash experiments on circular and octagonal tubes.
- Developed methods for strain-rate characterization in sub-Hopkinson velocity regime.
- Developed web-based database for display and analysis of impact experiments.

Future Direction

- Develop experiments to characterize fracture properties of advanced AHSS.
- Provide high-quality data for material and finite-element modeling (FEM) development.

Introduction

Crashworthiness characterization of AHSS requires testing of materials and structures under increased strain rates, large plastic strains, and large displacements that are characteristic of actual impact events. The AHSS characterization involves testing at several different length scales. The intrinsic material properties are investigated using the coupon-level specimens where the material is exposed to simple stress states that can be reduced to the equivalent stress and strain measures used in formulation of constitutive models. The coupon tests involve uniaxial tension and compression in plane-stress conditions. High-speed, hydraulic equipment is used to impose constant velocity in order to determine material response to different loading rates. At a higher length scale, the characteristic plastic-hinge mechanism responsible for crash-energy absorption in AHSS structures is investigated using the double-plate test. This test has shown that the strain-rate sensitivity of AHSS in bending under out-of-plane compression exhibit trends that cannot be fully explained using the plate-bending models derived from material behavior under uniaxial plane stress. At the component level, AHSS properties in tubular structures are investigated using specialized hydraulic equipment that allows constant crush speeds up to 8 m/s. In automotive design, the structural integrity of AHSS components is primarily provided by spot welds. The response of spot welds under different loading velocities and loading states have also been characterized in this project.

The above experiments provide high-quality data for development of material and structural FEM models for AHSS and, thereby, enable more accurate modeling and design of lightweight, crashworthy vehicles. The developed experiment technology is also directly relevant to other automotive materials as it provides a systematic approach to characterization and comparison of crashworthiness of new automotive materials.

Design of Experiments

The experiments conducted under this project have been compiled into interactive databases that are accessible over the World Wide Web. The portal page for the experiments is shown in Figure 1.

Figure 1. Web portal for AHSS experiments.

The experiments' data are integrated with the other project components. This provides mechanisms for data analysis and collaboration between project participants.

Strain-Rate Characterization in Sub-Hopkinson Regime

In support of the A/SP Strain Rate Characterization project, ORNL researchers are conducting high-rate experimental tests and analysis of base material specimens in uniaxial tension configuration (see 5.H). The objective of the test program is to provide the necessary experimental data in support of the A/SP efforts to determine high-strain-rate mechanical properties of AHSS. The test program consists of testing tensile specimens under strain rates of quasi-static, 0.1/s 1/s 10/s 100/s and maximum strain rates achievable in full open-loop configuration and the selected gage length. Among the unique features of the current approach is the ability to conduct tests across all speeds on the same apparatus and, thereby, eliminate variability associated with using different testing methods and actuators. The equipment allows for testing at speeds from quasi-static to 700 in/sec (18.5 m/s) over a range of 4 inches (100 mm) at maximum loads of 9000 lbf (40 KN). If an effective gage length for the chosen specimen is known, equipment can run non-linear velocities in the drive file to achieve global strain control (engineering or true strain rate as desired). The test equipment is shown in Figure 2.

Figure 2. High-speed hydraulic tester. The test stage is elevated to allow for actuator acceleration to desired test speed.

The dynamic-testing procedures from recent studies sponsored by the International Iron and Steel Institute [1,2] and published literature [3,4] are followed and further enhanced using the new measurement techniques and synchronization. The multiple measurement methods of both forces and displacements allow for correlation of the results and verification of the method. Schematic representation of the test specimen and the measurement locations are shown in Figure 3.

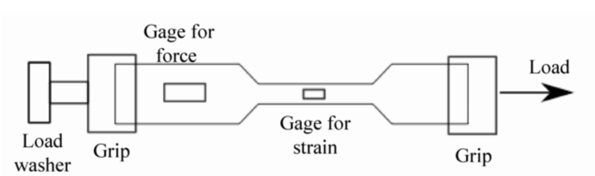

Figure 3. High strain-rate specimen design.

All the measurements are synchronized using the central trigger. High-speed video recording is used to provide detailed record of the test and to correlate optical measurement with the mechanical output data. An output of the program developed for optical measurement is shown in Figure 4. The measurement is based on the variations in color intensity along the prescribed scan lines. The distance between the found gage marks is shown in the images for increasing displacement.

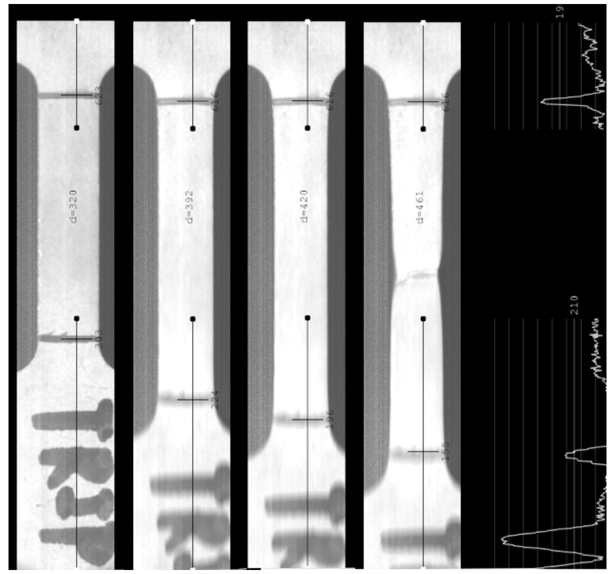

Figure 4. Optical strain-measurement output. Lines connecting black and white dots denote scan lines. Horizontal black lines denote found gage mark based on color intensity (shown on the right).

The multiple measurement methods of both forces and displacements allow for correlation of the results and verification of the method. All the measurements are synchronized using the central trigger. Web-based output for a transformation-induced plasticity (TRIP) 700 MPA specimen for 100/s rate is shown in Figure 5.

Component Crush Experiments

To improve experimental investigations of the material and structural behavior for automotive impact, the ORNL developed a new, integrated, virtual and physical test system for hydraulic, high-force, high-velocity crashworthiness experiments of automotive materials and structures. The system, a test machine for automotive crashworthiness (TMAC), permits controlled, progressive crush experiments at programmable velocity profiles and high force levels. The ability to control displacement (velocity) and the large lateral stiffness of the machine allows for strain history measurements that are not practical in inertia-based equipment. More details about the TMAC system can be found on http://www.ntrc.org. The TMAC system is shown in Figure 6. See also 12.B.

Figure 5. TRIP 700 test at 100 in/sec. Red (more varaiable) and yellow lines denote measurements from load washer and force strain-gage on specimen tab, respectively.

Figure 6. Test machine for automotive crashworthiness.

The component-level characterization of AHSS crashworthiness was examined using tube-crush tests of mild, high-strength low-alloy (HSLA) dual-phase (DP), bake-hardening and transformation-induced plasticity (TRIP) steels of various grades. The tests were run under constant crush velocities, 0.06 m/s, 0.6 m/s and 4 m/s. The crush data consist of time histories of force, displacement, strain measured in tube axial and hoop directions, and high-speed movies. Strain gages were positioned in regions where plastic folds form in order to investigate histories of strains and strain rates during crush in this crush-controlling region. An example of comparative effect of impact speed on the structural level of a spot-welded octagonal tube, representative of the latest vehicle front-end design, is shown in Figure 7.

Data from different sources are synchronized so that they can be used for detailed analysis of the crush progression. A synchronized frame with combined data from high-speed movie, impact force sensors and strain gages on the tube for a circular tube crush, is shown in Figure 8.

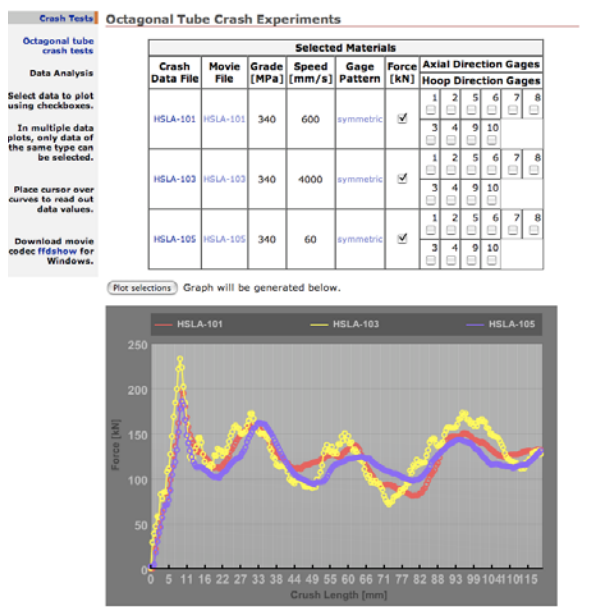

Figure 7. Force comparison for HSLA tubes for 0.06, 0.6 and 4 m/s crush. The data are selected from the Web database. Blue, red, and yellow lines denote crush tests at 0.06, 0.6 and 4m/s crush velocities, respectively.

Spot-Weld Experiments

Spot-welding is the principal method of joining steel sheets in today's automobiles. The spot welding of AHSS provides new challenges as it faces designers with new materials that draw their performance from tightly-controlled microstructure that inevitably changes under thermo-mechanical effects of welding. In addition, the stronger materials usually stiffen the joint regions so that forces and shocks are more intensive than in conventional, mild-steel designs.

In order to investigate behavior of AHSS welds under impact loading and to provide data for the modeling project on AHSS spot welds, static and dynamic strength tests were performed for spot-welded specimens made of DP 780 and drawing-quality special-killed (DQSK) mild steels at the University of South Carolina. Lap-shear (LS) and cross-tension (CT) as well as a newly-designed, mixed-mode specimen were tested using a MTS hydraulic universal testing machine for static and drop-weight tower for dynamic tests. Three weld nugget sizes for each steel and specimen geometry (LS and CT) were made. In the mixed-mode test, only DP 780 of one weld size was tested. Load and displacement as functions of time and failure mode of the spot welds were recorded in the tests. The three nugget sizes were selected such that one is smaller, one is equal (medium) and one is larger than the weld nugget size determined from the formula, $d = 5\sqrt{t}$, where d is the diameter of the weld nugget and t the thickness of the sheet. In addition, a newly-designed, mixed-mode specimen and fixture were also tested which was made of DP 780 with weld nugget size of 5.9 mm, i.e., the large size. Force-versus-displacement curves were generated and the failure mode of each specimen was recorded from the tests. The test data are used in developing a dynamic-failure criterion of spot welds made of AHSS. The experimental data are collected into the project Web-based database. The front page for test selection for analysis is shown in Figure 9.

Data for various impact tests are shown in Figure 10. The implemented data-fitting options allow for reduction of test artifacts and comparison.

The test data show that: 1) the peak load (or the strength) increases with weld nugget size; 2) as the nugget diameter decreases, the specimens are more prone to interfacial mode of failure; 3) the peak load for LS specimen is higher than that for CT specimen under the same test conditions and weld configuration. It is observed that in mixed-mode tests when the loading angle is 90°, most specimens had the pull-out mode of failure while the interfacial-failure mode prevailed in the other two loading angles (0°, 30°).

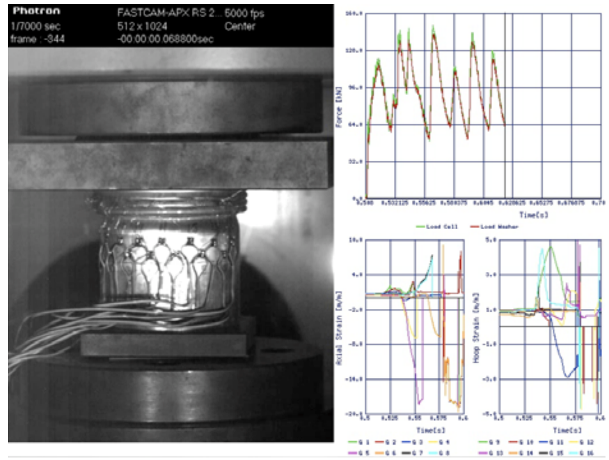

Figure 8. Synchronized data from crash test. Top graph shows force time history. Lower left and right graphs display strain-gage data in axial and hoop directions, respectively.

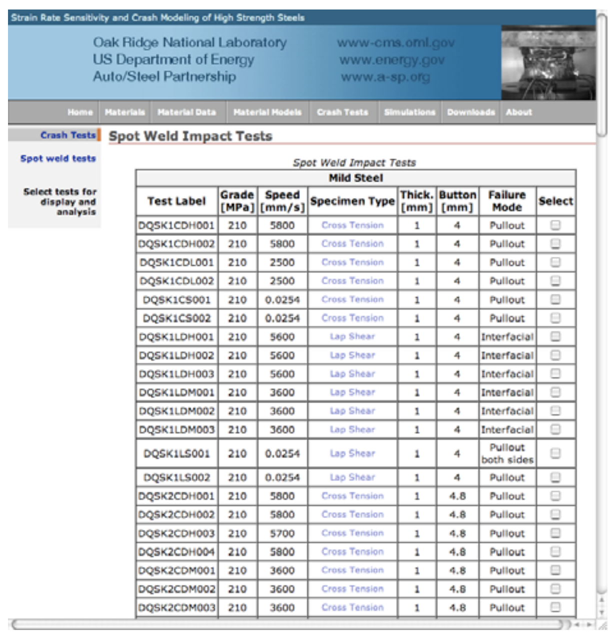

Spot Weld Impact Tests

Mild Steel

Test Label	Grade [MPa]	Speed [mm/s]	Specimen Type	Thick. [mm]	Button [mm]	Failure Mode	Select
DQSK1CDH001	210	5800	Cross Tension	1	4	Pullout	
DQSK1CDH002	210	5800	Cross Tension	1	4	Pullout	
DQSK1CDL001	210	2500	Cross Tension	1	4	Pullout	
DQSK1CDL002	210	2500	Cross Tension	1	4	Pullout	
DQSK1CS001	210	0.0254	Cross Tension	1	4	Pullout	
DQSK1CS002	210	0.0254	Cross Tension	1	4	Pullout	
DQSK1LDH001	210	5600	Lap Shear	1	4	Interfacial	
DQSK1LDH002	210	5600	Lap Shear	1	4	Interfacial	
DQSK1LDH003	210	5600	Lap Shear	1	4	Interfacial	
DQSK1LDM001	210	3600	Lap Shear	1	4	Interfacial	
DQSK1LDM002	210	3600	Lap Shear	1	4	Interfacial	
DQSK1LDM003	210	3600	Lap Shear	1	4	Interfacial	
DQSK1LS001	210	0.0254	Lap Shear	1	4	Pullout both sides	
DQSK1LS002	210	0.0254	Lap Shear	1	4	Pullout	
DQSK2CDH001	210	5800	Cross Tension	1	4.8	Pullout	
DQSK2CDH002	210	5800	Cross Tension	1	4.8	Pullout	
DQSK2CDH003	210	5700	Cross Tension	1	4.8	Pullout	
DQSK2CDH004	210	5800	Cross Tension	1	4.8	Pullout	
DQSK2CDM001	210	3600	Cross Tension	1	4.8	Pullout	
DQSK2CDM002	210	3600	Cross Tension	1	4.8	Pullout	
DQSK2CDM003	210	3600	Cross Tension	1	4.8	Pullout	

Figure 9. Spot-weld test database interface. The basic information for each test is shown in a table form and can be selected for further analysis.

Selected Materials								
Data File	Grade [MPa]	Speed [mm/s]	Test Type	Thck. [mm]	Btn. [mm]	Failure mode	Force [N]	Linear Fit Tolerance [N]
DP1CDH001	780	5700	Cross Tension	1.15	4.3	Interfacial	☐	Tol 100 ☐
DP1CDH002	780	5800	Cross Tension	1.15	4.3	Pullout	☑	Tol 1500 ☑
DP1CDM001	780	3500	Cross Tension	1.15	4.3	Interfacial	☐	Tol 100 ☐
DP1CS001	780	0.0254	Cross Tension	1.15	4.3	Interfacial	☑	Tol 100 ☐

Plot selections Graph will be generated below.

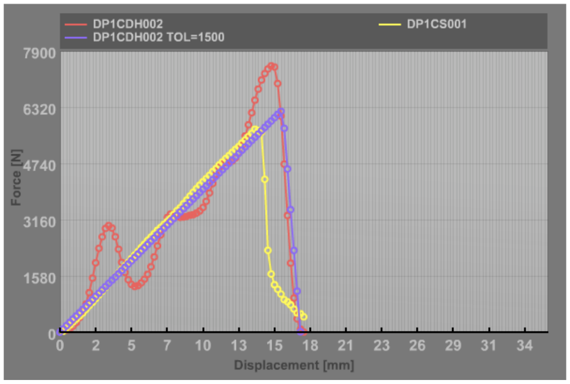

Figure 10. Force-displacement results for CT experiment. Yellow and red (more variable) curves denote tests at quasi-static and 5.7 m/s tests, respectively. Blue line denotes filtered data at high speed.

Conclusions

Several methods for characterization of AHSS crashworthiness have been developed. The material response at different length scales and under different deformation modes was investigated. The developed methods allow for accurate evaluation of crashworthiness properties, determination of material parameters to be used in computational modeling and design, and for development of modeling guidelines for AHSS materials and structures under impact loads.

Future Work

The future work on the project will focus on two topics:

1. Completing of base-material characterization tests.
2. Development of new coupon-level, crash-characterization experiments for AHSS fracture under impact.

Acknowledgements

Support from the Auto/Steel Partnership Strain Rate Characterization Team is acknowledged.

References

1. Recommendations for Dynamic Tensile Testing of Sheet Steels, International Iron and Steel Institute, 2005.
2. C. Wong, IISI-AutoCo Round-Robin Dynamic Tensile Testing Project, International Iron and Steel Institute, 2005.
3. D. Matlock, J. Speer, Constitutive Behavior of High Strength Multiphase Sheet Steels Under High Strain Rate Deformation, AISI/DOE Technology Roadmap Program, Report TRP 9904, 2005.
4. D.M. Bruce, "Dynamic Tensile Testing of Sheet Steels and Influence of Strain Rate on Strengthening Mechanisms in Sheet Steels", Ph.D. Thesis # MT-SRC-003-018, Colorado School of Mines, 2003.

---

[i] Denotes project 190 of the Auto/Steel Partnership (A/SP), the automotive-focus arm of the American Iron and Steel Institute (AISI). See www.a-sp.org. The A/SP co-funds projects with DOE through a Cooperative Agreement between DOE and the United States Automotive Materials Partnership (USAMP), one of the formal consortia of the United States Council for Automotive Research (USCAR, www.uscar.org.) set up by Chrysler, Ford and General Motors (GM) to conduct joint, pre-competitive research and development.

H. High Strain-Rate Deformation of Steel Structures

Principal Investigator: Srdjan Simunovic
Oak Ridge National Laboratory (ORNL)
P.O. Box 2008, MS6164
Oak Ridge, TN 37831-6164
(865) 241-3863; fax: (865) 241-0381; e-mail: simunovics@ornl.gov

Technology Area Development Manager: Joseph A. Carpenter
(202) 586-1022; fax: (202) 586-1600; e-mail: joseph.carpenter@ee.doe.gov

Expert Technical Monitor: Philip S. Sklad
(865) 574-5069; fax: (865) 576-4963; e-mail: skladps@ornl.gov

Contractor: ORNL
Contract No.: DE-AC05-00OR22725

Objective

- The objective of the project is to develop numerical-modeling guidelines in order to realistically assess the influence that the properties of strain-rate-dependent materials exert in crashworthiness computations. The dynamic-loading problems are modeled using diverse combinations of modeling approaches (sub-models) that are essential in describing strain-rate sensitivity in computational simulations. Sub-models examined include finite-element method (FEM) formulations, constitutive materials models, material properties under different strain-rates and loading conditions, contact conditions, etc, as well as material-property changes caused by component processing.

Accomplishments

- Investigated effects of stress transients for high-strength steel (HSS) and their effects on peak impact force.
- Developed experimental set-up for new crashworthiness characterization test based on parallel-plates buckling.
- Developed program for analysis of history of strain-rate calculations.
- Analyzed history of strain rates in unsymmetric crushing.
- Determined modeling effects on strain-rate history in unsymmetric crushing.
- Developed new constitutive models for HSS to account for strain-rate history and transients.
- Investigated forming and welding effects on steel tube crashworthiness.
- Developed model for tube roll-forming and validated it against manufacturing process.
- Developed modeling guidelines for modeling of tubular crush sections.

Future Direction

- Finding optimal formulations and approaches for modeling of spot-welded, polygonal advanced high-strength steel (AHSS) tubes.
- Development of models and experiments for damage and fracture of HSS in crash.

Introduction

The objective of the project is to develop numerical modeling guidelines for strain-rate-dependent materials in crashworthiness computations. The scope of the project is to study specific structural problems in automotive impact, develop new experimental and analytical techniques for characterization of strain-rate sensitivity of HSS and modeling of complex strain and strain-rate histories. The dynamic-loading problems are modeled using diverse combinations of modeling approaches (sub-models) that are essential in describing strain-rate sensitivity in computational simulations. Sub-models to be examined include finite-element formulations, constitutive materials models, contact conditions, etc. The trends, influences, and direct effects of employed modeling techniques will be identified and documented. The relative significance of employed sub-models is established, particularly in relation to the strain-rate effect resulting from the material constitutive models.

The research project is conducted as a team effort between the ORNL and the Auto/Steel Partnership Strain-rate Characterization Group (see 5.G). Recent results have been presented at the 2007 SAE World Congress and 2007 MS&T Conference.

Development of Crash Modeling Guidelines

Automotive structural components are primarily constructed of sheet metal. Under impact deformation, these components deform by formation of localized plastic zones that are responsible for dissipation of impact energy and containment of the deformation within the crash zones. The modeling of localized deformation and the response of metals under multiaxial states of stress and varying strain-rates are still far from being described by a unified theory. During multi-axial, large, plastic deformation, material undergoes significant changes of microstructure and texture that lead to changes in material properties on the macroscopic level. From a practical standpoint, the goal is that the selected material model is applicable to the range of loading and deformation for the problem at hand. In tubular crush devices that are used as energy absorbers in vehicles, metallic sheets are subjected to large, localized deformations that organize into global-collapse mechanisms. The standard practice for extracting strain-rate-relevant material parameters is to perform experiments with uniaxial-loading configurations. The ductility of uniaxial-tensile-loaded specimens is limited by the geometric instability. For automotive steel sheets, the magnitude of uniform plastic strains is limited to about 20%. However, the strains that are measured and modeled during tube crushing far exceed this limit. The physical reality of large deformations is not in question. The biaxial loading and bending provides additional stability that allows the utilization of a material's strain hardening, ductility and correspondingly large energy dissipation. The magnitude and distribution of plastic strains, large curvatures, and shifting of the neutral axis during fold formation clearly places the problem into the realm of large deformations.

Modeling of localized plastic deformation, plastic folds, is the area where material models and finite-element formulations are intrinsically linked. When shell elements are used to model tube crush, the issue of finite-element resolution comes down to the number and type of bi-linear shell elements that are used for modeling of a plastic fold. The experimentally-measured curvature of full plastic folds is of the order of the material thickness. For the fold representation to be accurate, the element length should approach the shell thickness. It is at this point that the assumptions of the standard shell theory are stretched beyond their limits and material models extrapolate far outside the experimentally-verified range. On the other end of the spectrum, when the finite-element resolution is fairly coarse (of the order of kinematic elements in analytical models), the material model extrapolation into large strains is not a concern because the strains get smeared over larger volumes and are within the range of uniaxial experimental data. However, the kinematics of the deformation are not met.

In both of the above FEM-meshing scenarios, in order to match the experimental results with models, material model parameters are commonly modified in engineering simulations. While the practice may be appalling to material scientists, the justification for modification in one case is to compensate for the inability to represent local deformations and, in the other, to account for the significance of the large-strain region for which experimental data are not available. The flexibility of computer programs now even provides methods for definition of optimization problems where the material parameters are determined so that they result in the optimal match between simulations and experiments for crush measures such as impact-force history and deceleration. These approaches are linked to specific structural problems, FEM-mesh configurations and loading situations. A more rigorous approach is to make sure that the FEM element resolution and element formulations are sufficient for accurate kinematic representation of the problem and then focus on compatible material modeling approaches.

Impact Simulations

The current research develops modeling guidelines in combination with a detailed experimental program. The experiments and accompanying simulations are conducted at different length scales (coupon level, plastic-fold formation, progressive tube crush) in order to investigate different mechanisms and their collaborative effect. At the highest length scale, tubular specimens are progressively crushed in the specialized, velocity-controlled, high-speed, hydraulic, Test Machine for Automotive Crashworthiness (TMAC) at ORNL. The tests are performed on different AHSS materials and simulated using different modeling approaches and formulations. (See also 12.B.)

Figure 1 shows the comparison of a computer simulation with a crush experiment. The simulation employs a combination of strain-rate constitutive model derived from uniaxial-loading experiments and shell-element discretization of characteristic dimension proportional to two sheet thicknesses. The overlap of simulation and TMAC progressive crush is very close. The current combination of model formulations gives the best correlation with the experiments for other crush conditions as well. The detailed discretization is necessary to match the experimentally-observed deformation features and measured strain and strain-rate history across the plastic folds.

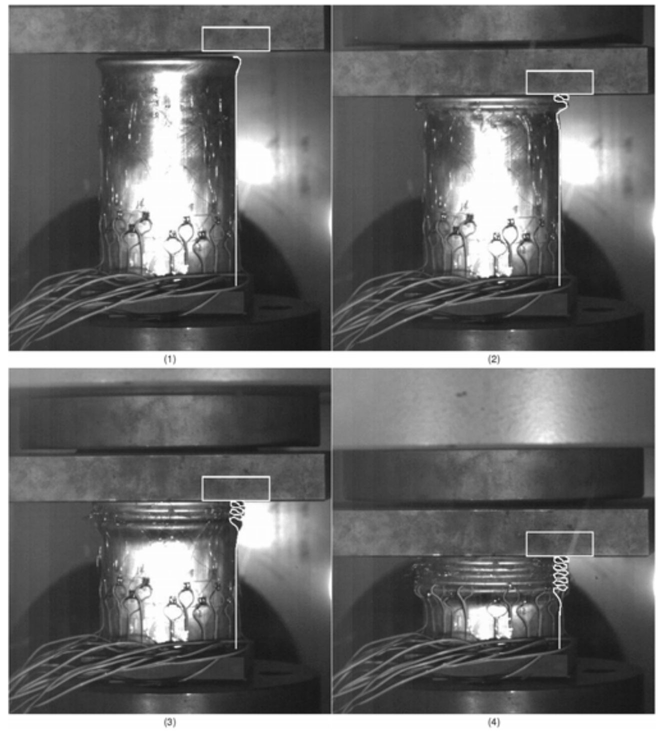

Figure 1. Comparison of experiment and simulation (white line) for 0.6 m/s crush of High-Strength Low-Alloy steel.

The comparison of simulated and measured impact force is shown in Figure 2. The discrepancy in the later part of the simulation is due to engagement of deceleration devices used to slow down the loading actuator.

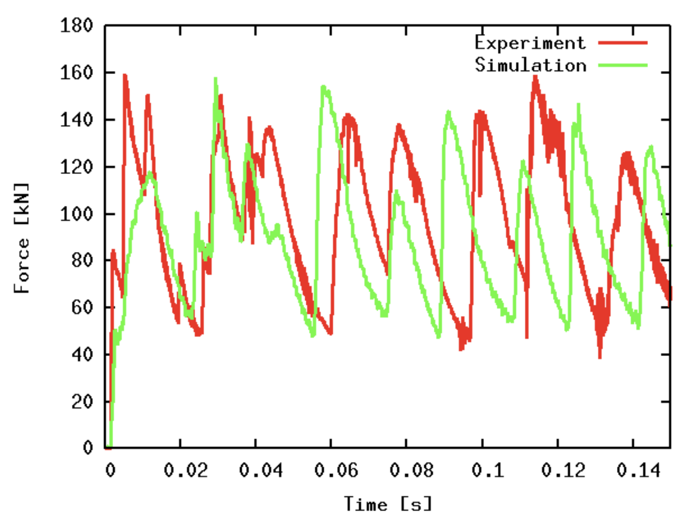

Figure 2. Comparison of simulation and experimentally-observed impact force.

Element formulation also has a significant effect on simulation accuracy. For a selected shell-element discretization, a combination of material model and shell-element formulations is sought that gives a stable folding pattern representative of the experiment. To determine this combination, we simulate the circular tube impact first as a fully-axisymmetric problem using a narrow, 1-element-wide strip with circular-symmetry boundary condition. At this level, all shell-element formulations have equally accurate performance as the problem involves decoupled bending and in-plane components. This can be seen in Figure 3 where shell-element simulations using different formulations lined up.

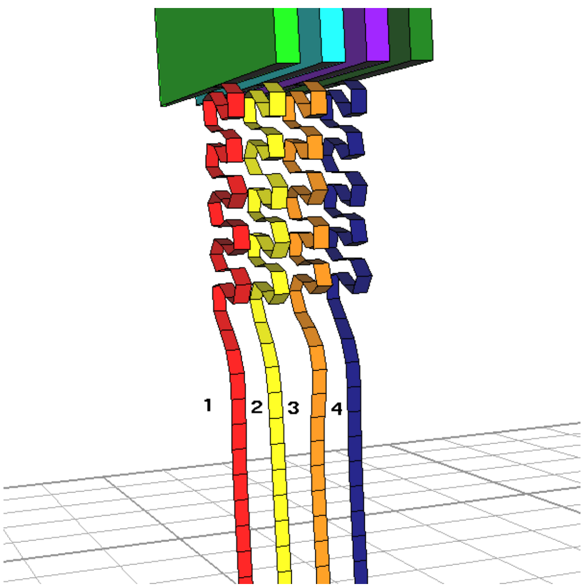

Figure 3. Results of axisymmetric problems using different shell formulations. The labels will be described in Figure 4.

As we increase the angle of the circular segment simulated, i.e., by attaching additional strips in the circumferential direction, we want to see if simulations with different shell-element formulations will remain axisymmetric as in experiments. As shown in Figure 4, only the formulation based on Bath-Dvorkin theory and on material model based on total strain-rate formulation (4) yields an axisymmetric mode as observed in experiments.

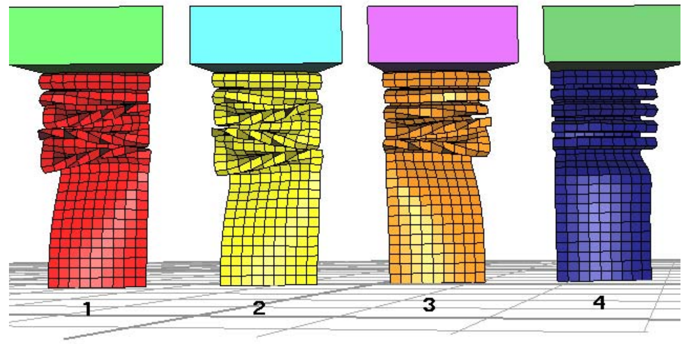

Figure 4. Shell-formulation stability analysis: 1) Belytshcko-Tsay shell formulation, strain-rate effect based on total strain-rate; 2) Belytshcko-Tsay shell, strain-rate effect based on plastic strain-rate; 3) Bathe-Dvorkin shell, strain-rate effect based on total strain-rate; 4) Bathe-Dvorkin shell, strain-rate effect based on plastic strain-rate.

Conclusions

An improvement in predictive capability of the crashworthiness models is linked to development of realistic material models and finite elements with better representation of complex strain and stress states in progressive crushing. Strain-rate sensitivity is an important component of the material models and needs to be incorporated in the crashworthiness models. The range of strains and strain rates calculated in the explicit FEM programs is of the order of 10 +3 /s, which provides a reasonable upper limit for the model. Strain-rate magnitudes of the order of 10 +2 /s are prevalent for shell-element sizes that are of the order of 2-4 tube shell thicknesses. The plastic rate for material modeling provides more realistically-feasible strain-rate histories. For modeling details of tube crushing, the FEM mesh discretization should be fine enough, as measured by the strain distribution, angle of shell directors, and resulting curvature, to model the crush fold formation. Simulation results indicate a close link between the strain-rate calculations and element type and discretization. Current technology can provide reasonable accuracy but at relatively high computational and technical cost due primarily to fine discretization. New, shell-element formulations are needed to model localized deformation at relatively high resolutions and improve modeling accuracy.

Future Work

The future work on the project will focus on two topics:

1. Finding optimal formulations and approaches for modeling of spot-welded polygonal AHSS tubes.
2. Development of models and experiments for damage and fracture of HSS in crash.

Acknowledgements

The research was performed at ORNL which is managed by UT-Battelle, LLC for the U.S. Department of Energy under contract DE-AC05-00OR22725. The tubes for the TMAC experiments were donated by the US Steel Corporation. The support of Auto/Steel Partnership Strain-Rate Characterization Team is acknowledged.

Presentations/Publications/Patents

1. S. Simunovic, J. M. Starbuck, P. V. K. Nukala; Characterization of strain and strain-rate histories in steel structures during impact; 2007 SAE World Congress, Detroit, 2007.
2. S. Simunovic, J. M. Starbuck, K. Wang, P. V. K. Nukala; Characterization of strain and strain-rate histories in HSS structures during progressive crush; MS&T Conference, Detroit, 2007.

I. Future Generation Passenger Compartment – Validation (ASP 241[i])

Project Manager: Pat J. Villano
Auto/Steel Partnership (A/SP)
2000 Town Center Drive, Suite 320
Southfield, Michigan 48075-1123
(248) 945-4780; fax: (248) 356-8511; e-mail: pvillano@a-sp.org

Co-Chairman: Joe Polewarczyk
General Motors Corporation (GM)
Body Systems & Closures
Engineering West
Mail Code 480-11-P64 Cube C1-1642
30200 Mound Road
Warren, Michigan 48092-2025
(586) 986-2157; fax: (586) 986-8592; e-mail: joseph.m.polewarczyk@gm.com

Co-Chairman: Jody R. Shaw
Manager, Automotive Marketing
United States Steel Corporation
5850 New King Court
Troy, Michigan 48098-2608
(248) 267-2608; fax: (248) 267-2581; e-mail: jrshaw@uss.com

Technology Area Development Manager: Joseph A. Carpenter
(202) 586-1022; fax: (202) 586-1600; e-mail: joseph.carpenter@ee.doe.gov

Field Project Officer: Aaron D. Yocum
(304) 285-4852; fax: (304) 285-4403; e-mail: aaron.yocum@netl.doe.gov

Expert Technical Monitor: Philip S. Sklad
(865) 574-5069; fax: (865) 576-4963; e-mail: skladps@ornl.gov

---

Contractor: United States Automotive Materials Partnership (USAMP)[i]
Contract No.: DE-FC05-02OR22910 through the National Energy Technology Laboratory

---

Objective

- Validate the greater-than-25% mass reduction demonstrated by Phase of 1 of the Future Generation Passenger Compartment (FGPC) project on a high-volume production vehicle while maintaining all.

Approach

The project is separated into five (5) phases:

- Phase 1 - Concept development,
- Phase 2a - Validation on a donated vehicle,
- Phase 2b – Development of advanced steels,
- Phase 2c – Concept development of large truck cab comprehending 2.5x roof-strength criteria,
- Phase 2d – Comprehend opportunities and influence of mass-compounding.

Accomplishments

Phase 1: Concept development

- On a concept vehicle, mass reduction of 30% has been achieved relative to current production vehicles while meeting all performance objectives.
- Robust solutions to a range of vehicle weights and bumper-height Insurance Institute for Highway Safety (IIHS) side impact are possible.
- Packaging of fuel-cell components is feasible within the constraints for the donor concept vehicle and can be designed for all structural criteria at equivalent structural mass of conventional powertrains.
- On small vehicles with B-pillars, the IIHS Side Impact and Side Pole Test performance criteria control the design, not the 2.5x roof-strength criteria. Large vehicles (sport-utility vehicles [SUVs] and trucks) will have more structure controlled by the 2.5x roof-strength criteria and the solution demonstrated in Phase 1 may not apply.
- Material properties that exceed the current advanced high-strength steel (AHSS) grades available can increase mass reduction of the passenger compartment from 30 percent to 36 to 38 percent.
- Mass-compounding effects have significant influence on the passenger-compartment structural mass.

Phase 2a: Validation of donor vehicle.

- Donor-vehicle model received and modified to apply results from Phase 1.
- Confirmations of the model and target settings were completed.
- Load-path optimization completed.
- Shape, gauge, and material optimization completed.
- Door shape and gauge completed.
- Mass-compounding effects have been quantified for modern vehicles and predict steel structures can achieve 50% FreedomCAR mass targets when all vehicle systems are resized accordingly.

Phase 2b: Development of advanced steels.
A separate project has been set up for the development of 3rd Generation AHSSs (ASP 280; see 5.A).
Eight research grants have been initiated at nine universities starting in the fall 2007.

Phase 2c: Concept development of a large truck cab comprehending 2.5x roof-strength criteria.
Study showed a hybrid solution of AHSS and composite reinforcements provided the most efficient solution.

Phase 2d: Comprehend opportunities for mass compounding:
Mass compounding effects have a significant influence on the passenger-compartment structural mass.

Future Direction

- Complete Phase 2a - Validation on a donated vehicle.
- Complete Phase 2b – Development of advanced steels.
- Complete Phase 2c – Validate Phase 1 results and correlate to the model that was developed.

Introduction

The FGPC project will incorporate current propulsion systems and fuel-cell technologies into concept architectures. This project will reduce passenger compartment mass by 25% or greater with cost parity relative to the FreedomCAR baseline while meeting the structural crash performance objectives for the IIHS side impact, anticipated future crash requirements for the Federal Motor Vehicle Safety Standard (FMVSS) pole-side impact test and FMVSS 2.5x vehicle weight roof-strength test. Further, it will maintain performance in static and dynamic stiffness, durability and front- and rear-crash requirements and also comprehend packaging requirements for fuel cell powertrain. The study will address a 5-passenger, 4-door, sedan, donor-vehicle design and finally identify opportunities for steel properties that exceed the capability of existing automotive steel grades to improve lightweighting potential. The project is separated into five (5) phases: Phase 1 – Concept development; Phase 2a – Validation on a donated vehicle; Phase 2b – Development of advanced steels; Phase 2c – Concept development of large truck cab comprehending 2.5x roof-strength criteria; and Phase 2d – Comprehend opportunities and influence of mass-compounding;

Project Status

Phase 2a – FGPC Validation

A current production donor vehicle has been selected and work initiated in February 2007. The project has completed Task 1, which establishes performance baseline for the donor vehicle and sets performance targets for the project. Task 2, part 1 has also been completed. Initial investigations indicate that critical load paths identified in Phase 1 will be applicable to the Phase 2a donor vehicle. Task 2, part 2, shape optimization is progressing.

Phase 2b – Development of 3rd Generation AHSS

Work carried out under Phase 1 demonstrated the need for a new family of steels so additional mass savings could be realized. Following the National Science Foundation (NSF) processes, NSF, DOE and A/SP have jointly funded basic steel research to provide experimental and a theoretical foundation to develop 3rd Generation AHSS steels to further reduce vehicle mass. Eight (8) universities have been funded for three years to carry out the research work. (See 5.A.)

Phase 2c – Mass-Efficient Architecture for Roof Strength (MEARS)

Passenger-compartment concepts for large vehicles (trucks and SUVs), where structure is controlled by 2.5x roof strength, were completed in 2007. The project focused on three different concepts: stamping-intensive, termed Concept-1; hydroforming intensive, termed Concept-2; and stamped-with-structural-insert-intensive, termed Concept-3. These were developed in this study, with all three concepts using AHSSs. Extensive optimization was carried out for each concept using HEEDS software.

In the stamping-intensive design (Concept 1), structural changes including panel geometry, part thickness, and material grades were proposed. The major reinforcements in the A-Pillar, roof rail, and C-Pillar were proposed to be made from hot-stamped boron steel. The inner parts of these sections were proposed to be of dual-phase (DP) 600 and DP 800 steels. The body-side outer material was not changed, but its thickness was increased. The most mass-efficient design from several concepts was optimized as a final design for Concept 1.

In the hydroforming-intensive design (Concept 2), the reinforcements in the A-Pillar, roof rail, and C-Pillar were replaced with hydroformed tubes made from DP 780. Tubes were also investigated for the roof header and roof bow. A total of four concepts were proposed with different tube configurations, the most mass-efficient design being optimized to obtain the final design for Concept 2.

In the stamped configuration with structural inserts design (Concept 3), the thickness of major load-carrying members was reduced in the baseline model while materials were upgraded to AHSS to make the structure lighter and to take advantage of the stiffness provided by the lighter inserts. A total of four concepts were proposed with different types of inserts (i.e., Steel-Concepts 3A and 3B, Nylon-Concept 3B, and Beta Foam-Concept 3C). Optimization was not carried out for these basic-concept levels.

A comparative study of all concepts was done from the perspective of mass, cost, manufacturability, and repairability. The concept with the nylon inserts was selected as the final design. Further studies were carried out on the design to optimize the size of nylon inserts and the design of the sheet-metal parts. Formability studies were carried out on the major structural parts to ensure that there were no major issues.

Phase 2 has been approved and will focus on improving the modeling of the nylon inserts, adhesive materials, and validating the predictions with physical testing to validate the models performance.

Phase 2d – Quantification of Mass Compounding
Vehicle design engineers intuitively know that an unplanned mass increase in a component during vehicle design has a ripple effect throughout the vehicle: other components need to be resized increasing vehicle mass even more. The phrase *mass begets mass* describes this phenomenon. A more encouraging view of this behavior considers a reduction in the mass of a component enabled by new technology resulting in a greater mass-reduction ripple effect throughout the vehicle. Published data on this effect are sparse and based on 1975-1981 model years. The purpose of the project was to update the data using contemporary vehicles.

The secondary mass change is the additional mass reduction resulting from primary mass reduction by the implementation of mass-reduction technology. When all subsystems can be resized, the secondary mass savings are from 0.8 to 1.5 kg/kg (1.25 kg/kg is the estimate for the *all* vehicle group). When the powertrain has been fixed and is not available for resizing, the secondary mass savings is from 0.4 to 0.5 kg/kg (0.5 kg/kg is the estimate for the all vehicle group).

The initial study is complete for sedans and SUVs, with a deliverable of a report and a calculator for estimating secondary mass savings.

Conclusions

Phase 1 – FGPC
The optimization methods applied to this study achieved an 11% mass reduction of the modified parts of the body-in-white (BIW) and Door Impact Beams (Table 1), and 30% mass savings over a conventional in-class vehicle's BIW and instrument panel (IP) beam (Table 2. Table 3 is a comparison of an industry-standard vehicle's safety cage to FGPC, which shows a 31% mass reduction.

Phase 2a
There are no conclusions for this phase at this time.

Phase 2b
There are no conclusions for this phase at this time.

Phase 2c – Mass-Efficient Architecture for Roof Strength
The optimized vehicle architecture met the target for roof-structure deflection of less than 4.5 inches under a load of 3 times the vehicle weight with only an increase of 1.2 kg.

Phase 2d – Mass Compounding
When all subsystems can be resized, the secondary mass savings is from 0.8 to 1.5 kg/kg (1.25 kg/kg is the estimate for the *all* vehicle group). When the powertrain has been fixed and is not available for resizing, the secondary mass savings is from 0.4 to 0.5 kg/kg (0.5 kg/kg is the estimate for the all vehicle group).

The study indicates that optimized steel structures can meet the FreedomCAR mass-reduction targets when mass compounding is considered. Realizing this objective requires additional technology development and is challenged by mass increases resulting from increased safety requirements, alternative powertrains and additional passenger amenities.

Acknowledgements:

Shawn Morgans of Ford Motor Company is recognized for his leadership on the MEARS project team.

Presentations/Publications/Patents

There are no patents or publications associated with this project.
Phase 1
Results of FGPC have been presented at several automotive conferences and within individual member company forums.

Phase 2c – Mass-Efficient Architecture for Roof Strength

A roadshow with the results has been presented to one original equipment manufacturer (OEM) to date.

Phase 2d – Mass Compounding

Results of this study have been presented to engineers at automotive companies and steel partnerships, as well as the USAMP Steering Committee and the Multi-Material Vehicle (see 12.D) Task Force.

MODIFIED PARTS	BASELINE FGPC-BO* (kg)	FINAL FGPC-FCD* (kg)	MASS SAVINGS (kg)	CHANGE (%)
BIW	130.6	121.0	9.6	7
Doors	12.6	6.4	6.2	49
TOTAL	143.2	127.4	15.8	11

Table 1: Final Mass Summary For FGPC Project – Modified Parts Only

STRUCTURE	INDUSTRY STANDARD (kg)	FINAL FGPC-FCD (kg)	MASS SAVINGS (kg)	CHANGE (%)
BIW + IP BEAM	310.0	217.6	92.4	30

Table 2: Final Mass Summary For FGPC Project – Comparison to Industry Standard

STRUCTURE	INDUSTRY STANDARD (kg)	FINAL FGPC-FCD (kg)	MASS SAVINGS (kg)	CHANGE (%)
Passenger Compartment	246.8	169.3	77.5	31%

Table 3: Final Mass Summary For FGPC Project – Comparison to Industry Standard Passenger Compartment

* Before Optimization (BO)
* Final Concept Design (FCD)

[i] Denotes project 241 of the Auto/Steel Partnership (A/SP), the automotive-focus arm of the American Iron and Steel Institute (AISI). See www.a-sp.org. The A/SP co-funds projects with DOE through a Cooperative Agreement between DOE and the United States Automotive Materials Partnership (USAMP), one of the formal consortia of the United States Council for Automotive Research (USCAR) set up by Chrysler, Ford and General Motors (GM) to conduct joint, pre-competitive research and development. See www.uscar.org.

J. Lightweight Rear Chassis Structure (ASP 601[i])

Project Manager: Jim Cran
Auto/Steel Partnership (A/SP)
2000 Town Center, Suite 320
Southfield, MI 48075
(905) 385-8276; fax: (905)-383-3200; e-mail: jim.cran@sympatico.ca

Co-Chair: Jamal Alghanem
Chrysler LLC
800 Chrysler Drive
CIMS 484-36-02
Auburn Hills, MI 48326
(248) 576-1915; fax: (248) 576-2046; e-mail: ga5@chrysler.com

Co-Chair: Michael Gulas
Dofasco Inc.
P.O. Box 2460
1330 Burlington St .E. Hamilton, Ontario, Canada L8N 3J5
(905) 548-4719; fax: (905) 548-4250, e-mail:michael_gulas@dofasco.ca

Technology Area Development Manager: Joseph A. Carpenter
(202) 586-1022; fax: (202) 586-1600; e-mail: joseph.carpenter@ee.doe.gov

Field Project Officer: Aaron D. Yocum
(304) 285-4852; fax: (304) 285-4403; email: aaron.yocum@netl.doe.gov

Expert Technical Monitor: Philip S. Sklad
(865) 574-5069; fax: (865) 576-4963; e-mail: skladps@ornl.gov

Contractor: United States Automotive Materials Partnership (USAMP)[i]
Contract No.: DE-FC05-02OR22910 through the National Energy Technology Laboratory

Objectives

- Obtain a minimum mass reduction of 25% for a baseline passenger-car rear-chassis structure with no more than a 9% cost premium.
- Develop and document integrated solutions that balance the interaction of materials, manufacturing and cost. The solutions will focus on high-volume production (200,000 plus vehicles per year).
- Demonstrate the successful use of advanced high-strength steels (AHSSs) in a passenger-car, rear-chassis structure.
- Address corrosion and durability issues associated with reduced thickness AHSS.

Approach

- Phase 1: Material optimization. Through material substitution and minimal size and shape changes, the mass of the baseline chassis was reduced 15% noting limited reduction in stiffness. Prototypes have been fabricated and are being physically tested. The lessons-learned are being used in Phase 2. Phase 1 completion is scheduled for June of 2008.

- Phase 2: Design optimization. Through a clean-sheet redesign, the goal is to obtain a minimum mass reduction of 25% with no reduction in stiffness. From the cost perspective, the goal is to obtain no more than a 9% cost premium. A preliminary Phase 2 design has been prepared. Phase 2 completion is scheduled for September 2008.
- Phase 3: Communications. The goal is to transfer the technology developed in the project to original equipment manufacturer (OEM) and Tier 1 chassis-structure designers. Phase 3 completion is scheduled for March 2009.

Accomplishments

- Fabricated seven Phase-1 prototypes.
- Modal tested one Phase-1 prototype.
- Fatigue tested the brackets on three Phase-1 prototypes.
- Awarded a contract to Altair to evaluate analytical fatigue-resistance methods for chassis structures.
- Coated with Electropoli two baseline chassis structures and two Phase-1 prototypes for corrosion testing.
- Addressed AHSS availability, AHSS forming, and AHSS welding-technology gaps.

Future Direction

- Conduct sub-system fatigue testing on a Phase 1 prototype.
- Compare analytical fatigue results with laboratory fatigue results for the Phase 1 prototypes.
- Corrosion test the Phase-1 prototypes.
- Finalize the preliminary Phase-2 design.
- Undertake a cost study for the Phase-2 Final Design.
- Prepare final report for the project.
- Transfer the technology through road shows to A/SP member companies and key Tier 1 suppliers.

Introduction

There has been significant progress on Phase 1. Seven additional prototypes were fabricated. Three of the five technology gaps were addressed: AHSS availability, AHSS forming, and AHSS welding. Work on the remaining two—fatigue resistance and corrosion resistance—is well underway. Fatigue activity will be completed in the first quarter of 2008 and corrosion-resistance activity, due to the length of time required for physical testing, will be completed by June 2008.

The project was set back one year when it was discovered that the wrong loads were being used in the project. Fortunately, Phase 1 was not affected because loads were not used to design the Phase 1 prototypes. Rather, stresses under unit loads in the prototypes were compared to stresses under unit loads in the baseline. Unfortunately, the incorrect loads did impact the preliminary Phase-2 design.

The baseline was changed from the derivative of the current production chassis to the current production chassis itself (Figures 1 and 2). This change allows a better comparison with work completed to date. An analysis of the preliminary Phase-2 design using the correct loads showed that the preliminary Phase-2 design has less overstress than the current production chassis (the new baseline) when the actual materials used are accounted for. Thus, a request for quotation (RFQ) to finalize the preliminary Phase-2 design will be issued. The preliminary Phase-2 design is 12% lighter than the new baseline. However, it is believed that joint refinement and durability analysis during final design will significantly increase this mass saving.

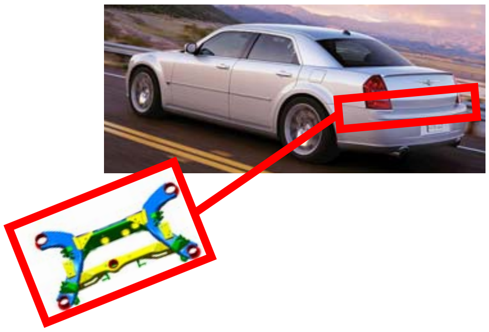

Figure 1. Donor vehicle and new baseline structure.

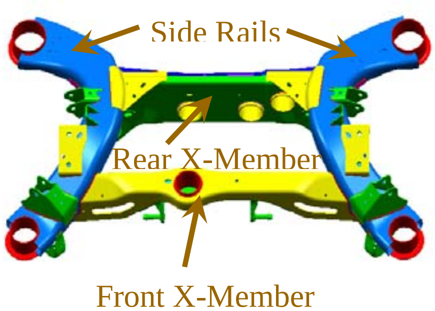

Figure 2. Baseline structure detail.

Phase-2 prototypes have been eliminated from the project. First, the technology gaps are being adequately addressed with the Phase-1 prototypes. Second, the Phase-2 design will be tested virtually. Third, if required, parts will be fabricated to check manufacturability. Fourth, if required, small specimens will be fabricated to address local issues.

The new completion date for the project is March 2009.

Phase 1: Materials Optimization

The project called for ten prototypes, three of which were fabricated in fiscal year (FY) 2006. The remaining seven were built during FY 2007. Prototypes 1 through 8 did not have gusset plates (as per the baseline chassis). They were allocated as follows: two for show pieces (Figure 3), one for modal testing (Figure 4), three for bracket fatigue testing (Figure 5) and two for corrosion testing. Prototypes 9 and 10 had gusset plates. They were allocated to sub-system fatigue testing.

Figure 3. Phase-1 prototype without gusset plates.

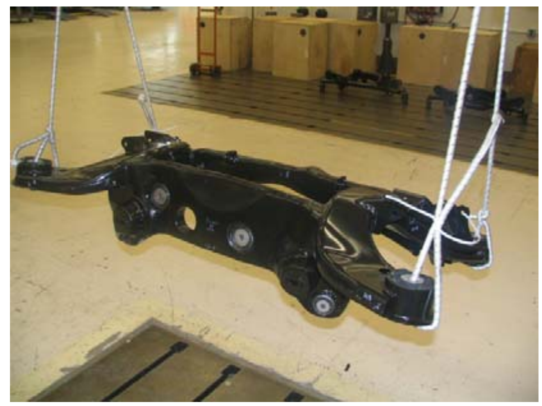

Figure 4. Modal test set-up.

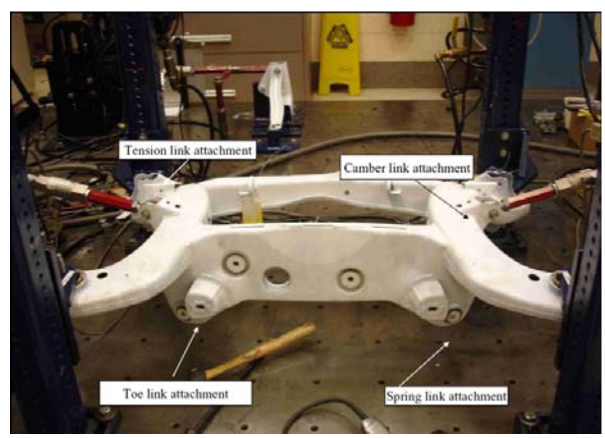

Figure 5. Bracket fatigue test.

Technology Gap Analysis – Availability of AHSS

The Team believes that the lack of a table showing the global availability of AHSS is hindering the use of AHSS for mass reduction in chassis structures. The Team pursued the development of a global table but discovered that the steel producers, for commercial reasons, do not want the availability of their AHSS in the public domain. Thus, the Team has reluctantly agreed that it is unable to address this technology gap.

Forming of AHSS

Very little AHSS has been used in chassis structures. Thus, the Team wishes to assure itself there are no major forming issues associated with the use of AHSS thicker than that commonly used in body structures.

In the baseline chassis structure, the side rails are made from 240 MPa steel and the rear crossmember is made from 208 MPa steel. In the Phase 1 prototypes, dual phase (DP) 590 steel was used for both the side rails and the rear crossmember.

Experi-Metal, the prototype fabricator, experienced no difficulties in forming the side rails and rear crossmember from DP 590 steel.

In the baseline chassis structure, the front crossmember is made from 362 MPa steel, while transformation-induced plasticity (TRIP) 780 steel was used for it in the Phase-1 prototypes. Experi-Metal experienced splitting in the front crossmember flanges. Forming analysis conducted by United States Steel indicated that material having a hole expansion >54% is required to prevent the splitting. For the prototypes, Experi-Metal overdrew the flanges and cut off the excess flange depth.

Based on its experience with the Phase-1 prototypes, the Team has concluded that globally-available AHSS grades may be formed into satisfactory chassis structure parts.

Welding of AHSS

Heat-affected zone (HAZ) softening, which depends on steel chemistry, is more pronounced in higher-strength steels. This softening reduces joint efficiency and must be taken into account when designing a chassis structure.

To address the softening issue, in conjunction with A/SP's Joining Team (see 5.B), the requirements were defined for a set of design rules applicable to chassis structures. The Joining Team has awarded Applied Engineering and Technology a contract to prepare gas metal arc welding (GMAW) Weld Design Rules for all steel grades including AHSS. The Joining Team anticipates the Rules will be published by December 2007.

Oak Ridge National Laboratory (ORNL) is developing a model to predict the effects of welding on AHSS microstructure. The model predicts softening in the HAZ. The Chassis Team is interacting with ORNL to ensure a simplified model suitable for inclusion into automotive finite-element analysis (FEA) models is developed.

Corrosion Resistance

Downgaging with AHSS means thinner steel. In chassis structures, the thickness of the steel is used as the second line of defense against corrosion. Thus, there is concern thinner steel may cause corrosion problems.

The Team's Corrosion Working Group has concluded that the performance of E-Coat over parts made from galvanized steel is a known technology for chassis applications. Hence, it can be used to protect thin AHSS members (less than 2.0 mm) in chassis structures. However, the Group feels it is desirable to have an alternate corrosion-protection method. Thus, it is evaluating the Electropoli hot-dip-galvanizing method used in Europe to coat chassis structures after fabrication. Two baseline rear-chassis structures and two Phase-1 prototypes have been coated with Electropoli in France. One baseline structure with E-coat, one baseline structure with Electropoli and one Phase-1 prototype coated with Electropoli are being sectioned by Ford to evaluate coating coverage. One baseline structure with E-coat, one baseline structure with Electropoli and one Phase-1 prototype coated with Electropoli will be trailer tested by General Motors from November 2006 to May 2008.

Fatigue Resistance

Durability is a major criterion in chassis design. AHSS brings not only mass reduction but higher stresses, which may reduce fatigue resistance if not properly accommodated. The Team has addressed the fatigue issue with the A/SP Sheet Steel Fatigue (see 5.D) Team. There is ample evidence that the fatigue strength of sheet steel is proportional to tensile strength. Thus, even though design stresses are higher in AHSS, the higher tensile strength of AHSS results in higher fatigue strength. The end result is the fatigue strength of AHSS material is not an issue. There is little data on the fatigue strength of metal inert gas (MIG) welded joints made with AHSS. However, fatigue experts agree that the fatigue strength of all MIG-welded joints depends on weld process and joint geometry, that is, the fatigue strength of MIG-welded sheet steel joints is independent of steel grade. To verify this conclusion, the Fatigue Team has launched a test program using DP 590, DP 780, DP 1000, and TRIP 780 AHSS joined by MIG and laser welds. The program should be completed in 2009.

The Team wants to compare the fatigue strength of the Phase-1 prototypes determined from the laboratory tests with the fatigue strength determined analytically. Altair was retained to construct as-built, computer-aided design (CAD) and finite-element (FE) models of the Phase-1 prototypes and to compare test and analytical results for the bracket fatigue tests, which have been completed. In addition, Altair is evaluating the use of FEsafe software with the BS 5400 module and the FEsafe software with the Verity module. The CAD and FE models have been constructed and Altair has concluded that the FEsafe and BS 5400 model predicted well fatigue life and fatigue-crack location. Altair will complete its assignment by December 2007.

Chrysler will start sub-system fatigue testing on a Phase-1 prototype early in 2008. It will use a half-rig test set-up and a standard Chrysler drive file. Chrysler will compare the physical test results with a CAE half-rig fatigue simulation.

Phase 2: Design Optimization

Martinrea prepared a preliminary Phase-2 design in FY 2006 (Figure 6). However, in order to properly incorporate the lessons learned from Phase 1 into Phase 2, work on Phase 2 was put on hold. When the Team discovered that the wrong loads were given to Martinrea for use in Phase 2, Martinrea was asked to determine the effect of the wrong loads on the preliminary design. The preliminary design is governed by stiffness and the Team believed the effect might be insignificant. Using linear static analysis and the correct loads, Martinrea found that the preliminary Phase-2 design has less overstress than the new baseline when the actual materials used for each are taken into account. Thus, the Team has agreed to finalize the Phase-2 preliminary design. The preliminary Phase-2 design is 12% lighter than the new baseline. However, the Team hopes to capitalize on additional mass reduction opportunities (e.g., improving the joints and additional durability analysis) during final design.

The original agreement with Martinrea to finalize the Phase-2 preliminary design did not include fatigue analysis or mass-compounding. Also, the Team has decided not to build Phase-2 prototypes because the technology gaps are being adequately addressed with the Phase-1 prototypes. Thus, support for a Phase-2 prototype build is no longer required from Martinrea. Lastly, Phase-2 work has been on hold for a year. To reflect the foregoing, the Team will issue a new RFQ to complete Phase 2.

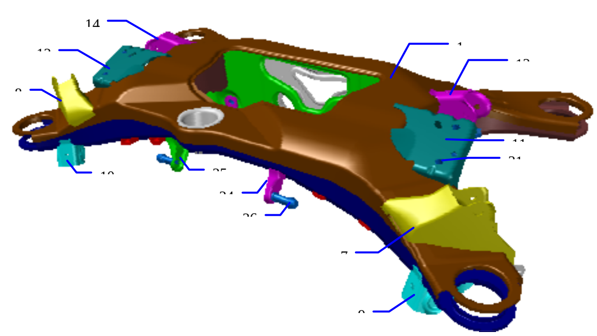

Figure 6. Phase-2 preliminary design.

Phase 3: Communications

Phase 3 communications activity is scheduled for January to March 2009.

Conclusions

Primarily due to design changes made to improve the Phase-1 prototypes, due to delays in obtaining test windows for prototype testing and due to the use of incorrect loads in Phase 2, it will take longer to complete the project than originally envisioned. The technology gaps that prevent mass reduction in chassis structures through the use of AHSS are steadily being broken down. The Team is confident the project objectives will be accomplished and the results will facilitate the use of AHSS by chassis engineers to achieve mass reduction.

Presentations/Publications/Patents

To date, no presentations or publications have been placed into the public domain. The first ones planned are at the end of Phase 1.

---

[i] Denotes project 601 of the Auto/Steel Partnership (A/SP), the automotive-focus arm of the American Iron and Steel Institute (AISI). See www.a-sp.org. The A/SP co-funds projects with DOE through a Cooperative Agreement between DOE and the United States Automotive Materials Partnership (USAMP), one of the formal consortia of the United States Council for Automotive Research (USCAR), set up by Chrysler, Ford and General Motors (GM) to conduct joint, pre-competitive research and development. See www.uscar.org.

K. Characterization of Thermo-Mechanical Behaviors of Advanced High-Strength Steels (AHSS): Formability, Weldability and Performance Evaluations of AHSS Parts for Automotive Structures

Principal Investigator: Moe Khaleel
Pacific Northwest National Laboratory (PNNL)
P.O. Box 999
(509) 375-2438; fax: (509) 375-6605; e-mail: moe.khaleel@pnl.gov

Technology Area Development Manager: Joseph A. Carpenter
(202) 586-1022; fax: (202) 586-1600; e-mail: joseph.carpenter@ee.doe.gov

Expert Technical Monitor: Philip S. Sklad
(865) 574-5069; fax: (865) 576-4963; e-mail: skladps@ornl.gov

Contractor: PNNL
Contract No.: DE-AC06-76RL01830

Objective

- Investigate the formability of advanced high-strength steels (AHSS) with emphasis on loading temperature, loading paths and “secondary” deformation effects on part ‘residual’ strength and microstructure.
- Develop a fundamental understanding of transformation kinetics of AHSSs by analyzing the crystallographic and morphological features of the phase transformations subject to different thermal- and mechanical-loading paths from forming and welding.
- Provide performance data and constitutive models for formed AHSS parts.
- Investigate the weldability of AHSS under various welding processes and parameter conditions applicable to auto-production environment.
- Generate weld-performance data including static strength, formability, impact strength, and fatigue life as a function of welding processes and parameters.
- Investigate welding techniques for improved AHSS weld performance and benchmark the performance against the current welding practices for roll-formed and hydro-formed AHSS frame and underbody-structure applications.
- Develop design guidelines on AHSS to assist rapid structure design and prototyping.

Approach

- Investigate formability and weldability of AHSS. This task includes: forming under complex loading paths (uniaxial and biaxial); quantification of formability and weldability for various grades of AHSS based on their chemistries and corresponding thermal-mechanical process.
- Investigate the interdependency of manufacturing processes: weldability of a formed part and formability of a welded part.
- Develop transformation-kinetics model and macroscopic constitutive relationships for AHSS (dual-phase (DP), transformation-induced plasticity (TRIP) and complex phase (CP)).
  - Systematically evaluate the effects of various welding process and process parameters on the microstructure and property of welds. Welding processes include gas-metal arc welding, laser welding, hybrid laser-arc welding, and resistance spot welding. Metallurgical and process models will be used to analyze the

microstructure evolution. The properties will be measured as a function of geometry, composition, process and process parameters. A performance evaluation procedure will be developed that allows for quantifying the performance improvement, weight and cost savings associated with use of AHSS.

- Evaluate structural-performance evaluation of formed and welded parts made of AHSS. This task will provide the automotive design engineers with accurate material performance data for design verification of AHSS structural parts.

Recent Accomplishments

- Finished detailed microstructural characterizations of deformed TRIP-steel samples on grain-size distributions, texture evolution and transformation kinetics under different loading modes, loading temperatures and loading rates.
- Developed transformation-kinetics model for multiphase TRIP steel and implemented it in metal-forming simulations.
- Quantify the effects of phase transformation during forming operation and its influence on TRIP steel side-rail impact performance.
- Finished preliminary micromechanical studies on DP 980 focusing on the effects of martensite volume fraction and strength on the macroscopic stress versus strain relationships as well as failure modes of AHSSs.
- Finished preliminary micromechanics modeling of TRIP 800 considering austenitic phase transformation.

Future Direction

- Investigate effects of through-thickness microstructural inhomogeneity and banding on the forming/bending performance of DP 980.
- Conclude the feasibility of using neutron diffraction in quantifying the retained-austenite volume fraction.
- Micromechanics modeling of DP steel considering grain-boundary effects.
- Micromechanics modeling of TRIP steel considering phase transformation of individual grains.

Introduction

This project is a collaborative effort between PNNL, Oak Ridge National Laboratory (ORNL), and the United States Automotive Materials Partnership (USAMP) of the U.S. Council for Automotive Research (USCAR). The work began in October 2005.

Because of their excellent strength and formability combinations, more and more AHSSs are being used in vehicle-body structures to reduce vehicle weight and improve vehicle-crash performance. Currently, the technical barriers hindering wider applications of AHSS in the domestic auto industry include: 1) the fundamental behaviors of AHSS parts subject to different thermal- and mechanical-loading paths (forming and welding) are not fully understood and quantified; 2) the constitutive behaviors for the formed parts are not available to computer-aided engineering (CAE) engineers for rapid prototyping; and 3) welding-induced complex microstructures and the effects of different welding processes and welding parameters on weld performance are not well understood.

In order to address these technical barriers, PNNL's role in this project includes investigating the formability of AHSS, with emphases on loading temperature, loading paths and secondary deformation effects on part 'residual' strength and microstructure. The project also develops a fundamental understanding of transformation kinetics of AHSS steels by analyzing the crystallographic and morphological features of the phase transformations subject to different thermal and mechanical-loading paths from forming. The goal is to provide the automotive design engineers with accurate material-performance data and constitutive models for design evaluations and verification of AHSS structural parts.

ORNL's focus is on the AHSS weld-performance evaluations and improvements. See 5.L.

<u>TRIP Steels</u>

Microstructure Characterizations of Deformed TRIP800 Steel Samples on Grain- Size Distributions, Texture Evolution and Transformation Kinetics Under Different Loading Modes, Loading Temperatures, and Loading Rates

Base material properties for TRIP 800 have been characterized under different original equipment manufacturer (OEM) manufacturing temperatures ranging from -40°C to 93°C under different strain rates. High strain-rate tensile tests under various temperatures were performed at ORNL's High-Temperature Materials Laboratory (HTML). It was previously reported that TRIP 800 has reduced ductility under dynamic loading compared to static loading.

In this reporting period, we studied the microstructure features and transformation kinetics under different loading conditions. For example, Figure 1 shows the electron backscatter diffraction (EBSD) map of as-received TRIP 800 with phase localization of ferrite (blue in color prints, dark background in black-and-white prints), austenite (red in color prints, dark gray in black-and-white prints) and zero-solution (green in color prints, light gray in black-and-white prints). Zero-solution zones can be ferritic grain boundaries, bainitic grains, martensitic grains, austenite with grain size smaller than 0.1µm, or zones with a high dislocation density. Results in Figure 1

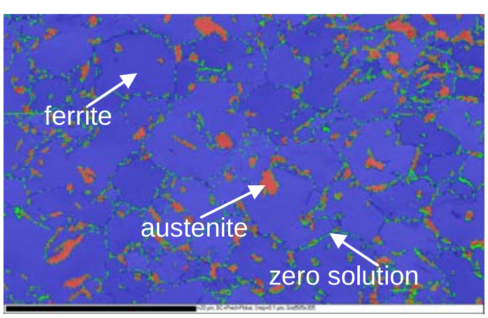

Figure 1. Phase map for as-received TRIP 800.

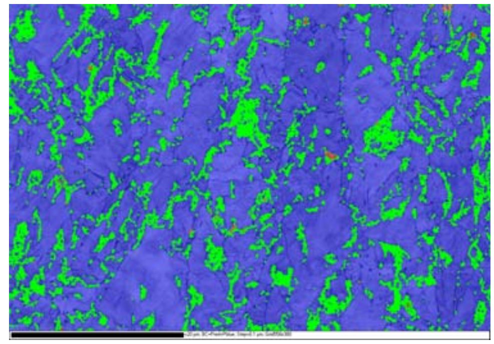

Figure 2. Phase map for deformed TRIP 800 under 256 in/sec loading rate and room temperature.

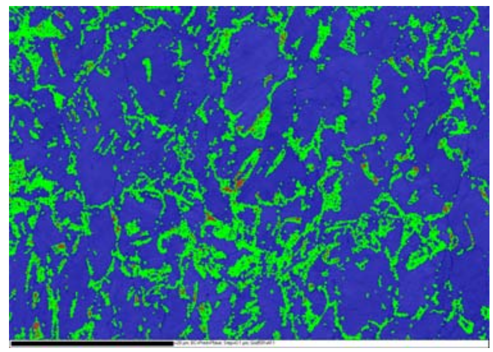

Figure 3. Phase map for deformed TRIP 800 under 640 in/sec loading rate and room temperature.

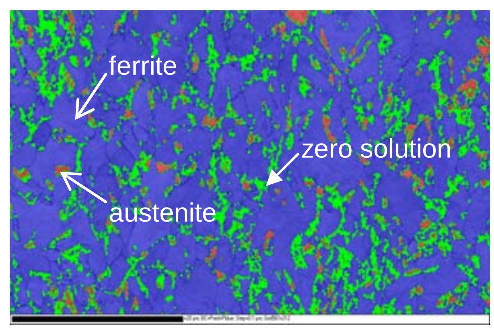

Figure 4. Phase map for deformed TRIP 800 under 256 in/sec loading rate and 93°C.

indicate that the microstructure of the "as-received" material consists of various phases with different grain sizes: the big grains are ferrite matrix and the small grains are essentially austenite, bainite or martensite. The average grain size for body-centered cubic (bcc) is close to 2 µm and for face-centered cubic (fcc) is 0.5 µm.

Figures 2 to 4 show the phase maps of deformed TRIP 800 samples under different deformation rate and temperatures. The results indicate that a slower austenite transformation rate occurs under higher loading temperature and higher loading rate. This explains the ductility reduction observed under high-rate tensile test. Essentially, the heat generated by the sample's plastic deformation inhibits martensitic transformation during high-rate loading rendering the sample with higher amount of retained austenite in the deformed microstructure without the additional plasticity provided by the TRIP effect.

The influences of loading temperature and loading rate on transformation kinetics, hence, strength and ductility of TRIP steels, should, therefore, be carefully considered in applications of this type of steel for crash members in automotive structural components.

Finite-Element Forming Simulation with TRIP-Steel Transformation Kinetics

In this section, results of finite-element forming simulation are presented in which the phase transformation during forming is predicted for TRIP steels. The commercial finite-element package ABAQUS is used in the forming simulation and the material's constitutive relations are implemented in a user-defined material subroutine to interface with the main analysis engine.

First, steel with a fully-austenitic structure is used as the forming example. Assuming a friction coefficient of 0.2, Figure 5 shows the predicted martensite distribution in a typical automotive hat section after forming. Results in Figure 5 indicate that the side wall of the formed part has much higher martensite volume fraction than the two flanges and the bottom of the hat section. Therefore, in addition to the wall thinning induced by the forming process, inhomogeneous material properties will also need to be considered in evaluating the crash performance of the hat section during impact.

Figure 6 illustrates the effects of lubrication on forming-induced phase transformation. In this case, a perfectly-lubricated part is assumed and the friction coefficient between the part and the die/punch is set to be zero. Under this perfectly-lubricated condition, martensitic phase transformation occurs primarily at the bent corners of the hat section for the same amount of forming depth. Therefore, the corresponding points on the as-formed hat sections will have different mechanical properties depending on different forming-lubrication conditions. The effects of forming-induced phase transformation on the hat section impact performance will be discussed next.

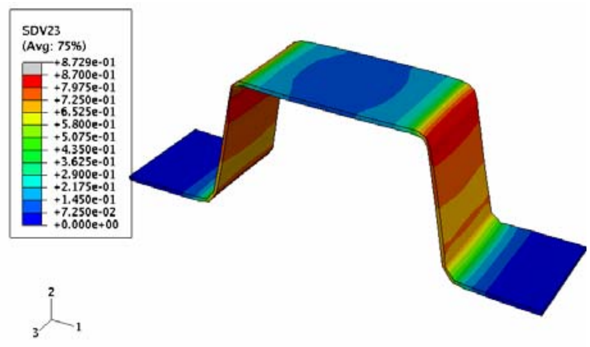

Figure 5. Distribution of martensite volume fraction after hat-section forming with friction coefficient = 0.2.

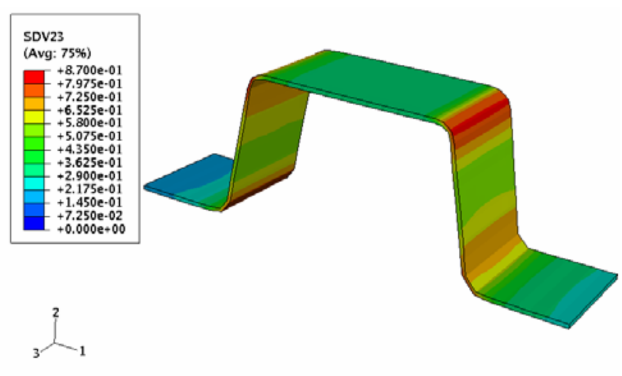

Figure 6. Distribution of martensite volume fraction after hat-section forming with friction coefficient = 0.

Effects of Phase Transformation During Forming Operation on Impact Performance of TRIP-Steel Side Rail

In this section, results of finite-element crash simulation are presented for a TRIP-steel side rail with and without considering the phase transformation during forming operations. The geometry for the two rails is the same with the same amount of wall thinning resulted from the forming operations. In the first case, a side rail with inhomogeneous material properties, as predicted by the forming simulation (friction coefficient = 0.2), is considered. In the second case, a side rail with uniform material property of austenite is considered. Figure 7 shows the evolution of von Mises stresses on the two side rails during crash simulation.

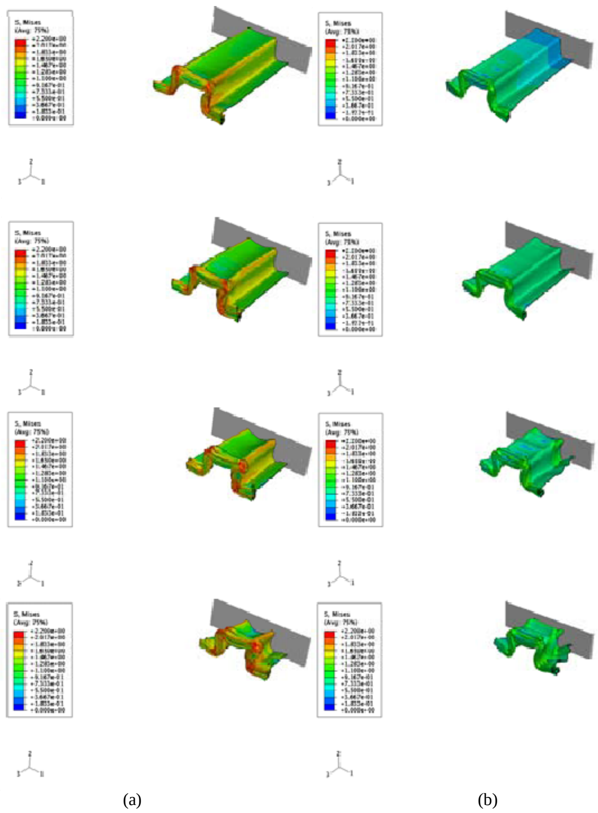

Figure 7. von Mises stress on deformed configurations during side-rail crash (a) with forming-induced phase transformation; (b) without forming-induced phase transformation.

For case (a), forming-induced martensite on the side wall of the hat section strengthens the side wall; therefore, much higher stress levels are predicted for case (a) than case (b). Figure 8 compares the energy absorption of the side rail versus time by considering and not considering the phase transformation strengthening resulted from forming operation. The results indicate that with the forming-induced phase transformation, higher energy absorption of the side rail can be achieved. On the other hand, if one only considers wall thinning from forming operations without considering phase transformation, the predicted hat-section energy-absorption level is much lower. Results here indicate that phase-transformation-induced strengthening should be considered by vehicle-structure engineers when TRIP steel is used as structural members.

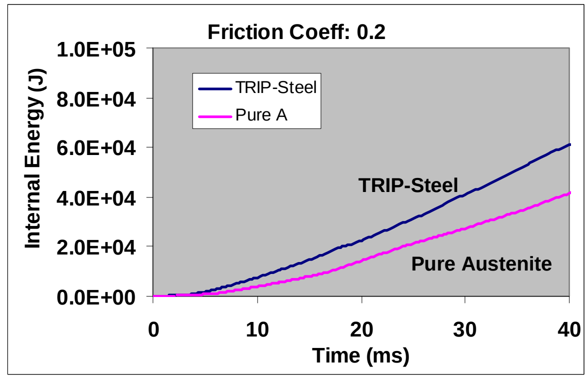

Figure 8. Effects of phase transformation on predicted side-rail energy absorption.

Dual Phase

Micromechanics Modeling for Dual-Phase Steel during Tensile Deformation

In previous studies, we have established the importance of various phase volume fractions on the macroscopic behaviors of the AHSS. In this section, we use micromechanics modeling approach to study the stress and strain partitions in the various phases of AHSS during deformation. The goal here is to gain a better understanding of the phase compatibility during deformation process for these steels and, therefore, to be able to predict the macroscopic strength and failure modes subjected to different loading conditions.

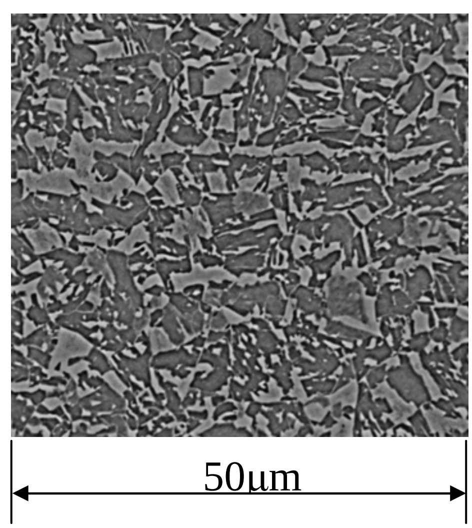

Figure 9. Typical microstructure used for micro-mechanics modeling of DP980.

Figure 9 shows the microstructure we started with for commercial DP 980 steel. The darker-color background represents the ferrite matrix and the brighter grains are the strengthening martensite phase. Figure 10 shows the finite-element mesh used for this representative volume element (RVE). In the micromechanics simulation, ferrite and martensite grains are given different material properties.

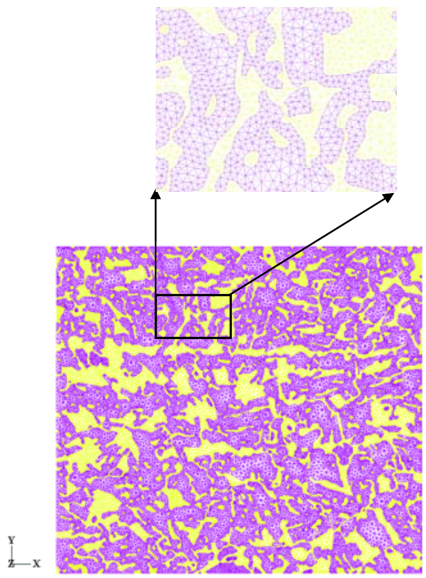

Figure 10. Finite-element discretization of the RVE.

The material properties for the individual ferrite and martensite phases are determined using the *in-situ* high-energy X-ray diffraction (HEXRD) method. The experiments were carried out at the 11-ID-C beamline of the Advanced Photon Source (APS) at Argonne National Laboratory (ANL). Figure 11 shows the measured lattice-strain partition among the different phases during the tension loading process. Based on the isotropic model, the three principal strain-tensor components, ε_{11}, ε_{22} and ε_{33}, were used to determine the stress-tensor components using Hooke's law:

$$\sigma_{ii} = E_{hkl}\left[\varepsilon_{ii} + \nu_{hkl}(\varepsilon_{11} + \varepsilon_{22} + \varepsilon_{33})/(1 - 2\nu_{hkl})\right]/(1+\nu)$$
$$i = 1,2,3$$

where E_{hkl} is diffraction elastic constants and ν_{hkl} is the Poisson's ratio in the subset of grains with their *hkl* crystal planes normal to the diffraction vector, determined by the Kröner model for each phase.

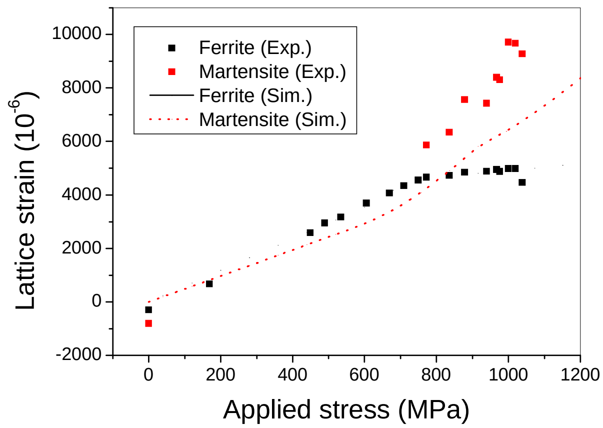

Figure 11. HEXRD-measured lattice strains along the loading direction for (200) reflections of ferrite and martensite during tensile loading.

The material properties used in the finite-element simulations are then:

$\sigma_y = 425 + 880\varepsilon_{ep}^{0.2}$ for ferrite and

$\sigma_y = 1130 + 1740\varepsilon_{ep}$ for martensite.

Note that no failure strain or ultimate elongation is specified for either phase. Finite-element analyses on the RVE level will be used to determine the macroscopic stress-versus-strain behaviors as well as the failure mode for this material subject to different loading and boundary conditions.

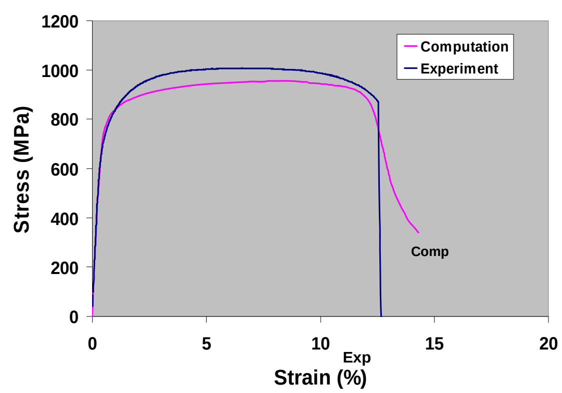

Figure 12. Predicted stress-versus-strain behavior for the RVE under plane-stress loading condition. The predicted failure mode under plane-stress loading condition is a macroscopic shear band.

Figure 12 compares the predicted and measured stress-versus-strain behaviors for this material under plane-stress loading condition. Overall satisfactory results have been obtained comparing with experimental results with final elongation around 12.5%.

Figure 13 illustrates the predicted von Mises stress and equivalent plastic-strain contours for the RVE during tensile loading. Results in Figure 13 indicate that much higher stress is experienced in the martensitic grains than the ferrite matrix during deformation, therefore confirming the martensite strengthening theory we presented earlier. In contrast to the stress partitioning, the matrix ferrite grains experience much higher plastic strains than the martensite grains. The final failure mode predicted is the coalescence of regions with large plastic strains in the form of a macroscopic 45° shear band. This prediction is in qualitative agreement with experimental observations for DP 980 under quasi-static tensile loading conditions; see Figure 14.

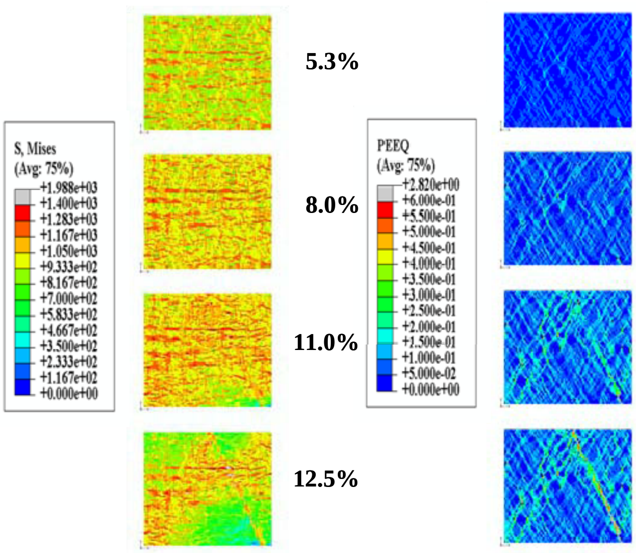

Figure 13. Predicted von Mises stress and equivalent plastic-strain contours for the RVE during tensile loading.

Future Direction

The next steps for our micromechanics modeling will be to include the grain-boundary effects and to consider the phase transformation of individual grains during deformation of TRIP steels. We are also planning on using ANL's APS facility in measuring the stress and strain partitioning in TRIP steels during deformation to validate the modeling results.

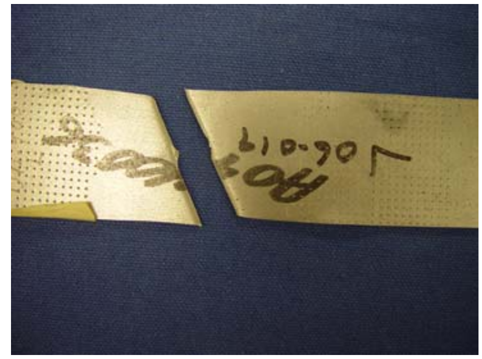

Figure 14. Experimentally-observed failure mode for DP 980 under quasi-static tensile loading.

Presentations/Publications/Patents

1. Sun, X, E.V. Stephens, and M.A. Khaleel. *Effects of Manufacturing Processes and In-Service Temperature Variations on the Properties of TRIP Steels.* SAE Paper No. 2007-01-0793. SAE World Congress 2007.
2. Liu, W.N., Choi, K.S., Sun, X., Khaleel, M.A., Ren Y. and Wang Y.D. *Modeling of Failure Modes Induced by Plastic Strain Localization in Dual Phase Steels.* To be presented at SAE2008 World Congress.
3. Liu, W.N., Choi, K.S., Sun, X., Khaleel, M.A. *Characterization of Thermo-Mechanical Behaviors of Advanced High Strength Steels (AHSS)*, presented at 2007 USCAR AMD annual offsite review. PNNL-SA-57747.

L. Characterization of Thermo-Mechanical Behaviors of Advanced High-Strength Steels (AHSS): Weldability and Performance Evaluations of AHSS Parts for Automotive Structures

Principal Investigator: Zhili Feng
Oak Ridge National Laboratory (ORNL)
1 Bethel Valley Road, Oak Ridge, TN 37831
(865) 576-3797; fax: (865) 574-4928; e-mail: fengz@ornl.gov

Participants:
Stan A. David, ORNL
John Chiang, Ford Motor Company
Cindy Jiang, AET Integration, Inc
Min Kuo, ArcelorMittal Steel

Technology Area Development Manager: Joseph A. Carpenter
(202) 586-1022; fax: (202) 586-1600; e-mail: joseph.carpenter@ee.doe.gov

Expert Technical Monitor: Philip S. Sklad
(865) 574-5069; fax: (865) 574-6098; e-mail: skladps@ornl.gov

Contractor: ORNL
Contract No.: DE-AC05-00OR22725

Objective

- Develop fundamental understanding and predictive capability to quantify the effects of welding and service loading on the structural performance of welded AHSS auto-body structures.
- Investigate the weldability of AHSS under various welding-processes and -parameter conditions applicable to auto-production environment.
- Investigate welding techniques and practices to improve AHSS weld performance and benchmark the performance against the current welding practices.
- Generate weld-performance data including static strength, impact strength, and fatigue life as functions of welding processes/parameters and steel grade and chemistry.
- Develop design guidelines and computer-aided engineering (CAE) methodology to assist rapid structure design validation and prototyping of AHSS parts, to achieve maximum vehicle weight reduction through intelligent selection and utilization of AHSS based on the fitness-for-purpose principle.

Approach

- Conduct comparative welding experiments on various AHSSs including high-strength low-alloy (HSLA), dual-phase (DP), transformation-induced plasticity (TRIP), and boron steels to develop the correlation among the joint properties, welding process conditions, and steel chemistry.
- Characterize and rank the factors controlling the weld geometry, weld microstructures and weld joint performance.
- Develop an integrated, thermal-mechanical-metallurgical welding process and performance modeling methodology to accurately predict the microstructure and mechanical-property gradients in the weld region; use the experimental data to validate the integrated model.

Accomplishments

- Initial development of welding process model capable of simulating the microstructural changes and the softening in the heat-affected zone (HAZ) of AHSS welds.
- Determined the fundamental metallurgical mechanisms causing HAZ softening of the current generation of AHSS.
- Developed initial correlation between the structural performance (static, dynamic and fatigue) and the microstructural changes of AHSS welds.
- Revealed the stress partitioning among different phases in TRIP steel during deformation and the effect of austenite-to-martensite transformation on the deformation and work hardenability of TRIP steel via *in-situ* neutron-scattering experiment.
- Demonstrated considerable fatigue-life improvement by means of refining welding conditions (within industry's acceptable welding practices).
- Close interactions with the industry, including different Auto/Steel Partnership (A/SP) technical committees and the Big 3, to exchange research progress and collaborate with other related projects.

Future Direction

- Continue to identify key factors controlling the weld joint performance under static- and fatigue-loading conditions.
- Further investigate the weld joint performance under impact/crash-loading conditions.
- Investigate the structural performance of AHSS weld joints under complex loading conditions (component-level behavior)
- Complete development of integrated thermo-mechanical-metallurgical modeling framework for AHSS welded structures.
- Continue to investigate welding techniques and practices to improve weld performance.
- Develop design guideline and CAE analysis methodology to assist rapid design and prototyping of AHSS structures.

Introduction

This project is part of collaborative research by ORNL and Pacific Northwest National Laboratory (PNNL, see 5.K) on "Characterization of Thermo-Mechanical Behaviors of Advanced High-Stress Steels (AHSS)." This joint effort aims at developing fundamental understanding and predictive modeling capability to quantify the effects of auto-body manufacturing processes (forming, welding, paint baking, etc) and in-service conditions on the performance of auto-body structures made of AHSS. ORNL's research (designated as Task 2 in this project) focuses on welding of AHSS. In the late part of the program, the interdependency of manufacturing processes – weldability of a formed part and formability of a welded part – will be investigated.

Specific background of Task 2 as related to the mission of DOE Lightweighting Materials and the needs of automotive industry for accelerated use of AHSS for body-structure lightweighting has been given in a previous annual report and will not be repeated here.

Task 2 has a technical steering committee with representatives from Chrysler, Ford, General Motors, A/SP Joining Committee (see 5.B), and steel companies.

In fiscal year (FY) 2006, the first year of the program, the research focused on obtaining the baseline knowledge and understanding about the static strength and fatigue life of AHSS welds. To this end, we experimentally investigated a wide range of AHSS types and grades most interesting to the US automotive industry. It was found, for the steels and welding conditions investigated herein, that:

- The static tensile strength of a gas metal arc welding (GMAW) process weld increases as the base-metal-steel strength increases. However, the joint efficiency (the ratio of weld strength to the base-metal strength) under static-loading condition can be greatly influenced by the HAZ softening of an AHSS weld. Ultra AHSS such as martensitic and boron steels have most noticeable HAZ softening and, thereby, lower joint efficiency. The lower-grade AHSS without HAZ softening maintain their high joint efficiency.

- Steel-grade dependency of weld fatigue life has been confirmed. The HAZ softening does not appear to be a major factor influencing the weld fatigue life.
- It is feasible to drastically improve the weld fatigue life of AHSS by manipulating welding-process conditions. The fundamental causes/mechanisms leading to the observed fatigue-life improvement re-quire further investigation.

In FY 2007, we began to focus on developing the fundamental understanding and predictive capability on the microstructural and property changes in the weld region of AHSS. Another major effort has been on investigating welding techniques to improve the weld durability (fatigue life) using a science-based approach. The experimental study on the welding effect expanded to the dynamic (impact) behavior of AHSS welds.

Steels and Welding

Based on the recommendations of Task 2 industrial technical steering committee, we have been focusing on welding of AHSS for chassis and underbody applications. The welding process was GMAW, the primary welding process for chassis and underbody structures. Five types of AHSS were selected in this study. They include dual-phase steels (DP 600, DP 780, DP 980), TRIP steels (TRIP 600, TRIP 780), martensitic steels (M130, M200), boron steel, and HSLA steel, with gauge thickness of 2-mm nominal. Details of the steels and welding conditions are provided in the FY 2006 annual report.

Improving Fatigue Life of AHSS Welds

In the past, the auto industry generally considered that the fatigue life of a weld joint is more or less independent of steel chemistry, and is dominated by the weld geometry (profile). Therefore, there is little room to improve the fatigue life of a steel weld from the welding perspective – the fatigue life of a steel weld will be primarily controlled by the load level (as indicated in the S-N curve). Such viewpoint stems from the experiences of conventional, low-strength, mild steels where the weld microstructure is not sensitive to welding. There have been very limited and systematic comparative studies on the fatigue behavior of different AHSS designed for automotive structural applications.

In FY 2006, we conducted a comparative study and found that there are noticeable differences in fatigue lives among different AHSS welds. Some of the higher-strength AHSSs studied such as boron steel had lower fatigue lives under the low-stress, high-cycle loading conditions (> 10^5 cycles) that are most relevant to the durability design of auto-body structures. In our FY 2006 study, all welds (of different AHSS) were made with the same set of welding parameters accepted by the industry for mild steels. This suggests that, in order to realize the benefits on the AHSS, different welding conditions would be required.

This year, we developed a new welding procedure that resulted in drastic improvement of the fatigue lives of AHSS welds. The new welding procedure involved adjusting different welding parameters to improve the weld profile, in particular the weld toe angle, to reduce the stress concentration at the weld toe. The adjustments of welding parameters developed in this study are readily transferable to a production environment. The welding speed (thus the productivity) is also within the range accepted by the industry. Figure 1 compares the different weld profiles produced using the baseline and improved welding conditions. The changes in weld profile resulted in a drastic increase in fatigue lives for AHSS, as shown in Figure 2. For comparison, the baseline fatigue lives of different AHSS welds made with the welding practice for mild steel are shown in Figure 3. An order-of-magnitude increase in fatigue lives has been achieved for DP and boron steels (relative to their respective baseline results).

The ability to improve the weld fatigue life of AHSS is significant. It addressed a critical concern in application of AHSS. The use of AHSS generally results in gage downsizing. This means that the AHSS structures will be subjected to higher fatigue stresses. If the fatigue life can not be improved through welding process innovations, the durability of the vehicle will suffer when mild steels are replaced with AHSS. Both A/SP Sheet Steel Fatigue Committee (see 5.D) and the Joining Technologies Committee (see 5.B) are interested in collaborating to further expand the study on this subject.

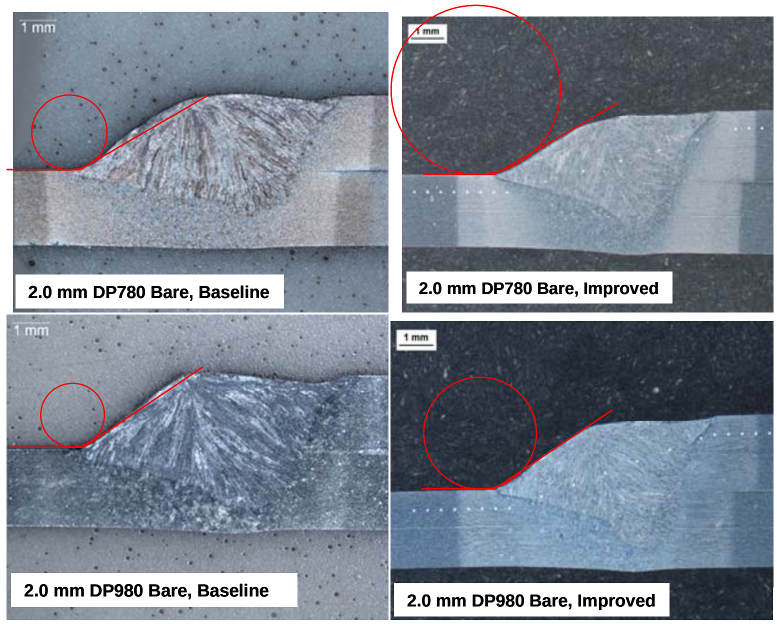

Figure 1. Weld-profile comparison between the baseline welding practice and the improved welding practice. The circles illustrate the changes in weld toe radius.

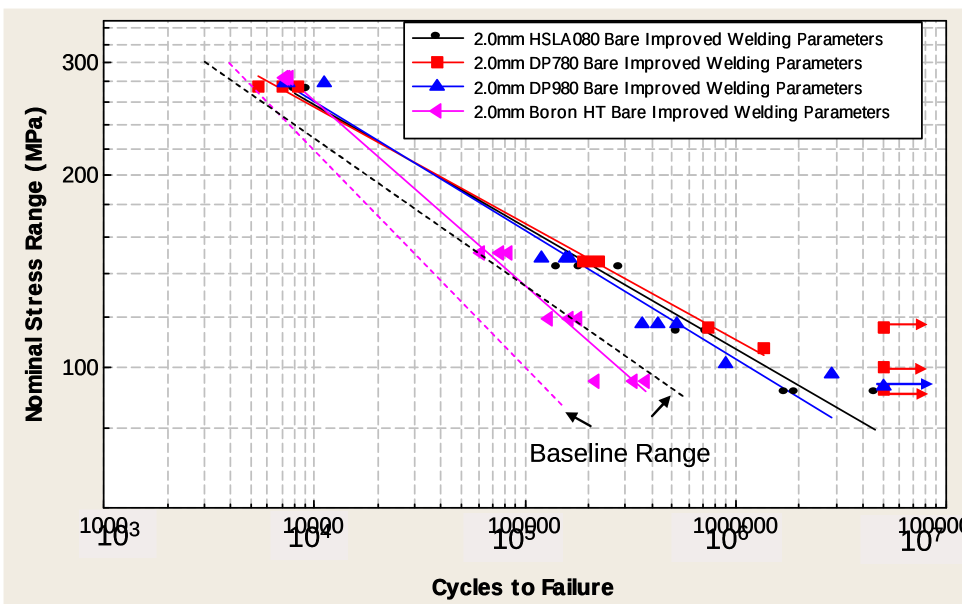

Figure 2. Improvement in fatigue life of AHSS welds by using AHSS-specific welding conditions.

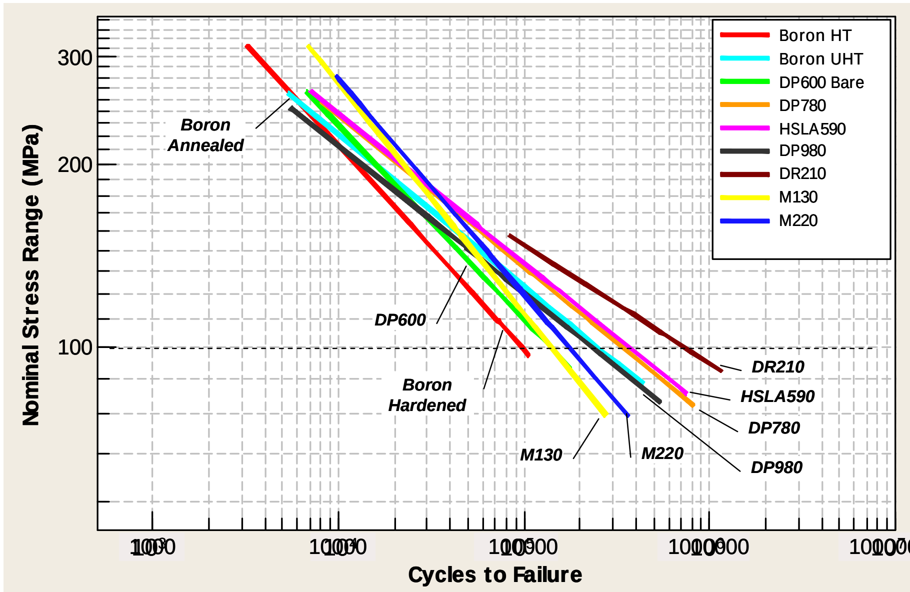

Figure 3. Comparison of fatigue S-N curves of different AHSS made under same welding conditions and having consistent weld profile. The regression curves are shown. R=0.1. Steel sheet thickness: 2 mm.

Predictive Models for Fatigue Life of GMAW Lap Joint of AHSS

In addition to the above experimental development of fatigue-life improvement of AHSS welds, we also completed the initial development of a weld fatigue-life prediction model that relates the fatigue life to the microstructure and geometry of AHSS weld joint. A summary of the model development is provided below.

We start with the local notch strain approach for welded joint [1,2]. In such an approach, the total fatigue life (N_t) of a welded joint consists of the crack-initiation part (N_i) and the subsequent cracking-propagation (to failure) part (N_p):

$$N_t = N_i + N_p$$

The propagation part can be estimated by the Paris law:

$$N_p = \frac{1}{C}\int_{a_i}^{a_c}\left(\frac{1}{\left(\Delta S\sqrt{\pi a}F(a)\right)}\right)da$$

Research in the past (for example, Lawrence et al. [1]) have shown that crack initiation is the dominant part in the total life of low-stress, high-cycle fatigue (i.e., in the stress range most relevant to auto-body durability design) in welded joints for high-strength steels and aluminum alloys. This differs from the case of mild construction steels where crack propagation takes up the majority in fatigue life of welded joints.

In this study, the Coffin-Manson equation is used for crack initiation life prediction:

$$N_i = \frac{1}{2}\left[\frac{2\left(\sigma_f' - \sigma_m\right)}{K_f \Delta S}\right]^{-1/b}$$

$$K_f = 1 + \frac{K_t - 1}{1 + a_p/\rho}$$

$$b = -0.1667\log\left(2.1 + \frac{917}{S_u}\right)$$

$$\sigma_f' = 0.95S_u + 370MPa$$

$$a_p = 1.187x10^5 / S_u^2$$

In the above equations, ΔS is the nominal stress range. σ_m is the mean stress. K_t is the stress concentration factor. K_f is the fatigue notch factor. ρ is the notch radius at the crack initiation site (weld toe or root in this study). *Su* is the local ultimate strength at the crack initiation site.

1 Lawrence F.V. 1973, "Estimation of fatigue crack propagation life in butt welds," *Welding Journal*, v53, 212s-220s.
2 Hou, C.Y. and Charng J.J. 1997, "Models for the estimation of weldment fatigue crack initiation life," *Int. J. Fatigue*, v19, 537-541.

The above equations relate the crack-initiation life to the three major factors governing the fatigue life of welded joint: (1) the stress state including the weld residual stress, (2) the local stress concentration due to weld geometry and discontinuity, and (3) the local material strength which is a function of the microstructure in the weld region.

The stress-concentration factors at the weld toe and weld root were determined using finite-element analysis. We analyzed the stress distributions for representative baseline and improved weld geometries under elastic deformation condition pertinent to the low-stress, high-cycle fatigue case. The actual weld profiles taken from weld cross-section metallographic pictures were used in building the finite-element mesh. The results are shown in Figure 4. The improved weld geometry reduces the stress concentration factor from 8.7 to 6.5 at the weld toe, and from 8.2 to 7.8 at the weld root.

Table 1 shows the drastic increase in the crack-initiation life of welded joint as result of reduction in fatigue notch factor, as determined from the fatigue-life prediction model described above. The improved weld geometry in our experiment would reduce the fatigue notch factor by about 20 to 30%. This translates into 5 to 10 times fatigue life improvement for mild steel (300 MPa ultimate strength). The improvement in fatigue life is even greater for AHSS, due to influence of material strength on crack initiation as indicated in the above equations. For example, fatigue life improvement for DP 780 is about 10 to 20 times. ***Thus, weld-geometry improvement can be particularly effective for higher-strength steels.*** The above analysis is supported by our experimental results, as shown in Figure 2 and Figure 3.

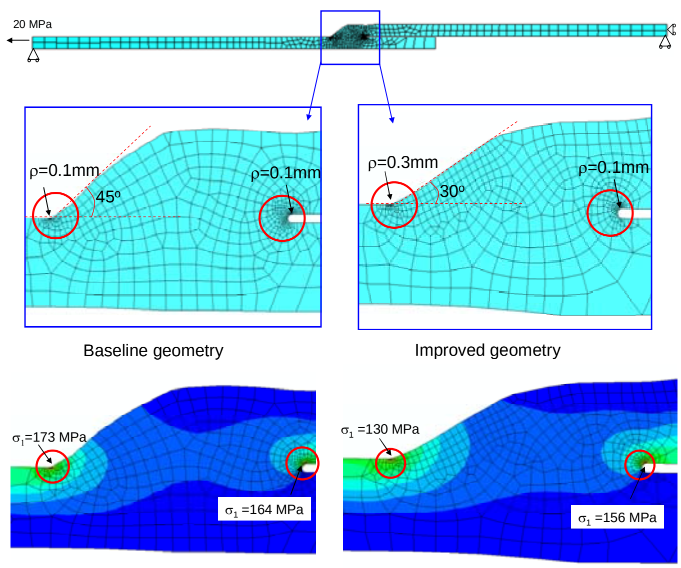

Figure 4. Finite-element analysis of local stress distributions around the weld toe and root region. The applied nominal stress is 20 MPa.

Table 1. Influence of fatigue notch factor on the crack-initiation life of a mild steel and a DP 780 steel.

Improvement in Kf	Improvement in Crack Initiation Life	
	Mild (300MPa)	DP780
5%	151%	176%
10%	223%	302%
20%	463%	829%
30%	906%	2098%
40%	1688%	4955%
50%	3014%	11032%

The fatigue-crack-initiation life-prediction model was further evaluated against the experimental testing data for a number of the steels and weld geometries studied in this project. The comparison and evaluation is summarized in Figure 5. Overall, the fatigue-life prediction model can capture the observed variations in fatigue lives due to steel grade, weld geometry and HAZ microstructure and local property variations of AHSS. However, the model underpredicts the experimentally-observed total fatigue lives as it does not contain the fatigue-crack-propagation part yet. The fatigue-crack-propagation life-prediction part of the model is being developed and verified.

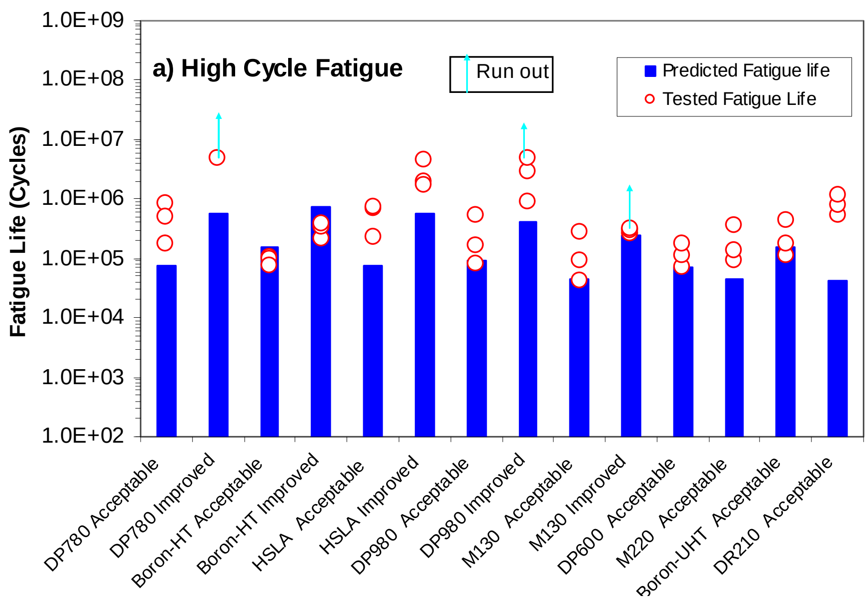

Figure 5. Comparison between experimental fatigue-life data and predicted fatigue crack initiation lives of GMAW lap joints for different grade steels and weld geometries [high-cycle fatigue case $N_f > 10^5$].

Modeling of Weld Microstructure Changes and HAZ Softening

As evidenced in our FY 2006 work and others, AHSS exhibit considerable microstructure changes in the weld region. The microstructural changes can result in the HAZ softening which impairs the static (and possibly the impact/crash) strength of AHSS welded structures. A major objective of Task 2 is, then, to develop the predictive capability to quantitatively relate the microstructure and property changes to the steel chemistry and welding-process conditions and to integrate the weld model into CAE-based design and engineering methodology for use in the industry.

We have completed the initial development of a welding thermo-metallurgical model for AHSS GMAW welds. This model is capable of correctly predicting the microstructure changes and the HAZ softening for the AHSS studied so far. As an example, Figure 6 shows the comparison between the predicted microhardness distribution and the experimental mapping of the microhardness for a boron steel weld. As shown in the figure, the weld model is able to predict the minimum hardness location (away from the weld fusion line) and the overall distribution of the microhardness changes in the HAZ. Modeling approaches dealing with the weld metal are being developed.

By correlating the temperature and microstructure information obtained from the weld process simulation, it is possible to explain the observed HAZ softening in AHSS welds. The minimum hardness region in the HAZ (approximately 2 mm away from the weld fusion line in Figure 6 for boron steel) corresponds to the intercritical temperature range in the Fe-C phase diagram (i.e., between A1 and A3 in Figure 7).

During welding, the minimum-hardness region is heated into the intercritical temperature range in which two phases (austenite and ferrite) co-exist. On cooling, the austenite can decompose to hard, low-temperature phases such as martensite or bainite. On the other hand, the ferrite phase in the intercritical temperature range will stay untransformed on cooling as it is a stable phase at room temperature. The presence of the soft ferrite will result in reduced strength and hardness, thus the minimum hardness of the HAZ. Such explanation is consistent with the observations that the most-pronounced HAZ softening takes place in martensite and boron steels.

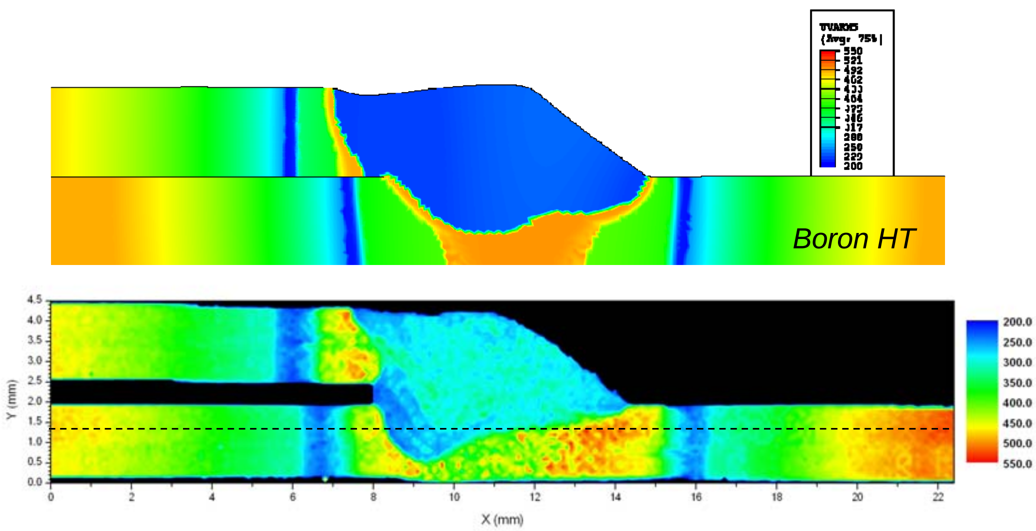

Figure 6. Comparison of predicted microhardness distribution (top) and experimental microhardness mapping (bottom). Boron steel is shown here. The model for the weld region is still under development.

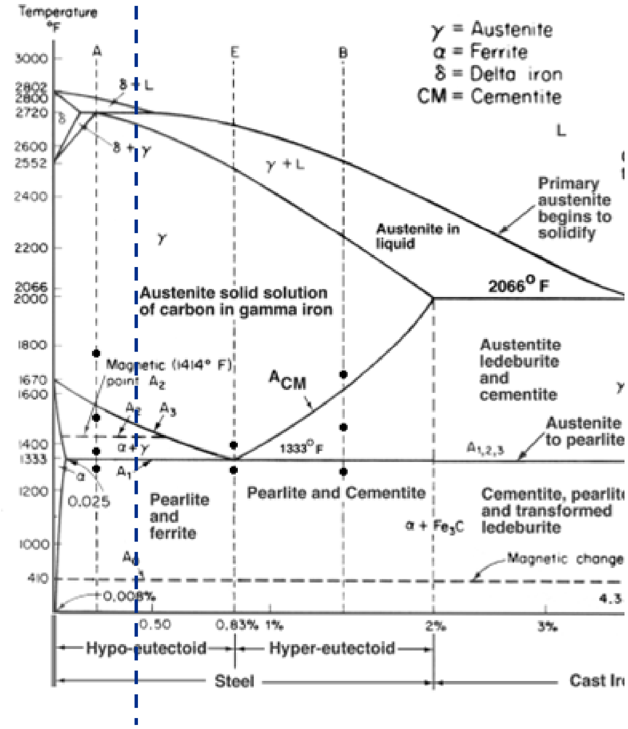

Figure 7. Fe-rich corner of Fe-C phase diagram.

The weld process model also reveals other mechanisms contributing to the HAZ softening of AHSS welds. Below the A1 temperature, the martensite in the base metal will undergo the tempering process, resulting in the observed gradual decrease in the hardness as the peak temperature approaching to A1. Above the A3, the steel will transform fully to austenite on heating. On cooling, whether the austenite will transform to martensite, bainite, or other hard phase depends on the hardenability of the steel (related to the steel chemistry). This explains the differences in the microstructure and microhardness in the near HAZ region (i.e., the region between the fusion line and the minimum-hardness region) of different AHSSs.

The above discussions on the fundamental metallurgical causes for the profound HAZ softening in AHSS are supported by the detailed microstructure-characterization analysis conducted in this study. A series of microstructure metallographic photos were systematically taken at different locations in the weld and HAZ region of a weld. The precise locations of these photos were determined by the distance from the fusion line and from the bottom surface of the sheet. With their locations being precisely known, these photos were then reconciled with the micro-hardness mapping results to yield the correlation between the microhardness and the underlining microstructures at various locations of the weld region. As example, Figure 8 and Figure 9 contrast the microstructures in different regions of a boron steel weld and a HSLA590 steel weld.

It is important to point out that the HAZ-softening phenomenon is an inherent characteristic for high-strength steels relying on allotropic phase transformation (i.e., decomposition of austenite to mixture of soft phases such as ferrite and hard phases such as martensite or bainite) to achieve a balance of strength and ductility. Such a phenomenon is not unique to automotive AHSS; it has also been observed in various high-strength steels such as low-carbon alloy steels such as X100 for natural-gas transmission pipelines and high-alloy steels such as 9Cr-1Mo steel for pressure vessels. On the other hand, the ferrite phase in the intercritical temperature range will stay untransformed on cooling as it is a stable phase at room temperature. The presence of the soft ferrite will result in reduced strength and hardness, thus the minimum hardness of the HAZ. Such explanation is consistent with the observations that the most-pronounced HAZ softening takes place in martensite and boron steels.

It is also important to point out that, while the HAZ softening is unavoidable in the current generation of AHSS, the degree of HAZ softening varies as a function of steel chemistry, base-metal microstructure, and welding process conditions. Various options can be explored to reduce the HAZ softening effect, from steel chemistry optimization, welding process selection, and effective structural design.

Other Progress

In-situ Neutron Diffraction Study of TRIP Steel.

In the past, the deformation behavior and the effects of phase transformation in TRIP steels have been studied post-mortem. Deformed samples are sectioned and examined using various metallographic techniques. The transformation-induced plasticity phenomenon is inferred from microstructure observations. What has been missing from these studies is the stress information within different phases that controls the transformation process in TRIP steels

In this project, we took the advantage of a neutron source to perform *in-situ* neutron experiments to study the phase-transformation kinetics in TRIP steels under loading. The goal was to determine the effect of deformation on austenite-to-martensite phase transformation in TRIP steels. Two TRIP steels, TRIP 590 and TRIP 780 were studied. By utilizing the unique time-of-the-flight feature of a pulsed neutron source, the lattice spacing changes of multiple crystallographic planes in two orthogonal directions were determined simultaneously. The *in-situ* measurement allowed for direct measurement of the phase-transformation process and the stress partitioning among different phases as the sample is being deformed. Figure 10 shows the changes in the lattice strains during the deformation process. The interplays between the austenite-to-martensite phase transformation and the deformation process are clearly revealed. Our *in-situ* neutron experiment, for the first time, provides direct and quantitative measurement of the TRIP behavior which can greatly assist and validate the constitutive model development effort at PNNL for forming simulation of TRIP steels.

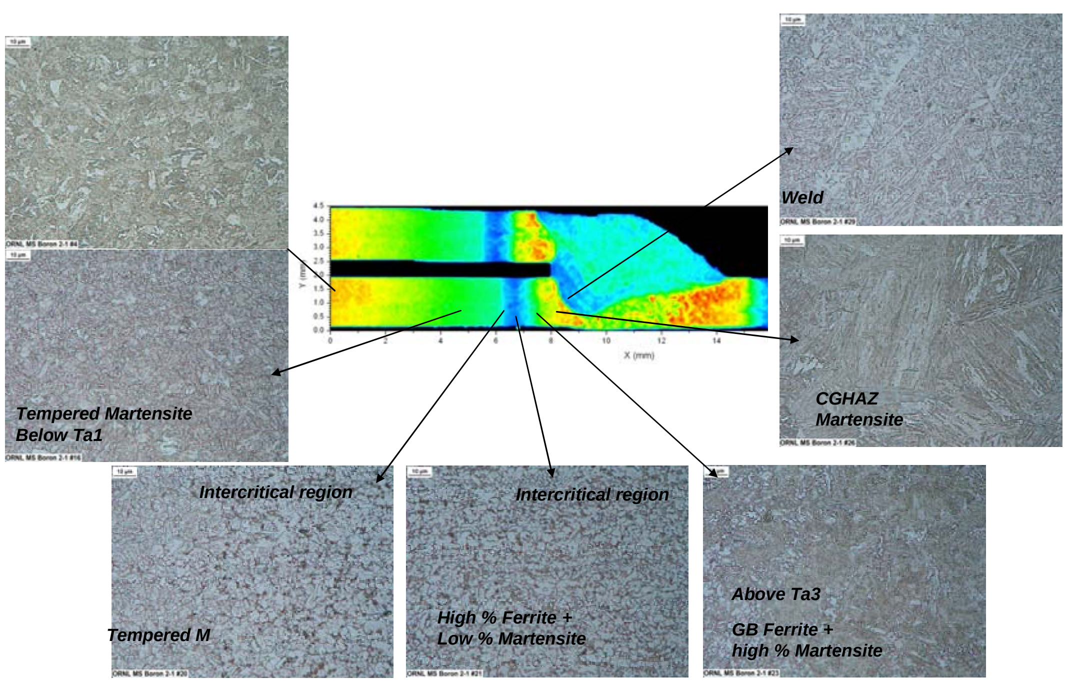

Figure 8. Microhardness distribution in a boron-steel weld and the corresponding microstructures in different locations in HAZ and weld. The drastic variations in microhardness result from considerable microstructure variations in different regions of HAZ. The lowest microhardness location corresponds to the intercritical region with high percentage of ferrite formed on heating and a low percentage of martensite transformed on cooling.

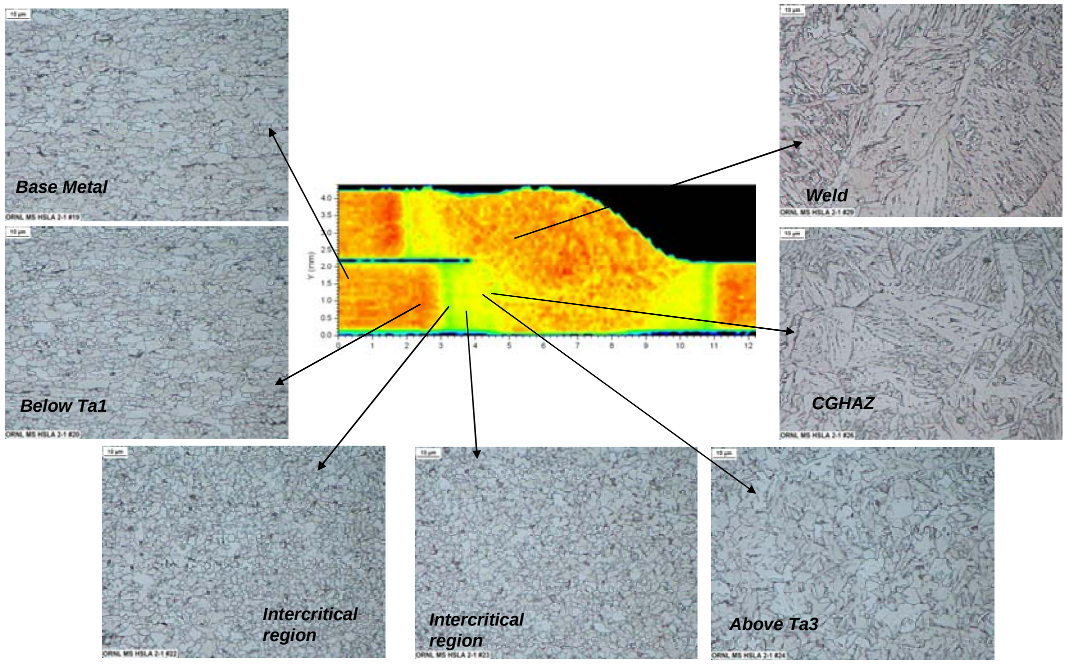

***Figure 9**. Microhardness distribution and the underlining microstructures in different part of HAZ of a HSLA590 steel.*

Interactions with the Auto and Steel Industry

The weldability task (Task 2) has received strong support from the industry from the start of the project. Since then, we have maintained active interactions with the auto and steel industry through the technical steering committee and A/SP. Such interactions have been mutually beneficial to the project and to the industry. We were invited to A/SP's Joining Technologies Team, Sheet Steel Fatigue Committee, and Lightweight Chassis Structures Team (see 5.J) to exchange research results. We also were invited to Ford, General Motors (GM) and Chrysler to discuss our research progress and understand the needs of the industry. Several collaborative efforts have come out of these interactions. For example, the Joining Technology Committee has decided to conduct a follow-on, static joint-strength-efficiency study to cover a wider range of steels, gage thickness and other welding processes. The Fatigue Committee is interested in incorporating our findings on fatigue-life improvement into their studies. Ford, GM, ArcelorMittal Steel and A/SP's joining and lightweight chassis design committees are looking into the feasibility of incorporating our weld microstructure model in some of their CAE design and research activities. We plan to maintain the strong interactions with the industry in this program.

Plan for FY 2008

The R&D activities in FY 2008 will be built on the strong progress of the project, focusing on completing the following tasks:

1) Complete the microstructure model development to include weld metal.
2) Initiate the integration of the welding process/microstructure model with mechanical-performance model that will enable simulation of the deformation and failure behavior of AHSS welds.
3) Continue on weld fatigue-life prediction model development.
4) Complete microstructure characterization of different AHSS welds to further validate the weld microstructure model.
5) Complete several topical reports on weld joint-efficiency study, microstructure characterization and weld-microstructure model development.

Presentations/Publications/Patents

1. Great Designs in Steel Seminar 2007, AISI, Livonia, MI, March 7, 2007
2. SAE World Congress & Exhibition, April 16-19, 2007, Detroit, MI (Invited Talk).

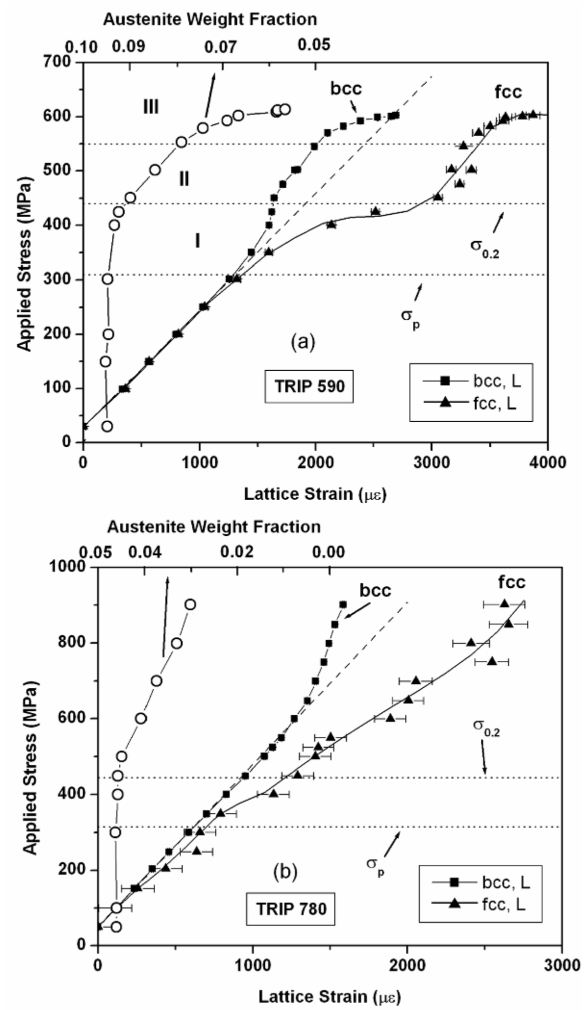

Figure 10. The lattice-strain evolution in the longitudinal direction of the face-centered cubic (fcc) phase and body-centered cubic (bcc) phases during the *in situ* neutron measurements in (a) TRIP 590 steel and (b) TRIP 780. The weight fraction of retained austenite (open symbols) was plotted to correlate to the lattice strain evolution. Note that bcc refers to the sum of ferrite and martensite phases, whose peaks overlap, after the martensitic transformation is induced. The weight fraction scale of (b) was adjusted to match that of (a), in order to illustrate the difference in phase transformation.

Acknowledgements

We would like to acknowledge the following individuals and A/SP committees who contributed to this project:

Chrysler: W. Marttila
Ford Motor: Paul Geck, J. Bonnen
General Motors: S. Gayden, J. Bohr, C. Chen
AK Steel: T. Montroy
Defasco: W. Bernert
Severstal N.A.: R. Mohan, Y.W. Wang
US Steel: M. F. Shi
A/SP Joining Technologies Team
A/SP Sheet Steel Fatigue Committee
A/SP Lightweight Chassis Structure Team

M. Materials Design for Steel Alloys

Co-Principal Investigator: Seong-Gon Kim
Assistant Professor
Physics and Astronomy
Hilbun Hall, Rm 237
Mississippi State University (MSST), P.O. Box 5405
Mississippi State, MS 39762-5405
(662) 325-8031; e-mail: kimsg@ccs.msstate.edu

Co-Principal Investigator: Mark F. Horstemeyer
Chair in Solid Mechanics & Professor, Mechanical Engineering
Center for Advanced Vehicle Systems (CAVS)
MSST
206 Carpenter Bldg., PO Box ME
Mississippi State, MS 39762
(662) 325-7308; fax: (662) 325-7223; e-mail: mfhorst@me.msstate.edu

Co-Principal Investigator: Randall German
Director and Professor
CAVS
MSST, P.O. Box 5405
Mississippi State, MS 39762-5405
(662)325-5431; (662)323-3906; fax: (662) 325-5433; e-mail: german@cavs.msstate.edu

Co-Principal Investigator: Hongjoo Rhee
Postdoctoral Associate
CAVS,
MSST, P.O. Box 5405
Mississippi State, MS 39762-5405
(662) 325-9221; e-mail: hrhee@cavs.msstate.edu

Co-Principal Investigator: Sungho Kim
Postdoctoral Associate
CAVS,
MSST, P.O. Box 5405
Mississippi State, MS 39762-5405
(662) 325-9241; e-mail: sk5@msstate.edu

Technology Area Development Manager: Joseph A. Carpenter
(202) 586-1022; fax: (202) 586-1600; e-mail: joseph.carpenter@ee.doe.gov

Contract Monitor: Aaron Yocum
(304) 285-4852; fax: (304) 285-4403; e-mail: aaron.yocum@netl.doe.gov

Contractor: MSST
Contract No.: 4000054701

Objective

- Design low-cost steel alloys with improved strength and formability for automotive applications.

Approach

We use a hierarchical, multiscale methodology to investigate the effect of nanoscale precipitates and additives to the overall strength and formability in steel-alloy design for automotive applications. Critical issues being addressed include: selection of key combination of precipitates and matrices, interaction of precipitate and matrix phases and, ultimately, composition-structure-property relationship. At the electronic level, quantum-mechanical, first-principles simulations based on Density Functional Theory (DFT) will be performed to investigate the interfacial interactions between matrix and the primary and the secondary precipitates. At the atomistic level, accurate atomistic simulations will be performed using efficient and reliable empirical interatomic potentials such as modified embedded-atom method (MEAM) or force-matching, embedded-atom-method (FMEAM) potentials. The interatomic potentials are constructed by optimizing the potential parameters to reproduce various experimental materials properties and atomic-force data from DFT calculations. Large-scale, atomistic simulations will be conducted to study the effects that size, shape, and volume fraction of different precipitates have on the thermo-mechanical properties of steel alloys. Many factors that govern the yield and hardening behavior of solids such as crack-tip propagation, dislocation nucleation, dislocation motion, and the interaction of dislocations with grain boundaries will be investigated through these simulations. Results will be used to guide quantitative alloy-composition designs to improve strength and formability of steel alloys.

- Construct and validate reliable interatomic potentials to model various phases of high-strength steel alloys.
- Obtain the electronic, structural and mechanical properties of the main phases of steel alloys.
- Investigate the effect of various precipitates present in modern high-strength steel alloys on their thermo-mechanical properties.
- Investigate the efficacy of novel additives to design new high-strength steel alloys with improved strength and ductility.
- Perform experiments to test new materials and validate the results.

Accomplishments

The first year objectives were met by accomplishing the followings:

- The DFT calculations were performed on iron (Fe) – carbon (C) alloy systems using the full spin-polarized, local-density approximations (LDA) to correctly account for the ferromagnetism in Fe atoms.
- Developed a new, multi-objective optimization (MOO) methodology as a robust procedure to construct reliable and transferable interatomic potentials for steel-alloy systems.
- Applied the MOO procedure to construct transferrable interatomic potential for Fe using the FMEAM.
- Applied the MOO procedure to construct transferrable interatomic potential for C using the FMEAM.
- Established a basic framework for the accelerated development of reliable and efficient interatomic potentials for other combination of alloy systems to perform large-scale, realistic atomistic simulations.
- Established a procedure to achieve a close integration with other tasks of the project. The task “Simulation-Based Design Optimization” (see 6.G) assists the present task in developing empirical interatomic potentials, which will be used by many other tasks including the present task and the task ”Examining Fundamental Mechanisms of Tooling Wear for Powder Processing” (see 4.D). The simulation results from the present task are then fed into the task “Multiscale Microstructure-Property Plasticity Considering Uncertainty” (see 6.J) for simulations in larger length scales.
- Established a close collaborative relationship with industrial partners including POSCO, SAC, Inc., and Wade Service.
- Submitted one paper on MOO methodology to Phys. Rev. B.
- One paper on the DFT calculations on cementite is in preparation.
- One paper on the development of FMEAM interatomic potential for Fe atoms is in preparation.
- One paper on the development of FMEAM interatomic potential for C atoms is in preparation.

Future Direction

- Develop interatomic empirical potentials for silicon (Si), nitrogen (N) and molybdenum (Mo) using the MOO procedure.
- Develop interatomic empirical potentials for various alloys involving Fe, C, Si, N, and Mo using the MOO procedure.
- Perform DFT simulations of ferrite-cementite interfaces (shear, debonding, etc).
- Perform large-scale, atomistic simulations of ferrite-cementite interfaces using empirical interatomic potentials.
- Perform DFT simulations of martensitic phase and Fe-Mo intermetallic compounds.
- Perform large-scale, atomistic simulations of martensitic phase and Fe-Mo intermetallic compounds.
- Obtain various high-strength steels and perform experiments on those materials to understand fundamental materials/mechanical properties and to provide information to design and simulation efforts.
- Validate numerical models using structure-property data obtained from experiments.

Introduction

The fabrication of desired automobile components is often the largest barrier to new materials, since automotive designs call for specific aerodynamic considerations. Despite their desirable material characteristics, high-strength steels have limited fabrication capability because they inherently resist deformation and wear the tooling. Therefore, we have the challenge and opportunities to perform compositional design of high-strength steel alloys in a manner that lowers mass, increases strength and retains workability, but generates required strength after the fabrication step.

Potential components for lightweighting and ultra-strength materials are the front end, powertrain, instrument panels, the chassis system, and car bodies including door panels, for example. We propose to perform compositional design of steel alloys to lower these barriers with a better understanding of the quantum-mechanical and atomistic structure of various constituent composite crystal structures and their interactions, the influence of alloying additions, and the effects of thermo-mechanical treatments on wrought materials during and after processing.

Ductility of materials can be improved by alloying and by the resulting activation of slip systems. We will investigate the origin of these alloying effects by using quantum-mechanical, first-principles methods such as DFT [Kresse96, Kohn65]. We will focus on the "gamma" surfaces (surface energy versus imposed shear) to understand the extent to which these effects are governed primarily by electronic structure or crystallography. Results will be integrated into thermo-dynamic-database extensions supporting quantitative alloy-composition designs to improve ductility.

Previous research on "triple-phase" sheet steels exploiting retained-austenite transformation plasticity for enhancement of sheet formability at high strength levels has identified the key role of austenite particle size and composition in optimizing transformation stability. We will investigate the control of austenite stability through isothermal bainitic transformation. The results will enable the prediction of new compositions and processing to increase austenite stability to a theoretically-predicted optimum and improve ultra-high-strength sheet-steel formability.

The use of precipitation reactions, such as Fe-Mo precipitates, is one of the ways to allow softer forming and high use strength. The other attractive option is to use laminates, such as Fe and aluminum (Al). Both Fe and Al are easily rolled into sheets and should have good roll bonding. After stamping, a thermal cycle could be used to induce diffusional alloying to produce FeAl, which is a ductile intermetallic. As the hard-soft laminates might prove optimal in toughness, it may not be necessary to fully homogenize the laminates. The low-density Al will reduce weight and the high-strength intermetallic will provide strength while the advantage of easy processing is retained by using laminated foils.

Experimental Approach

Figure 1 shows an overall flowchart of the project procedure along with proper technical approaches. First, reliable empirical interatomic potentials to model various phases of high-strength steel alloys are constructed and validated. Next, the structural, electronic, and mechanical properties of the main phases of advanced high-strength steel (AHSS) alloys are obtained by DFT and atomistic simulations. In order to design a novel AHSS alloy with improved strength and ductility, the effects of various phases, novel additives, heat treatment and manufacturing processes on the materials and mechanical properties of the AHSS are investigated by DFT and atomistic simulations. At this stage, various base alloys of interest with different intrinsic materials properties will be provided by industrial partners, such as POSCO and SAC, Inc. Various experiments on the base alloys will be carried out to understand fundamental materials/mechanical properties and the output will be provided for designing efforts. Such experiments include chemical analysis, microstructure observation, micro- and macro-mechanical tests. The overall chemical analysis of the base alloys will be performed by using a spectrometer. The quantitative and qualitative chemical compositions of each phase present in the alloys will be individually analyzed by an energy-dispersive x-ray (EDX) spectroscopy technique. Microstructures of the alloys will be investigated by an optical microscope (OM) and a scanning electron microscope (SEM). Conventional hardness tests will be conducted to gain overall properties of the alloys, while nano-indentation tests (NITs) will be performed to obtain micromechanical properties of various phases found in the alloys.

In order to obtain fundamental mechanical properties related to strength and ductility such as yield strength, elongation, tensile strength, work-hardening exponent (*n*-value), stress-strain relations and strain-rate effects, tensile tests will be carried out at various strain rates. The yield strength and tensile strength of the alloys are important because their relations are not only intrinsic materials properties but also general designation systems for high-strength steels. Such designation systems also classify different yield strength with equal tensile strength and vice versa, thereby, allowing some assessment of the stress-

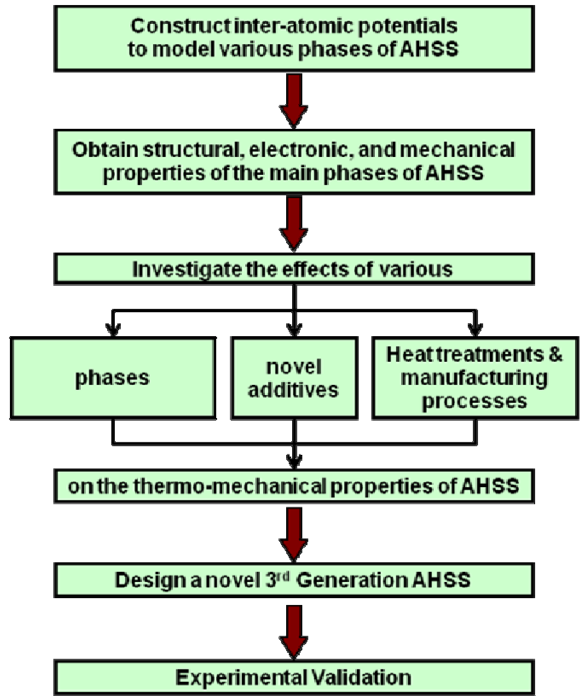

Figure 1. A flowchart showing the overall project procedure and technical approaches.

strain curves and amount of work hardening [IISI06]. The requirement of AHSS with improved formability and crash-energy absorption is strongly affected by the work hardening exponent (*n*) – the higher the *n*-value, the better stretch ability. Total elongation is also the traditional measure of the steel's general stretch ability over wide areas of the stamping. The modification of microstructure to create a novel AHSS for increased *n*-value, greater stretch ability, crash-energy absorption and higher total elongations is desired for application requirements demanded by the automotive industry. One of the critical problems to adapt high-strength steels to automotive is pure formability with increased strength. Therefore, the press formability will be investigated under different press modes. By utilizing the composition-structure-property relationship extracted by aforementioned experiments and various simulations, a novel AHSS will be designed. A small amount of sample will be manufactured and supplied by the industrial partners and model validation by various experiments will be carried out.

Computational Approach

We use a hierarchical, multiscale methodology to investigate the effect of nanoscale precipitates and additives to the overall strength and formability in steel-alloy design for automotive applications. In a hierarchical, multiscale framework, numerical methods are run independently at disparate length scales. Then, a bridging methodology such as statistical-analysis methods, homogenization techniques, or optimization methods are used to distinguish the pertinent cause-effect relations at the lower scale to determine the relevant effects for the next higher scale [E03]. One effective hierarchical method for multiscale bridging is the use of thermodynamically-constrained internal state variables (ISVs) that are physically based on microstructure-property relations [Coleman67, Rice71, Kestin70, Hasan95, Espinosa01, Gailly02]. We will adopt the strategy developed by Horstemeyer and his co-workers who used ISVs as a top-down hierarchical approach to bring the pertinent nanoscale, microscale, and mesoscale phenomena into the macroscale [Horst01, Horst03, Olson98, Olson00, Hao03, Hao04].

Critical issues being addressed include: selection of key combination of precipitates and matrices, interaction of precipitate and matrix phases and, ultimately, composition-structure-property relationship. At the electronic level, quantum-mechanical, first-principles simulations will be performed to investigate the interfacial interactions between matrix and the primary and the secondary precipitates. All first-principles, total-energy calculations and geometry optimizations are performed within the DFT [Kresse96, Kohn65] using Blöchl's all-electron projector augmented wave (PAW) method [Bloch194] as implemented by Kresse et al. [Kresse99]. For the treatment of electron exchange and correlation, we generally use the local density approximation (LDA) [Ceperley80, Perdew81] and sometimes the generalized gradient approximation (GGA) [Perdew96] depending on the accuracy required. The Kohn-Sham equations are solved using a pre-conditioned, band-by-band, conjugate-gradient (CG) minimization [Kresse93].

At the atomistic level, accurate atomistic simulations will be performed using efficient and reliable empirical interatomic potentials such as the MEAM [Baskes92, Daw84, Daw83] or FMEAM [Li03, Liu96] potentials. The interatomic potentials are constructed by optimizing the potential parameters to reproduce various experimental materials properties and atomic-force data from DFT calculations. Large-scale, atomistic simulations will be conducted to study the effect that size, shape, and volume fraction of different precipitates have on the thermo-mechanical properties of steel alloys. Many factors that govern the yield and hardening behavior of solids, such as, crack-tip propagation, dislocation nucleation, dislocation motion, and the interaction of dislocations with grain boundaries, will be investigated through these simulations. Results will be used to guide quantitative alloy composition designs to improve strength and formability of steel alloys.

FMEAM

In the FMEAM [Li03, Liu96], a force-matching method [Ercolessi94] is applied to the conventional embedded-atom method (EAM) [Daw84, Daw83]. Within the EAM approach, the total energy of the system can be written as

$$E = \sum_i E_i \tag{1}$$

where

$$E_i = \frac{1}{2} \sum_{j(\neq i)} V(r_{ij}) + F(n_i) \tag{2}$$

$V(r)$ is the pair interatomic potential, $F(n)$ is the embedding energy function, n_i is the total 'atomic density' at atom i from the surrounding atoms, and it is assumed that

$$n_i = \sum_{j(\neq i)} \rho(r_{ij}) \tag{3}$$

where $\rho(r)$ is the 'atomic density' around an isolated atom [Daw84].

Unlike the MEAM, the FMEAM approach does not use any analytic functional form for $\rho(r)$, $V(r)$, or $F(n)$. Instead, each of these functions is described as a set of control points, whose values are the parameters to be optimized. A cubic spline function is used to interpolate the values between the control points. The control points are optimized by matching the forces of this potential to those of quantum-mechanical, *ab initio* calculations for a large set of different configurations. The potential parameters are simultaneously fit to several critical experimental data such as equilibrium lattice constant, cohesive energy, bulk modulus, and elastic constants.

MOO

A generic, MOO problem can be formulated as [Kim05, deWeck04]:

$$\begin{aligned} &\min\ \vec{J}(\vec{x}) \text{ s.t. } x \in S \\ &\text{where } \vec{J} = \left[J_1(\vec{x}) \cdots J_m(\vec{x})\right]^T \\ &\vec{x} = \left[x_1 \cdots x_n\right]^T \end{aligned} \tag{4}$$

Here, $\vec{J}$ is a column vector of *m* objectives, whereby $J_i \in \Re$. The individual objectives are dependent on a vector $\vec{x}$ of *n* design variables in the feasible domain *S*. The design variables are assumed to be continuous and vary independently. Typically, the feasible design domain is defined by the design constraints and the bounds on the design variables. The problem is to minimize all elements of the objective vector simultaneously. The most widely-used method for MOO is scalarization using the weighted-sum method. The method transforms the multiple objectives into an aggregated scalar objective function $\vec{J}$ that is the sum of each objective function J_i multiplied by a positive weighting factor w_i:

$$J(\vec{x}) = \sum_{i=1}^{m} w_i J_i(\vec{x}) \tag{5}$$

In this project, the overall goal is to develop FMEAM potentials for steel alloys. The individual objective functions are constructed from the normalized differences between the FMEAM-generated values and the target values:

$$J_i(\vec{x}) = \left[\frac{Q_i(x) - Q_i^0}{Q_i^*}\right]^2 \tag{6}$$

Here, Q_i is the physical quantity computed using the current FMEAM potential parameters and Q_i^0 is the target value to reproduce. The target values are usually experimental values, but the computed values from the first-principles method are chosen when the experimental data are not available. The normalization factor Q_i^* is a typical value for the given materials parameter and often $Q_i^* = Q_i^0$ is assumed. The overall objective function $J(\vec{x})$ can be minimized using usual multi-dimensional optimization routines. To avoid unnecessary complications, we use the *downhill simplex method*, [Press92] which requires only function evaluations, not derivatives.

Fe Interatomic Potential

The multi-objective optimization procedure was applied to develop a new interatomic potential for Fe based on FMEAM. We used the EAM potential by Chamati *et al.* [Chamati06] as the initial set of the parameters for our multi-objective optimization.

Figure 2 shows the cohesive energy of Fe atoms in a body-centered (bcc) crystal structure, its lowest-energy crystal structure, as a function of the nearest-neighbor distance. FMEAM potential calculations (blue open squares) are compared with DFT calculations (red open circles) and Rose equation-of-state (black line). The Rose equation-of-state is constructed from experimental data, namely optimum lattice constant, the cohesive energy, and the bulk modulus. Our results show that FMEAM potential for Fe reproduces experimental data extremely accurately over a wide range of separation distances. As it is generally accepted, DFT estimates the equilibrium bond length to be slightly smaller than the experimental value [Droogenbroeck04].

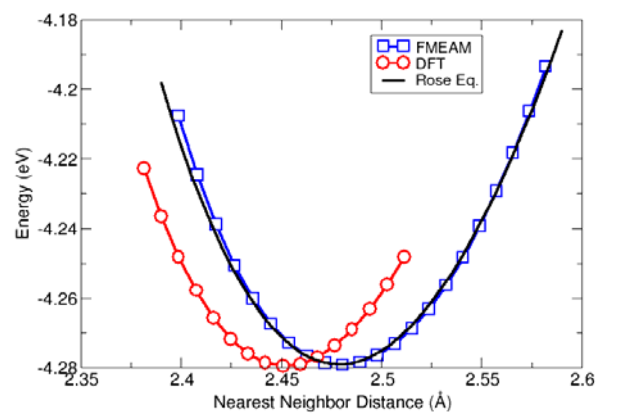

Figure 2. The cohesive energy of Fe atoms in a bcc crystal structure as a function of the nearest neighbor distance. FMEAM potential calculations (blue open squares) are compared with DFT calculations (red open circles), and Rose equation-of-state (black line) constructed from experimental data.

To validate the transferability of our new FMEAM potential, we calculated the cohesive energies of Fe atoms in other configurations such as face-centered cubic (fcc), and hexagonal close-packed (hcp) crystal structures as a function of the atomic volume. The results are summarized in Figure 3. Our results show that the new FMEAM potential for Fe atoms correctly predicts the order of stability among these common structures. In addition, the differences in equilibrium cohesive energies among these configurations are reasonably close to those of DFT calculations. However, FMEAM predicts the equilibrium atomic volumes for hcp and fcc to be similar to that of bcc while DFT predicts those values to be much smaller. Since other configurations are also relevant to various phases of steel alloys, we plan to further optimize the FMEAM potential for these configurations in the next year.

We also tested the transferability of the new FMEAM potential on a Fe dimer. Dimer interaction is an important indicator of the validity of empirical potentials because it is closely related to adsorption of atoms on surfaces, interfaces structures, and grain-boundary morphology and dynamics. As shown in Figure 4, our new FMEAM potential reproduces the total energy of a dimer reasonably well compared to more rigorous and time-consuming DFT calculations. The equilibrium bond length predicted by FMEAM potential is slightly larger than DFT's prediction. Also, the binding energy computed using the FMEAM potential is about 1.0 eV smaller than that of DFT calculations. Despite these minor discrepancies, these numbers represent an excellent validation result considering the fact that DFT calculations are known to underestimate the bond length and overestimate the binding energies compared to the experimental data [King94].

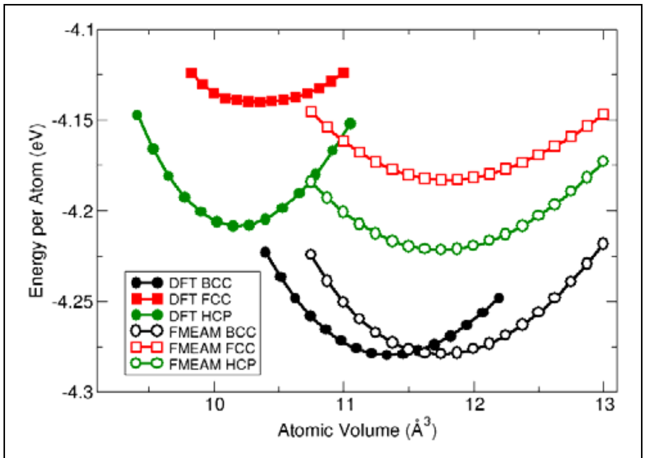

Figure 3. The cohesive energies of Fe atoms in bcc, fcc, and hcp crystal structures as a function of the atomic volume. The values reproduced with FMEAM potentials are compared with DFT calculations.

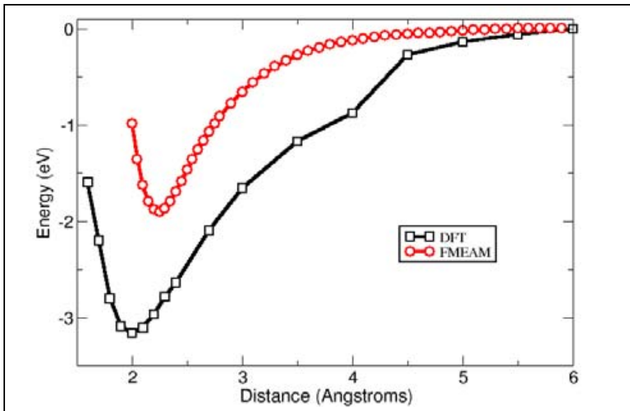

Figure 4. Total energy of a Fe dimer as a function of the separation distance. FMEAM potential calculations (red open circles) are compared with DFT calculations (black open squares).

C Interatomic Potential

The multi-objective optimization procedure was applied to develop a new interatomic potential for

C based on FMEAM. We used the MEAM potential by Lee [Lee06] as the initial set of the parameters for our multi-objective optimization. Figure 5 shows the cohesive energy of C atoms in a diamond structure as a function of the nearest-neighbor distance. The values obtained from FMEAM potential (black circles) are compared with the ones from DFT calculations (blue triangles). The Rose equation-of-state is constructed from experimental data, namely, optimum lattice constant, the cohesive energy, and the bulk modulus. Our results show that the energy values from FMEAM potential lie nearly on top of the Rose equation-of-state indicating that the new FMEAM potential for C atom works extremely well for C atoms in diamond lattice configuration, which is one of the most relevant structures for C in general.

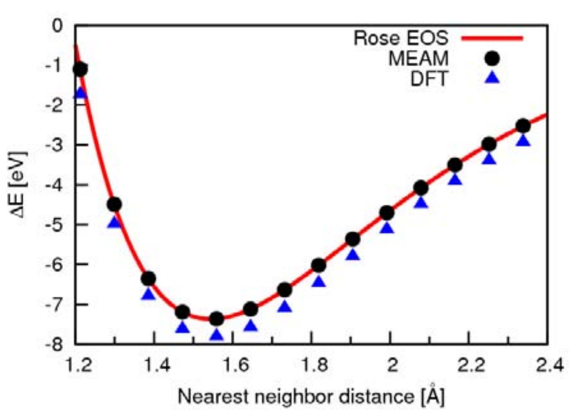

Figure 5. The cohesive energy of C atoms in diamond structure. The values obtained from FMEAM potential (black circles) are compared with the ones from DFT calculations (blue triangles) and the Rose equation-of-state constructed from experimental data.

Figure 6 shows the cohesive energies of C atoms in different configurations as a function of the atomic volume obtained from FMEAM potential calculations [Figure 6(a)] and DFT calculations [Figure 6(b)]. The plot shows that our FMEAM potential for C atoms correctly predicts that diamond structure is the lowest energy configuration. However, it fails to predict that the graphene sheet will have lower energy than cubic structure. Since graphene and graphite are also common and relevant structures for C atoms, we plan on improving this shortcoming in the next year.

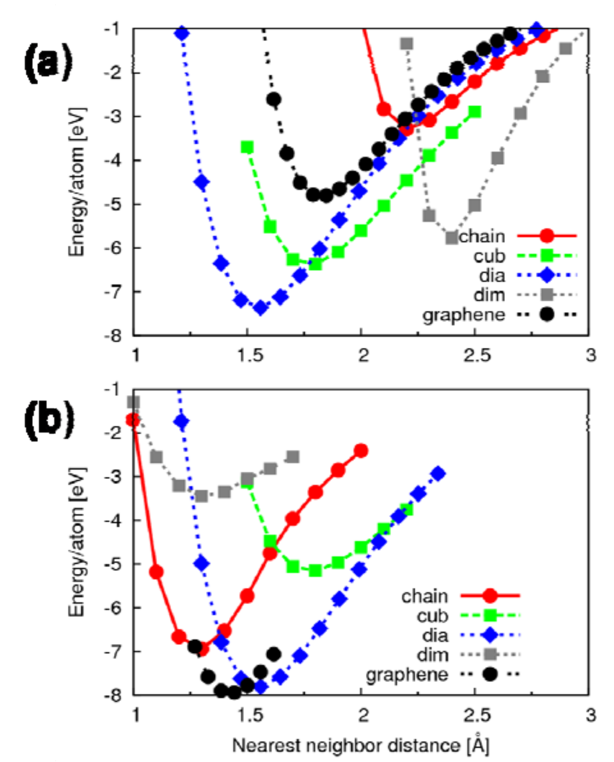

Figure 6. The cohesive energies of C atoms in different configurations as a function of the nearest-neighbor distance. (a) FMEAM potential calculations. (b) DFT calculations. The notations for configurations are: chain = linear chain, cub = cubic lattice, dia = diamond lattice, dim = dimer, grapheme = a single sheet of graphene.

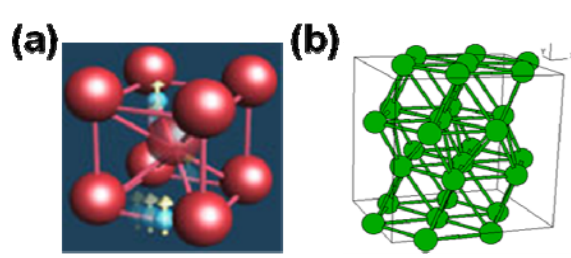

Figure 7. The crystal structure of Fe atoms. (a) bcc structure and (b) hcp structure.

Ferrite Phase

To establish the baseline of the simulations for the project, we performed the quantum-mechanical, first-principles calculations on the ferrite phase. Figure 7 shows the Fe atoms in bcc and hcp structures. It is well known that DFT total-energy calculation of Fe atoms using LDA to treat electron exchange-correlation predicts the hcp nonmagnetic structure as the ground-state structure instead of the correct bcc ferromagnetic structure [Stixrude94]. We performed DFT calculations using different exchange-correlation functionals and pseudopotential models with and without spin polarization. Our results, summarized in Table 1, show that, when the full spin-polarized DFT calculations with the generalized gradient approximation (GGA) exchange-correlation energy were used, the correct ferromagnetic bcc structure is determined as the lowest-energy structure. We also found that the projector augmented wave (PAW) method is superior to the ultrasoft pseudopotential (US-PP) method as it gives much better energy differences between bcc FM and hcp NM structures. Our results also confirm previously reported calculations by Kresse *et al.* [Kresse99].

Table 1. Relative energy of Fe crystals in various crystal structures and magnetic states. Energy values are given in meV. PAW and US-PP denote the different methods to handle electron-ion interaction while LDA and GGA indicate the different methods to treat electron exchange-correlation:

	PAW[a]		US-PP[b]	
	LDA[c]	GGA[d]	LDA[c]	GGA[d]
bcc Fe NM	431	387	430	383
bcc Fe FM	151	**-66**	87	-238
fcc Fe NM	87	79	86	76
hcp Fe NM	0	0	0	0

[a]Projector augmented wave (PAW) method
[b]Ultrasoft pseudopotential (US-PP) method
[c]Local density approximation (LDA)
[d]Generalized gradient approximation (GGA)

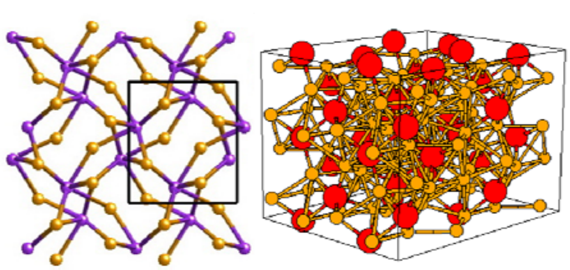

Figure 8. Two different views of the crystal structure of cementite. Gold spheres represent Fe atoms and red/purple spheres represent C atoms.

Table 2. Crystal structure parameters for cementite. *a*, *b*, and *c* are the lattice constants. *x*, *y*, and *z* are the relative coordinates for basis atoms.

	This work	Other[a]	Exp.[b]
a	5.03	5.06	5.09
b	6.72	6.74	6.74
c	4.47	4.51	4.53
C-x1	0.876	0.877	0.890
C-z1	0.438	0.440	0.450
Fe(I)-x2	0.035	0.038	0.036
Fe(I)-z2	0.837	0.837	0.850
Fe(II)-x3	0.176	0.176	0.186
Fe(II)-y3	0.068	0.068	0.063
Fe(II)-z3	0.332	0.332	0.328

[a]Chiou *et al.* [Chiou03]
[b]Fasiska *et al.* [Fasiska65]

Cementite Phase

The second main phase of the steel is the cementite (Fe_3C). We use the DFT method to investigate the materials properties of the cementite phase and its interactions with the ferrite phase. Figure 8 shows the structure of cementite phase which has the space group *Pnma* (No. 62) [Hahn83]. The unit cell contains four iron atoms in "first" positions [4 Fe(I)], eight iron atoms in "second" positions [8 Fe(II)], and four carbon atoms in large interstices [4 C], see Figure 8. The unit-cell structure of the cementite and the position of basis atoms are determined by the parameters listed in Table 2.

We performed DFT calculations to optimize the structure parameters listed in Table 2 simultaneously. The values obtained in the present work agree well with previously published results by Chiou *et al.* [Chiou03] and experimental values [Fasiska65]. Figure 9 shows the total energy of Fe_3C cementite as a function of the atomic volume. Our results indicate that the equilibrium volume for cementite is 151 Å^3 where the experimental value is 155 Å^3. Again, DFT calculations underestimate the equilibrium volume by 2.7%, confirming a well-known tendency of the DFT method

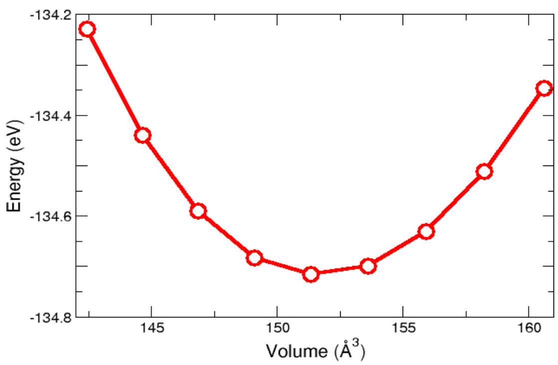

Figure 9. The total energy of cementite as a function of the atomic volume.

In the next year, we plan to perform large-scale, atomistic simulations of the interaction between the two main phases of steel, cementite and ferrite, using the FMEAM potentials developed in this project.

Conclusions

The goal of this project is to investigate the effect of nanoscale precipitates and novel additives to the overall strength and formability in steel-alloy systems. DFT calculations were performed on Fe-C alloy systems using the full spin-polarized LDAs to correctly account for the ferromagnetism in Fe atoms. We developed a new MOO methodology as a robust procedure to construct reliable and transferable interatomic potentials for steel-alloy systems. This MOO procedure was applied to construct transferrable interatomic potentials for Fe and C atoms using the FMEAM. We also established a basic framework for the accelerated development of reliable and efficient interatomic potentials for other combination of alloy systems to perform large-scale, realistic atomistic simulations. Full spin-polarized density-functional theory calculations have been performed on ferrite and cementite phases and compared with experiments.

This investigation should facilitate the design of a new generation of AHSSs by providing fundamental understanding of several critical issues that include the selection of key combinations of precipitates and matrices, interaction of precipitate and matrix phases and, ultimately, composition-structure-property relationship.

Presentations/Publications/Patents

1. Seong Jin Park, M.F. Horstemeyer, and Seong-Gon Kim, *"Atomistic Simulations for Steel Alloy Design"*, Colloquium at POSTECH, Pohang, KOREA, June 4, 2007.
2. Seong Jin Park, M.F. Horstemeyer, and Seong-Gon Kim, *"Atomistic Simulations for Steel Alloy Design"*, Seminar at Technical Research Laboratory of POSCO, Pohang, KOREA, June 5, 2007.

References

1. [Baskes92] M. I. Baskes, *"Modified embedded-atom potentials for cubic materials and impurities"*, Phys. Rev. B 46, 2727 (1992).
2. [Blochl94] P. E. Blöchl, Phys. Rev. B vol. 50, pp. 17953 (1994).
3. [Ceperley80] D. M. Ceperley and B. J. Alder, *"Ground State of the Electron Gas by a Stochastic Method"*, Phys. Rev. Lett. vol. 45, pp. 566—569 (1980).
4. [Chamati06] H. Chamati, N.I. Papanicolaou, Y. Mishin, D.A. Papaconstantopoulos, *"Embedded-atom potential for Fe and its application to self-diffusion on Fe (100)"*, Surf. Sci. vol. 600, pp. 1793—1803 (2006).
5. [Chiou03] W. C. Chiou, Jr., and E. A. Carter, *"Structure and stability of Fe3C-cementite surfaces from first principles,"* Surf. Sci. vol. 530, pp. 87—100 (2003).
6. [Coleman67] B. D. Coleman and M. E. Gurtin, *"Thermodynamics with internal state variables"*, J. Chem. Phys., vol. 47, 597—613 (1967).
7. [Daw83] M. S. Daw and M. I. Baskes, *"Semiempirical, Quantum Mechanical Calculation of Hydrogen Embrittlement in Metals"*, Phys. Rev. Lett. 50, 1285 (1983).
8. [Daw84] M. S. Daw and M. I. Baskes, *"Embedded-atom method: Derivation and application to impurities, surfaces, and other defects in metals"*, Phys. Rev. B 29, 6443 (1984).
9. [Droogenbroeck04] Joris Van Droogenbroeck, Karla Tersago, Christian Van Alsenoy and Frank Blockhuys, *"A systematic study of the effect of correlation, DFT functional and basis set on the structure of Roesky\u2019s ketone"*, Chem. Phys. Lett. vol. 399, pp. 516—521 (2004).

10. [deWeck04] O. L. de Weck, *"Multiobjective Optimization: History and Promise (The Third China-Japan-Korea Joint Symposium on Optimization of Structural and Mechanical Systems",* Kanazawa, Japan, (2004).
11. [E03] W. E and B. Engquist, *"Multiscale Modeling and Computation"*, Notices of the AMS, vol. 50, 1062-1070 (2003).
12. [Espinosa01] H. D. Espinosa, H. -C. Lu, P. D. Zavattieri, and S. Dwivedi, *"A 3-D Finite Deformation Anisotropic Visco-Plasticity Model for Fiber Composites,"* J. of Composite Materials, vol. 35, 369-410 (2001).
13. [Ercolessi94] F. Ercolessi and J.B. Adams, *"Interatomic potentials from first-principles calculations: the Force-Matching method"*, Europhys. Lett. vol. 26, pp. 583 (1994).
14. [Fasiska65] E. J. Fasiska and G. A. Jeffrey, *"On the cementite structure"*, Acta Cryst., vol. 19, 463—471 (1965).
15. [Gailly02] B. A. Gailly and H. D. Espinosa. *"Modelling of Failure Mode Transition in Ballistic Penetration with a Continuum Model Describing Microcracking and Flow of Pulverized Media*", Int. J. for Numerical Methods in Engineering, vol. 54, 365—398 (2002).
16. [Hahn83] T. Hahn (ed.), *International Tables for Crystallography*, vol. A, Reidel, Dordrecht (1983).
17. [Hao03] Su Hao, Brian Moran, Wing Kam Liu, and Gregory B. Olson, *"A hierarchical multi-physics model for design of high toughness steels"*, Journal of Computer-Aided Materials Design, vol. 10, 99—142 (2003).
18. [Hao04] Su Hao, Brian Moran, Wing Kam Liu, and Gregory B. Olson, *"Multi-scale constitutive model and computational framework for the design of ultra-high strength"*, Computer Methods in Applied Mechanics and Engineering, vol. 193, 1865—1908 (2004).
19. [Hasan95] O. A. Hasan and M. C. Boyce, "A Constitutive Model for the Nonlinear Viscoelastic Behavior of Glassy Polymers," Polymer Engng. and Sci., vol. 35, 331—344 (1995).
20. [Horst01] M. F. Horstemeyer, S. J. Plimpton, and M. I. Baskes. *"Size Scale and Strain Rate Effects on Yield and Plasticity of Metals"*, Acta Matallurgica, vol. 49, 4363—4374 (2001).
21. [Horst03] M. F. Horstemeyer and P. Wang. *"Cradle-to-grave simulation-based design incorporating multiscale microstructure-property modeling: Reinvigorating design with science"*, Journal of Computer-Aided Materials Design, vol. 10, 13—34 (2003).
22. [IISI06] *Advanced high strength steel (AHSS) application guidelines*, prepared by International Iron & Steel Institute, September 2006.
23. [Kim05] I. Y. Kim and O. L. de Weck, "Structural and Multidisciplinary Optimization", vol. 31, 105 (2005).
24. [King94] R. D. King-Smith and David Vanderbilt, *"First-principles investigation of ferroelectricity in perovskite compounds"*, Phys. Rev. B vol. 49, pp. 5828—5844 (1994).
25. [Kohn65] W. Kohn and L. J. Sham, "*Self-consistent Equations Including Exchange and Correlation Effects*", Phys. Rev. Vol. 140, pp. A1113—A1138 (1999).
26. [Kresse93] G. Kresse and J. Hafner, *"Ab initio molecular dynamics for liquid metals"*, Phys. Rev. B vol. 47, pp. 558 (1993).
27. [Kresse96] G. Kresse and J. Furthmüller, *"Efficient iterative schemes for ab initio total-energy calculations using a plane-wave basis set"*, Phys. Rev. B 54, 11169 (1996).
28. [Kresse99] G. Kresse and D. Joubert, "*From ultrasoft pseudopotentials to the projector augmented-wave method*," Phys. Rev. B vol. 59, pp. 1758 (1999).
29. [Kestin70] J. Kestin and J. R. Rice, *"Paradoxes in the application of thermodynamics to strained solids"*, in "A Critical Review of Thermodynamics", edited by E.G. Stuart, B. Gal-Or, and A. J. Brainard, Mono Book Corp., Baltimore, 275-298 (1970).
30. [Lee06] Byeong-Joo Lee, *"A modified embedded-atom method interatomic potential for the Fe—C system,"* Acta Materialia, vol. 54, pp. 701—711 (2006).
31. [Li03] Youhong Li, Donald J. Siegel, James B. Adams, and Xiang-Yang Liu, "*Embedded-atom-method tantalum potential developed by the force-matching method*," Phys. Rev. B vol. 67, pp. 125101 (2003).
32. [Liu96] Xiang-Yang Liu, James B Adams, Furio Ercolessi and John A Moriarty, "*EAM potential for magnesium from quantum mechanical forces*," Modelling Simul. Mater. Sci. Eng. vol. 4, pp. 293—303 (1996).
33. [Olson98] G. Olson. *"Systems design of hierarchically structured materials: Advanced*

steels", Journal of Computer-Aided Materials Design, vol. 4, 143—156 (1998).
34. [Olson00] G. Olson. *"New age of design"*, Journal of Computer-Aided Materials Design, vol. 7, 143--144 2000).
35. [Perdew81] J. P. Perdew and A. Zunger, *"Self-interaction correction to density-functional approximations for many-electron systems"*, Phys. Rev. B 23, 5048 (1981).
36. [Perdew96] J. P. Perdew, K. Burke, and M. Ernzerhof, *"Generalized Gradient Approximation Made Simple"*, Phys. Rev. Lett. vol. 77, pp. 3865 (1996).
37. [Press92] William H. Press and Brian P. Flannery and Saul A. Teukolsky and William T. Vetterling, *Numerical Recipes in C: The Art of Scientific Computing*, 2nd ed., Cambridge University Press, Cambridge (1992).
38. [Rice71] J.R. Rice, *"Inelastic constitutive relation for solids: An internal variable theory and. its application to metal plasticity"*, J. Mech. Phys. Solids, vol. 19, 433—455 (1971).
39. [Stixrude94] Lars Stixrude, R. E. Cohen, and D. J. Singh, "Iron at high pressure: Linearized-augmented-plane-wave computations in the generalized-gradient approximation", Phys. Rev. B vol. 50, pp. 6442—6445 (1994).